TÉCNICO LISBOA

Investigation of the impact of wake modelling approaches on wind farm yield via yaw-based control optimization

Bartłomiej Paweł Rak

Thesis to obtain the Master of Science Degree in

Energy Engineering and Management

Supervisor: Dr. Ricardo Balbino dos Santos Pereira

Examination Committee

Chairperson: Prof. Edgar Caetano Fernandes

Supervisor: Dr. Ricardo Balbino dos Santos Pereira

Member of the Committee: Prof. José Alberto Caiado Falcão de Campos

January 2021

I declare that this document is an original work of my own authorship and that it fulfils all the requirements of the Code of Conduct and Good Practices of the *Universidade de Lisboa*.

To those working towards a more sustainable future.

Acknowledgements

Completion of this Master's Thesis marks the end of a two-year challenging educational journey made possible by the European Institute of Innovation & Technology and KIC InnoEnergy Master's School. I would like to thank all the people involved in creating and coordinating such an extraordinary study programme that provided great opportunities for personal and professional development. Also, I would like to acknowledge the Silesian University of Technology in Poland and Instituto Superior Técnico in Portugal and their incredible academic staff I had the opportunity to learn from throughout the master's programme. Lastly, I want to thank my dear colleagues and friends who have been an important part of this journey and with whom I have many fond memories of the numerous adventures we have been through together.

Not until the last year of my energy engineering studies had I the opportunity to take a course on offshore wind energy, taught by dr. Ricardo Balbino dos Santos Pereira. Fascinated by how complex and challenging wind energy harvesting is, I decided to undertake a Master's Thesis project on wind farm control under the supervision of dr. Pereira. This research journey let me explore many unfamiliar topics, broaden my understanding of wind energy engineering and contribute to the fight for a more sustainable future. Dr. Pereira, the inspiration you gave me, the challenging questions you asked and the continuous guidance you provided were invaluable throughout the development of this thesis project. I sincerely thank you.

Lastly, I cannot forget about the two incredible people, my parents Paweł and Joanna, who gave the very beginning to this adventure by awakening my curiosity about the world and inspiring me to study abroad. Your continuous support and faith in me helped me overcome every challenge that I have faced on my way to achieving my Master's Degree.

Abstract

The exploitation of offshore wind resources is considered to have tremendous potential in providing carbon-free energy. In order to increase the economic viability of wind farms, improvement in power generation is sought by mitigating the wake losses. While the industrial standards still favour turbine-level power maximization, a concept of collaborative yaw-based plant-level control has gained significant attention in recent years. This thesis investigates the potential of such a control strategy based on predictions of different wake modelling approaches under a range of atmospheric conditions and plant layouts. The utilized wake velocity deficit models are the top-hat Jensen model, the Gaussian-shaped Bastankhah model and its novel extension, termed Gauss–Curl Hybrid (GCH) model that accounts for secondary steering effects. The yaw control optimization is conducted on a row of eight NREL 5-MW turbines using the FLORIS modelling utility and SLSQP optimization algorithm. Generally speaking, the Jensen model shows lack of robustness and is not recommended for yaw control studies. In contrast, the two Gaussian-shaped models are well handled by the optimization algorithm and produce consistent results. More specifically, the Bastankhah model prefers yaw offsets of nearly equal magnitude throughout the whole wind farm except for the most downstream machine that remains aligned with the freestream. On the other hand, the GCH model suggests a large offset at the most upstream turbine, which is gradually reduced at consecutive machines. For a reference wind farm considered, the achieved power improvement yielded 3.59% and 14.66% for the Bastankhah and GCH models, respectively.

Keywords

Offshore Wind Energy, Wind Farm Optimization, Wind Farm Control, Wake Steering, Yaw Control, Wake Models

Resumo

A energia eólica tem um enorme potencial no fornecimento de energia verde. Para aumentar a viabilidade económica dos parques eólicos, tenta-se aumentar a produção de energia mitigando as perdas de esteira. Embora os operadores de parques favoreçam ainda a maximização da potência em cada turbina, recentemente o controlo colaborativo do parque baseado no desalinhamento intencional das turbinas tem ganho atenção significativa. Esta tese investiga tal estratégia de controlo utilizando diferentes modelos de esteira sob uma variedade de condições atmosféricas e disposição geométrica das turbinas. Os modelos de déficit de velocidade utilizados são o modelo Jensen, o modelo Bastankhah e o modelo Gauss-Curl Hybrid (GCH), este último considerando os efeitos secundários de desalinhamento das turbinas. A optimização do controlo do parque é efectuada numa linha de oito turbinas NREL de 5 MW usando o software FLORIS e o algoritmo de optimização SLSQP. Em geral, o modelo Jensen mostra falta de robustez e não é recomendado para este tipo de estudos. Os dois modelos com perfil de velocidades gaussiano quando utilizados pelo algoritmo de optimização produzem resultados consistentes. Concretizando, o modelo Bastankhah resulta em ângulos de desalinhamento de magnitude quase igual em todo o parque, excepto para a máquina mais a jusante que permanece alinhada com o escoamento não perturbado. Já o modelo GCH sugere um desalinhamento maior na turbina mais a montante, que é gradualmente reduzido em máquinas consecutivas. Para as condições do parque eólico de referência, o aumento de energia alcançado é de 3,59% e 14,66% para os modelos Bastankhah e GCH, respectivamente.

Palavras-chave

Energia Eólica Offshore, Otimização de Parque Eólico, Controlo de Parque Eólico, Direção de Esteira, Controlo Yaw, Modelos de Esteira

Table of Contents

List of Figures

List of Tables

List of Acronyms

ABL	Atmospheric Boundary Layer
AWC	Active Wake Control
BEM	Blade Element Momentum
BFGS	Broyden-Fletcher-Goldfarb-Shanno
COE	Cost Of Energy
CVP	Counter-rotating Vortices Pairs
DOWEC	Dutch Offshore Wind Energy Converter
FLORIS	FLOw Redirection and Induction in Steady-state
GCH	Gauss-Curl Hybrid
HAWT	Horizontal Axis Wind Turbine
HTI	High Turbulence Intensity
HWS	High Wind Speed
IPC	Individual Pitch Control
LCOE	Levelized Cost Of Energy
LES	Large Eddy Simulation
LIDAR	LIght Detection and Ranging
LS	Large Spacing
LSEI	Equality- and Inequality-constrained Least Squares
LTI	Low Turbulence Intensity
LWS	Low Wind Speed
NLP	Non-Linear Programming
NREL	National Renewable Energy Laboratory
QP	Quadratic Programming
RC	Reference Case
RECOFF	Recommendation for Design of Offshore Wind Turbines
SLSQP	Sequential Least SQuares Programming
SOWFA	Simulator fOr Wind Farm Applications
SS	Small Spacing
TKE	Turbulent Kinetic Energy
USA	United States of America
WD_265°	Wind Direction 265°
WD_275°	Wind Direction 275°
WFC	Wind Farm Control
WindPACT	Wind Partnerships for Advanced Component Technology

List of Symbols

Roman letters

A	Rotor swept area [m^2]
A_d	Actuator disc area [m^2]
C	Maximum normalized velocity deficit in Gauss wake model[-]
C_D	Drag Coefficient [-]
C_L	Lift Coefficient [-]
C_P	Power Coefficient [-]
$C_{P,max}$	The Betz limit [-]
$C_{P,eff}$	Effective Power Coefficient [-]
C_T	Thrust Coefficient [-]
D	Rotor diameter [m]
D_r	Wake width at the rotor [m]
D_w	Width of a wake cross-section [m]
F	Force [N]
F_D	Drag force [N]
F_L	Lift force [N]
N	Number of blades [-]
N_r	Number of points in rotor domain [-]
N_t	Number of turbines [-]
P	Power [W]
Q	Torque [Nm]
R	Rotor radius [m]
T	Thrust force [N]
U	Streamwise wind velocity component [m/s]
U_{avg}	Average wind velocity at a non-yawed rotor [m/s]
U_{br}	Wind velocity just behind the rotor [m/s]
U_d	Wind velocity at an actuator disc [m/s]
U_{def}	Wind velocity deficit [m/s]
U_{eff}	Effective wind velocity [m/s]
U_i	Wind velocity at *i-th* turbine [m/s]
U_{ki}	Wake velocity of turbine k at turbine i [m/s]
U_r	Wind velocity at the rotor [m/s]
U_{rel}	Relative wind speed [m/s]

U_w	Wind velocity in the far wake [m/s]
V	Spanwise wind velocity component [m/s]
V_r	Spanwise wind velocity within the rotor domain [m/s]
W	Vertical wind velocity component [m/s]
a'	Angular induction factor [-]
a	Axial induction factor[-]
c	Chord length [m]
k	Wake growth rate in the Jensen velocity deficit model [-]
k^*	Wake growth rate in the Gauss velocity deficit model [-]
k_d	Tuneable parameter of the Jiménez velocity deflection model [-]
k_y	Spanwise wake growth rate in the Gauss velocity deficit model [-]
k_z	Vertical wake growth rate in the Gauss velocity deficit model [-]
$\dot{m}$	Mass flow [kg/s]
p	Pressure [Pa]
p_d^-	Pressure immediately downstream of an actuator disc [Pa]
p_d^+	Pressure immediately upstream of an actuator disc [Pa]
p_w	Pressure in the far wake
r_w	Radial position in the wake [m]
r_a	Width of the annular ring [m]
w	Tangential velocity component in the wake [m/s]
x	Streamwise distance [m]
x_{nw}	Length of near wake [m]
y	Spanwise coordinate in the wake [m]
y_t	Spanwise position of turbine [m]
z	Vertical coordinate in the wake [m]
z_h	Hub height [m]

Greek letters

Γ	Circulation strength of a vortex [m/s]
Γ_{wr}	Circulation strength of the wake rotation vortex [m/s]
X	Wake skew angle [deg]
X_{init}	Initial wake skew angle at the rotor [deg]
Ω	Angular velocity of the rotor [rad/s]
α	Angle of attack [deg]
α_r	Tuning parameter for the yaw-induced wake recovery [m]
γ	Yaw angle [deg]
γ_t	Yaw angle applied at a turbine in GCH wake model [deg]
δ	Infinitesimal quantity [-]
δ_w	Wake deflection [m]
ε	Dimensionless step size for the numerical approximation of Jacobian [-]

ε_n	Normalized step size for the numerical approximation of Jacobian [-]
ε_w	Wake expansion parameter in the Gauss wake model [-]
η_g	Generator efficiency [-]
θ	Section pitch angle [deg]
λ	Tip speed ratio [-]
λ_r	Local tip speed ratio [-]
λ_h	Local speed ratio at the hub [-]
υ_T	Mixing length in the free atmosphere [m^2/s]
ρ	Air density [kg/m^3]
σ	Standard deviation of the Gaussian-like velocity profile [m]
σ_y	Gaussian wake width in spanwise direction [m]
σ_z	Gaussian wake width in vertical direction [m]
τ_g	Generator torque [Nm]
φ	Inflow angle [deg]
ϵ	Size of vortex core [m]

Other symbols

5D	Distance expressed as a number multiplied by the rotor diameter [m]
f_tol	Precision goal in the stopping criterion
maxiter	Maximum allowed number of iterations
T1	Abbreviation to denote “first turbine” of the row of turbines
x0	Initial guess of the vector of arguments
x0_0	Vector of baseline yaw angles
x0_G	Vector of the guessed yaw angles

Indices

∞	Freestream conditions
bottom	Due to rotor-released bottom vortex
top	Due to rotor-released top vortex
wake	In the wake
wr	Due to wake rotation
eff	Effective

Chapter 1

Introduction

This chapter gives a brief overview of the undertaken dissertation project. The role of offshore wind energy in the global energy transition process is discussed. Further, the background information on wake problem within wind farms is presented, followed by the motivation behind the research into wind farm control. Next, the scope of the study is established and the addressed research question is stated. At the end of the chapter, the work structure is provided.

1.1 Overview

The energy transition is a process of shifting from fossil fuel-based towards zero-emission renewable sources of energy, shaping the development of the global energy sector in the 21st century. This transformation requires collaborative action of governments, industry and research to seek new and improve existing ways of carbon-free electricity production, that not only ensure sustainability and minimal environmental impact but also are economically competitive in the energy market.

Wind energy production has experienced spectacular growth over the last decades marking this renewable resource as a recognised alternative to the conventional ways of electrical power generation. As the wind technology becomes more mature, the global averaged levelized cost of electricity (LCOE) continuously falls, amounting to 0.06 USD/kWh for onshore wind, and 0.13 USD/kWh for its offshore counterpart in 2018. While onshore wind projects are highly restricted by the availability of land and the resource, strong interest is now focused on harvesting offshore wind power, which offers tremendous potential [1].

A number of reasons justify the superiority of the wind energy capture offshore over onshore. Starting from environmental impacts, civil works related to the construction of transportation infrastructure are unnecessary. Also, the visual and audible concerns are mitigated. This gives the possibility to construct larger wind farms consisting of more powerful machines. As many major cities are located close to the seaside, shorter transmission lines are required. Besides, the resource quality is more favourable away from the land, since winds are stronger and less turbulent due to the absence of obstructions and uneven terrain [2, 3]. As a consequence, offshore wind turbines accumulate less fatigue damage and can produce more electricity relative to their onshore kin, quantified by the average annual capacity factor of 43% and 34% for the respective technologies [4].

Despite these benefits, in many regions, offshore wind power still lacks competitiveness against onshore wind and fossil-fuel-based alternatives. To increase its economic viability, improvements are constantly being made in turbine design and materials, wind farm planning and control [5]. Further advancement in these core areas is therefore imperative for the proliferation of offshore wind power, which is currently the priority within the wind energy research communities [6].

1.2 The motivation behind wind farm control

The number, size and complexity of wind farms have been gradually increasing over the past years, resulting in remarkable development in the design of large-scale wind energy conversion systems. While this approach helps to reduce the overall cost of energy due to many economies of scale, it introduces the problem of aerodynamic interaction between the machines via their wakes, as depicted in Figure 1.2.1. The term “wake” refers to the volume of the flow affected by the kinetic energy extraction, that travels downstream of the turbine rotor. It is characterised by a reduced streamwise velocity, high vorticity and increased turbulence levels compared to the freestream conditions. The two major issues related to such aerodynamic coupling are reduced power output of

downstream turbines because of lower incident wind speeds, and shortened lifespan of the rotors due to enhanced fatigue loads caused by increased turbulence and operation in partial wake overlap. In the global scale, the wake effect contributes to considerable losses in power generation of wind farms as well as significantly increased operation and maintenance costs [7, 8, 9].

Figure 1.2.1 Wakes at Horns Rev wind park made visible by weather conditions [10]

Many research efforts have been undertaken to decrease the adverse influence of wind turbine wakes through wind farm layout optimization. To avoid excessive layout related wake losses, the minimum turbine spacing of 5 rotor diameters (5D) is maintained as a design standard [11]. Although placing turbines further apart would decrease the level of their aerodynamic interaction, it is not economically viable to fully eliminate it due to farm-size dependent costs. Therefore, the general idea is to place wind turbines as far apart as possible in the local dominant wind directions and group them closely in wind sectors that on average receive less wind or are perpendicular to the dominant winds. However, due to the unsteadiness of wind direction and externally imposed design restrictions, there is still a high occurrence of wake losses even for aerodynamically optimized wind plant layouts [7]. In the case of direct alignment between the wind direction and a row of turbines, the power drop at the second machine can amount to as much as 40%, relative to the front one, showing a large, still existing potential for improvement [12]. Therefore, a large subdivision of wind energy research is now seeking ways to overcome the wake problem by investigating the potential of various wind farm controls strategies.

Modern wind turbines are equipped with control systems allowing the machines to maximize their power output in the time-varying atmospheric conditions. The current industrial standards of controlling a wind farm, which, in fact, is a distributed control of individual turbines, still favour the power maximization of each turbine alone, ignoring the negative effects that the machines have on one another through their wakes. As wind farms constantly grow in size and more knowledge on the wake effect has become available, the scientists' perception of the optimal wind farm control undergoes a paradigm shift, moving from so-called "greedy" into more collaborative inter turbine control strategies [13].

In brief, this broad concept explores the possible ways of adjusting the available degrees of freedom of individual turbines to intentionally manipulate the wind field across the wind farm. This way a plant level objective of either power maximization or power set-point tracking with loads reduction can be achieved [6]. In recent years, yaw-based wake redirection technique has gained significant attention and is considered as a

promising solution for the wake loss mitigation in existing and future wind farms, showing encouraging results obtained via simulations [14, 15, 16], wind tunnel experiments [17, 18, 19], and field tests [20, 21, 22].

The crucial part in wind farm control is the understanding of the flow behaviour when control actions are being implemented, necessary for the development of a control algorithm. The role of such algorithm includes supervision of the plant operation and adjustment of the control settings of the machines in real-time, based on present wind conditions. Such an algorithm can be either model-free, utilizing, for example, Game-Theoretic methods [23] or model-based, utilizing mathematical models of wind turbine and wake aerodynamics. The latter approach assumes that, when applying a model-based controller in a real wind farm, its resulting performance will be equivalent to the predictions of the models used to design the controller. The main challenge associated with this assumption lies in the credibility of the implemented models, especially these accounting for the wake effects, which have stochastic nature and are still not fully understood. Thus, assessment of the reliability of the mathematical models in terms of capturing control-relevant wake behaviour and their impact on the suggested control actions remains an open research question [6].

This Master's Thesis aims to investigate the impact of several wake modelling approaches on the solution of yaw-based plant-wise control optimization with the objective of farm yield maximization. The present study mainly involves testing the effectiveness of yaw control under a range of wind conditions and farm layouts in steady-state. It is of interest to assess how different characteristics of the employed wake models affect the incident distribution of yaw settings and the resulting power gains at individual turbines. From the perspective of a real wind farm operation, the optimal control would rely on finding the compromise between the level of power generation and fatigue loading on the machines. However, the present investigation does not take into account the effect of the imposed yaw settings and the resulting partial wake overlap situations on the loads experienced by the turbines, focusing solely on power maximization. In this work, a control-oriented modelling framework developed at National Renewable Energy Laboratory in the U.S. (NREL) – FLOw Redirection and Induction in Steady-state (FLORIS) is used [14]. FLORIS consists of a range of wake models and optimization tools that allow to determine the optimal control set-points for each turbine of an arbitrary wind farm, under given wind conditions, neglecting any unsteady aerodynamic phenomena, such as wake meandering [8].

1.3 Document outline

The remaining body of this Master's Thesis is structured as follows. **Chapter 2** covers the theoretical background of wind turbine and wind farm aerodynamics. Some fundamental concepts behind the mechanism of wind energy extraction are introduced and the utilized wake modelling approaches are described. **Chapter 3** addresses the possible ways of controlling an individual wind turbine and a wind farm as a whole. In **Chapter 4** the applied methodology together with some preliminary optimization studies is covered. **Chapter 5** is intended for the discussion of the optimization results. The impact of the wake modelling method on the proposed yaw control strategy under various wind conditions and farm layouts is assessed. Finally, in **Chapter 6** the most important conclusions from the present research are drawn and suggestions for further investigations are made.

Chapter 2

Wind energy aerodynamics

This chapter covers some basic concepts of aerodynamics, which is one of the main scientific disciplines of wind energy engineering. First, the physics of the interaction between moving particles of fluid with the blades of a rotor, known as rotor aerodynamics, is discussed, and some fundamental theories of this subfield are brought up. Then, the wind farm aerodynamics, which addresses large scale inter turbine flow effects is covered. The physical phenomena related to creation and evolution of the wake are elaborated, followed by the presentation of the employed wake velocity deficit, deflection and combination models.

2.1 Wind turbine aerodynamics

Wind energy capture is a consequence of the aerodynamic interaction between the flowing air and wind turbine blades. Major aspects of wind turbine performance rely on the aerodynamic forces generated by the mean wind. The analysis of rotor aerodynamics can be subdivided into two categories: (1) induction aerodynamics, dealing with the global flow field around a wind turbine to determine the induced velocities at the blade, and (2) blade aerodynamics, accounting for the loads experienced by the blades as a response to this flow field [24]. Although there exist many highly advanced engineering approaches to simulate wind turbine behaviour [25], it is deemed appropriate to introduce here only the most basic and commonly known models of rotor aerodynamics. This subchapter provides an overview of the Momentum Theory accounting for the wake rotation, the Blade Element Theory and their combination known as the Blade Element Momentum (BEM) Theory. The theories and derivations presented below are based on the two widely known and comprehensive books on wind energy [2, 26], with no further references made.

2.1.1 Momentum Theory and the Betz Limit

Momentum Theory, also commonly referred to as Actuator Disk Theory, is a very basic approach to describe the process of extraction or injection of kinetic energy between flowing fluid and a conceptual device created for such purpose, called an actuator disc. The formulation of this theory dates back to the late 19th century and to the three prominent figures of the aerodynamics: W. J. M. Rankine, A. G. Greenhill and R. E. Froude. The theory is based on one-dimensional momentum and mass conservation laws and does not account for any specific design of a wind turbine.

A wind turbine rotor, represented as an actuator disc, extracts the kinetic energy carried by the wind. The affected part of the airflow forms a stream-tube with the cross-sectional area upstream of the turbine smaller than the one downstream, as visualized in Figure 2.1.1. The expansion of the stream-tube is due to the mass conservation law of the flowing fluid. The control volume in this analysis is made of the stream-tube surface area and its two cross-sections: far upstream and far downstream. The following assumptions are introduced: (1) homogenous, incompressible, inviscid, steady-state fluid flow, (2) an infinite number of blades, (3) uniform thrust over the disc or rotor area, (4) a non-rotating wake, (5) the static pressure far upstream and far downstream of the rotor is equal to the ambient static pressure.

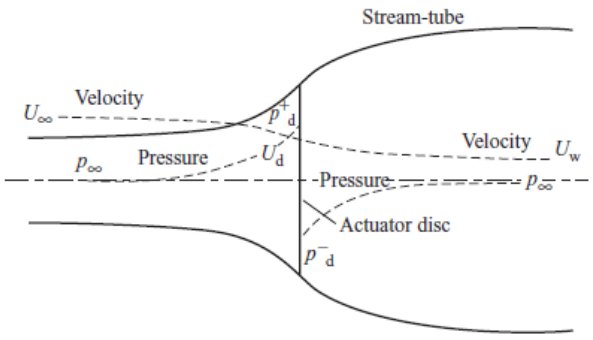

Figure 2.1.1 The concept of an actuator disc from [26]

As indicated in Figure 2.1.1, the symbol ∞ refers to conditions far upstream, d to conditions at the actuator disc and w to conditions in the far wake. The air which passes through the actuator disc undergoes an overall rate of change in momentum equal to the total change in velocity $U_\infty - U_w$ multiplied by the mass flow $\dot{m}$. The force causing this drop in momentum comes entirely from the pressure difference across the disc, therefore:

$$F = (p_d^+ - p_d^-)A_d = (U_\infty - U_w)\rho A_d U_d \tag{2.1}$$

where A_d denotes disc area and ρ air density. The pressure drop on the left side of the equation can be found by applying Bernoulli's principle, separately to the upstream and the downstream region, this yields:

$$\frac{1}{2}\rho U_\infty^2 + p_\infty = \frac{1}{2}\rho U_d^2 + p_d^+ \quad \text{and} \quad \frac{1}{2}\rho U_w^2 + p_\infty = \frac{1}{2}\rho U_d^2 + p_d^- \tag{2.2}$$

Subtracting these equations gives:

$$(p_d^+ - p_d^-) = \frac{1}{2}\rho(U_\infty^2 - U_w^2) \tag{2.3}$$

The rate of momentum drop can be then described by:

$$\frac{1}{2}\rho(U_\infty^2 - U_w^2)A_d = (U_\infty - U_w)\rho A_d U_d \tag{2.4}$$

After some simple mathematical transformations one arrives at the following dependency:

$$U_d = \frac{U_\infty + U_w}{2} \tag{2.5}$$

Thus, the application of this model implies that the wind velocity at the rotor plane is equal to the average of upstream and downstream wind speeds. An axial induction factor, denoted by a is then defined as a fractional decrease in wind velocity between the free-stream and the rotor plane and will be used in further considerations.

$$a = \frac{U_\infty - U_d}{U_\infty} \tag{2.6}$$

Then,

$$U_d = U_\infty(1 - a) \quad and \quad U_w = U_\infty(1 - 2a) \tag{2.7}$$

The term aU_∞ is often referred to as the induced velocity at the rotor. The value of the axial induction factor ranges from 0 to 0.5, which means no wind speed reduction in the system and wind speed reduction to zero velocity behind the rotor, respectively. The latter value is the limit of applicability of this simple theory and for cases with $a \geq 0.5$ empirical modifications have to be made. The thrust force exerted on the wind by the actuator disc becomes:

$$T = 2\rho A_d U_\infty^2 a(1 - a) \tag{2.8}$$

The power, considered as the rate of work done by this force on the flowing fluid is concentrated at the actuator disc and expressed as force T times the velocity U_d, which yields:

$$P = 2\rho A_d U_\infty^3 a(1 - a)^2 \tag{2.9}$$

The efficiency of a wind turbine rotor is usually characterized by its power coefficient C_P. This parameter is defined as a ratio of the power extracted by the rotor and the total available power in the wind with the absence

of actuator disc.

$$C_P = \frac{Rotor\ Power}{\frac{1}{2}\rho A_d U_\infty^3} \tag{2.10}$$

Therefore,

$$C_P = 4a(1-a)^2 \tag{2.11}$$

The maximum value of the power coefficient is found for $a = \frac{1}{3}$ and it is known as The Betz Limit named after Albert Betz, German aerodynamicist.

$$C_{P,max} = \frac{16}{27} = 0.5926 \tag{2.12}$$

Similarly, the thrust coefficient can be defined as a non-dimensional thrust force exerted on the rotor.

$$C_T = \frac{Thrust\ Force}{\frac{1}{2}\rho A_d U_\infty^2} \tag{2.13}$$

2.1.2 Momentum Theory with wake rotation

An extension to the previous analysis could be made by accounting for the rotational effects. As the airflow exerts a torque on the rotor disc, the conservation of angular momentum implies that a torque of equal magnitude and the opposite direction is imposed upon the air. When passing through the rotor, the air gains a tangential velocity component which is expressed in terms of an angular induction factor a' and equals:

$$w = 2a'\Omega r \tag{2.14}$$

where Ω is an angular velocity of the rotor and r a radial distance from the rotor axis. The tangential velocity differs for all radial positions and therefore it is more convenient to consider the annular control volume of width δr_a at the radial distance r. The resulting torque on the annular element δQ is equal to the rate of change of angular momentum of air passing through its area $2\pi r \delta r_a$, thus:

$$\delta Q = 2\rho U_\infty a'(1-a)\Omega r^2 2\pi r \delta r_a \tag{2.15}$$

The incremental thrust force δT exerted on the annular ring can be obtained similarly using the previous one-dimensional analysis:

$$\delta T = 2\rho U_\infty^2 a(1-a)2\pi r \delta r_a \tag{2.16}$$

An important parameter that often occurs in aerodynamic equations for the wind turbine rotor and relates both induction factors is the tip speed ratio λ. It is defined as a ratio of the blade tip speed to the freestream wind velocity, given by:

$$\lambda = \frac{\Omega R}{U_\infty} \quad and \quad \lambda_r^2 = \frac{a(1-a)}{a'(1+a')} \tag{2.17}$$

where R stands for the rotor radius while the local speed ratio $\lambda_r = \frac{\Omega r}{U_\infty}$ defines this proportion at any radial

distance. The infinitesimal power generated by each annual element is then given by:

$$\delta P = \Omega \delta Q = 2\rho U_\infty a'(1-a)\Omega^2 r^2 2\pi r \delta r_a \tag{2.18}$$

2.1.3 Blade Element Theory

Blade element theory is based on an approach in which a wind turbine blade is divided into a certain number of sections along its radius that are addressed individually. Each of these sections has an aerofoil shape characterized by its lift C_L and drag C_D coefficients, as shown in Figure 2.1.2 b). Due to the rotor rotation movement, the apparent wind speed U_{rel} seen by an aerofoil is a vector sum of the freestream velocity $U_\infty(1-a)$ and the tangential wind speed $r\Omega(1+a')$. The angle formed by the local velocity and the rotor plane is called the inflow angle φ, the angle between the chord line and the rotor plane is the section pitch angle θ, and the angle of attack α is the difference between φ and θ, as presented in Figure 2.1.2 a).

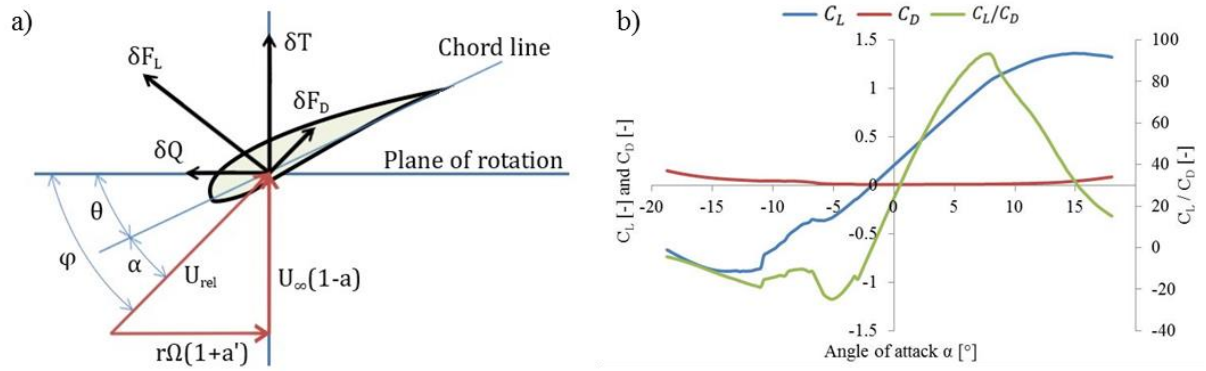

Figure 2.1.2 a) Illustration of rotating aerofoil section aerodynamics, b) Exemplary lift and drag characteristics of an aerofoil, based on [27]

As a result of the aerodynamic interaction between the airflow and the blade section, incremental lift δF_L and drag δF_D forces arise on the aerofoil, which act perpendicularly and parallel to the apparent flow direction, respectively. The projections of these forces on the directions normal and tangential to the plane of rotation allow finding their contributions to the incremental thrust δT and torque δQ, as illustrated in Figure 2.1.2 a). Thus, the following relationships apply:

$$tan\varphi = \frac{U_\infty(1-a)}{r\Omega(1+a')} = \frac{1-a}{(1+a')\lambda_r} \tag{2.19}$$

$$U_{rel} = \frac{U_\infty(1-a)}{sin\varphi} \tag{2.20}$$

$$\delta F_L = \frac{1}{2}\rho U_{rel}^2 c C_L \delta r \tag{2.21}$$

$$\delta F_D = \frac{1}{2}\rho U_{rel}^2 c C_D \delta r \tag{2.22}$$

$$\delta T = \delta F_L cos\varphi + \delta F_D sin\varphi \tag{2.23}$$

$$\delta Q = \delta F_L sin\varphi - \delta F_D cos\varphi \tag{2.24}$$

where c stands for the chord length of the aerofoil. Considering a wind turbine rotor with N blades, and expressing the relative velocity U_{rel} as a function of the freestream velocity as in equation (2.20) the total normal force (thrust) on the section at the distance r from the rotor axis equals:

$$\delta T = \frac{1}{2} Nc\rho \frac{U_\infty^2 (1-a)^2}{sin^2\,\varphi} (C_L cos\varphi + C_D sin\varphi)\delta r \tag{2.25}$$

while the total force contributing to the sectional torque would be:

$$\delta Q = \frac{1}{2} Nc\rho \frac{U_\infty^2 (1-a)^2}{sin^2\,\varphi} (C_L sin\varphi - C_D cos\varphi) r\delta r \tag{2.26}$$

At this point, it is worth to notice that the effect of the aerodynamic drag is to reduce the torque and as a consequence the power while at the same time to increase the thrust loading. By applying blade element theory one also obtains the normal and tangential forces on an annular section of a rotor. However, their magnitude is directly related to the blade geometry, the characteristics of the aerofoil and the inflow conditions.

2.1.4 Blade Element Momentum Theory

Blade Element Momentum (BEM) theory combines the previously described formulations of the Momentum and the Blade Element Theories. In this way, the relationship between blade shape, flow conditions and turbine performance can be found. By imposing equality between the forces: equations (2.16) and (2.25), and torques: equations (2.15) and (2.26), derived previously, after some algebraic manipulations one can arrive at the following expressions for axial a and angular a' induction factors:

$$a = \left(\frac{4\,sin^2\,\varphi}{\frac{cN}{2\pi r}(C_L cos\varphi + C_D sin\varphi)} + 1 \right)^{-1} \tag{2.27}$$

$$a' = \left(\frac{4 sin\varphi cos\varphi}{\frac{cN}{2\pi r}(C_L sin\varphi - C_D cos\varphi)} - 1 \right)^{-1} \tag{2.28}$$

Then, the forces and flow conditions at each blade section can be determined iteratively. According to [28], once the axial induction factor has been obtained for each section of the blade, the forces on the blade can be determined and the overall rotor power coefficient can be calculated from the expression:

$$C_P = \left(\frac{8}{\lambda^2}\right) \int_{\lambda_h}^{\lambda} \lambda_r^3 a'(1-a) \left[1 - \left(\frac{C_D}{C_L}\right) cot\varphi\right] \delta\lambda_r \tag{2.29}$$

where λ_h is the local speed ratio at the hub.

2.2 Wind farm aerodynamics

The study of the wind farm aerodynamics has become a very prominent area of wind energy research, as nowadays the majority of turbines both, onshore and offshore, got clustered into large wind farms. The process of optimal wind farm planning involves two major objectives: (1) maximization of the capacity factor, and/or (2) minimization of the Cost of Energy (COE) [29]. Therefore, owing to the costs of land, civil works, electric current transmission infrastructure and operations & maintenance activities, wind turbines should be placed close to each other, in tight clusters. On the other hand, the proximity of turbines introduces two major issues of aerodynamic nature: reduced power production due to wake velocity deficits, and increased dynamic loads on the blades due to higher turbulence levels and operation in partial wake overlap. As a result, the overall energy output of a wind farm is always less than the sum of energy extracted by each stand-alone turbine. According to the studies of Barthelmie et al. [30, 31], the power losses of a single downstream turbine being completely in the wake of an upstream one can easily reach 40%, depending on the inter turbine spacing and wind conditions. When considering the full operational performance of a wind farm, the averaged losses caused by the wake effect can amount to approximately 8% for onshore and 12% for offshore wind farms. Thus, a good understanding of the turbine interaction through their wakes is crucial for both optimal wind farm planning and development of collaborative wind turbine control strategies. This subchapter provides a description of physical phenomena involved in the wake development as well as a presentation of the wake models utilized in this study.

2.2.1 The wake effect

As mentioned before, wind turbine wake is a flow region behind a rotor characterized by decreased wind velocity, high vorticity and increased turbulence levels. As the wake propagates downstream, it slowly recovers to the freestream conditions as a result of turbulent mixing with the flowing air particles unaffected by the turbine. Depending on the downstream distance behind a turbine rotor, it is common to consider two different flow regions: near and far wake.

In general, the near wake is a region just behind a turbine, where flow field characteristics are directly affected by the geometry and operational conditions of the machine. The longitudinal length of near wake region depends on many factors like atmospheric stability, inflow conditions, number of blades and blade aerodynamics, and scientists state different values for this distance, ranging from one [9] up to four [32] rotor diameters. Nevertheless, it is known that air movement in this zone is driven by a non-zero pressure gradient together with strong turbulence caused by vortices that emanate from the blade tips. As the wake propagates downstream, these vortices break down and the impact of the axial pressure gradient vanishes marking the transition to the far wake.

In the far wake, the actual shape of the rotor impacts the flow indirectly through reduced axial velocity and increased turbulence intensity, causing the flow profile to depend more on atmospheric and topographic effects. In this region turbulence is the dominating physical phenomena acting as an efficient mixer, which comes from three sources: (1) atmospheric turbulence related to surface roughness and thermal effects, (2) turbulence induced by the rotor blades and the presence of the nacelle and tower, and (3) turbulence from tip vortices

breakdown. As a result of turbulent mixing in the flow, the velocity deficit and overall turbulence intensity level recover to the freestream conditions. Progressing downstream, the velocity profile becomes approximately Gaussian, axisymmetric and self-similar. Also, large-scale energetic oscillatory motions of the entire wake might be observed, commonly referred to as wake meandering [8, 33].

Accurate prediction of the aerodynamic interaction between the turbines in a wind farm and associated wake losses is a challenging task due to a combination of the numerous processes involved. Firstly, the wind hits the blades of a turbine and induces rotational movement of the rotor at a rate that simultaneously depends on many meteorological, aerodynamic and control factors such as wind speed, wind shear, turbulence intensity, aerodynamic properties of the aerofoils, incident yaw and blade pitch angle settings. Then, the inflow conditions combined with the amount of extracted kinetic energy from the wind, the angular velocity of the blades and the nacelle yaw alignment angle determine the airflow characteristics as it leaves the rotor plane. The resulting wake expands in the lateral and vertical direction, meanders and eventually dissipates in a chaotic manner governed by ambient turbulence, atmospheric stability and presence of other wakes overlapping with the original one [34]. The attempts to describe and relate these processes in a mathematical form have led to the development of many wake models of varying fidelity and computational cost.

2.2.2 Wind turbine wake models

Studying and modelling of wind turbine wakes is in itself a broad, ongoing research area, aiming to understand, explain and mathematically describe the observed behaviour of wakes. Over the years, extensive analytical, numerical and experimental efforts have been taken to develop models that can reliably predict this type of flows. The range of models available today varies from low to high fidelity, where the latter describes the wake more precisely and tries to capture more of its characteristics than the former, at the expense of higher computational costs. In the context of wake steering, model-based controllers require computationally efficient models that capture enough physics to predict wake behaviour while running fast enough to allow real-time optimization. Therefore, simple analytical wake models are still considered as a very useful tool for wind farm aerodynamics studies [6].

The wake characteristics are space-, time- and parameter-dependent. The flow field behind a wind turbine differs with the downstream distance from the machine and is time-dependent as both, the turbine operation and surrounding free-stream flow change over time. Wake behaviour is also influenced by external factors such as temperature or surface roughness. A model giving a full description of the wake would account for: (1) wind velocity deficit, as a consequence of kinetic energy extraction, (2) increased turbulence intensity due to the presence of rotating turbine blades and other components, (3) wake recovery, denoting that downstream of a turbine the flow recovers to freestream conditions due to turbulent mixing, (4) wake meandering, being large-scale stochastic oscillations of the entire wake structure in the horizontal and vertical directions. (5) wake expansion, resulting from the fact that in incompressible flows the decrease in velocity means a proportional increase in the wake's cross-sectional area, (6) wake deflection, caused by the rotational effect of the blades and/or non-perpendicular orientation of the rotor with the incoming wind, (7) wake skewing, as a result of veer, (8) vertical wind shear, meaning the change of wind velocity with height, and lastly (9) kidney-shaped wake

deformation due to operation in yaw misalignment [6].

Certain groups of abovementioned components of a wake are usually accounted for separately by different wake models, namely wake velocity deficit, wake deflection and wake combination models. In the remainder of this chapter, the corresponding wake models employed in the present study will be discussed.

2.2.2.1 Jensen velocity deficit model

The Jensen wake model [35, 36] is one of the oldest and most widely known models for predictions of the wind velocity field in the wake. It is characterized by a high degree of simplicity, low computational cost and relatively accurate performance, being the reason for its numerous implementations in wind energy studies.

The model assumes a steady inflow, linear wake expansion, and uniform velocity field inside the wake, as illustrated in Figure 2.2.1. By applying a conical control volume limited by the cross-sectional area making up the rotor plane and a cross-section of the wake at an arbitrary downstream distance, coinciding with the turbine's axis of rotation, the conservation of mass equation for the flow of air can be written as:

$$D_r^2 U_r + (D_w^2 - D_r^2) U_\infty = D_w^2 U_w \tag{2.30}$$

where D_r [m] and U_r [m/s] stand for the wake width and streamwise wind velocity at the rotor while D_w [m] indicates wake width in the far wake cross-section. Then, assuming turbine operation with an induction factor a, the velocity profile at a given downwind distance x and radial position r_w can be computed as:

$$U_w(x, r_w, a) = U_\infty \left(1 - U_{def}(x, r_w, a)\right) \tag{2.31}$$

where the velocity deficit U_{def} is given by:

$$U_{def}(x, r_w, a) = \begin{cases} 2a\left(\dfrac{D_r}{D_r + 2kx}\right)^2, & if\ r \le \dfrac{D_r + 2kx}{D_r} \\ 0, & otherwise \end{cases} \tag{2.32}$$

In this model, wind velocity in the wake U_w, is defined in the axial direction only, and depends on the magnitude of the induction factor a, distance behind the machine x and a tuneable non-dimensional wake decay constant k. Typical values of k range from 0.01 to 0.1 depending on the ambient turbulence, topographical effects and turbine operation region.

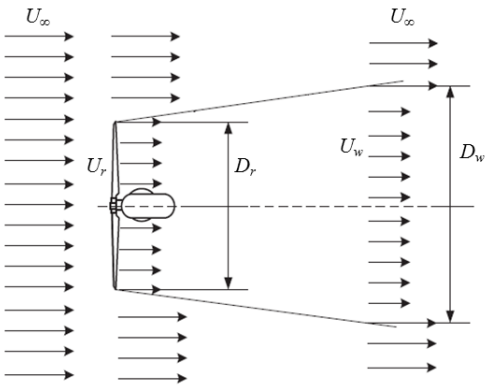

Figure 2.2.1 Visualization of a single Jensen's wake, modified from [37]

The simplicity of the Jensen wake model determines many limitations to the description of the factual wake behaviour. To mention just a few, it does not conserve the momentum as shown in [38], it is only applicable in the far wake region as it does not account for the vortex shedding from the rotor and has no notion of the added turbulence due to varying turbine operating conditions. Additionally, the unrealistic velocity field description due to presumably too large wake expansion and the uniform velocity profile within the wake (whereas it follows a Gaussian profile as shown by P. Vermeulen [39] in a wind tunnel test and G. Taylor [40] in a field test) often leads to an overestimation of downstream turbine power in full wake conditions and underestimation of power in partial wake conditions. These deficiencies of Jensen wake model might severely impact the effectiveness of the wake steering in which accurate flow field prediction is crucial.

2.2.2.2 Gauss velocity deficit model

Many studies on wind turbines wakes reported that after some downwind distance, the factual velocity deficit profile within the wake approximately follows the Gaussian shape, as shown in Figure 2.2.2. This velocity profile was observed by numerical simulations [41], wind tunnel measurements [42] and data from operating wind farms [43]. Thus, it was deemed appropriate to use the Gaussian curve to describe the velocity deficit in the far wake regions, regardless of the inflow conditions. The model proposed by M. Bastankhah and F. Porté-Agel [38], further referred to as Gauss wake model represents a large group of analytical velocity deficit models assuming the self-similar Gaussian velocity profile.

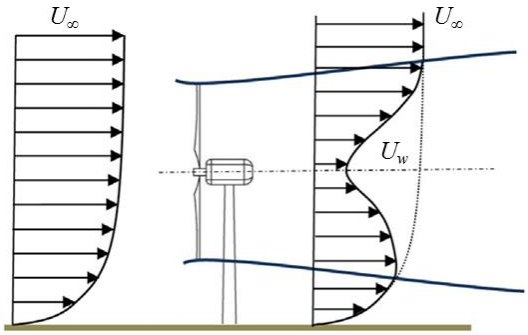

Figure 2.2.2 Visualization of Gaussian-shaped wake velocity profile with wind shear, modified from [38]

To find the velocity distribution downwind of a wind turbine, the integral form of the streamwise momentum equation is considered. By neglecting the viscous and pressure terms and applying mass and momentum conservation, the rate at which momentum is removed at the turbine rotor plane can be given as follows:

$$\rho \int U_w(U_\infty - U_w)\delta A = T \tag{2.33}$$

where A is the rotor swept area. Next, assuming self-similar Gaussian shape of the velocity deficit in the wake, the incident velocity profile at the given downstream location can be expressed by:

$$U_w = U_\infty \left(1 - Ce^{-\frac{r_w^2}{2\sigma^2}}\right) \tag{2.34}$$

where C represents the maximum normalized velocity deficit at each downwind location x at the centre of the

wake and σ is the standard deviation of the Gaussian-like velocity deficit profiles at each x.

Inserting equations (2.13) and (2.34) into equation (2.33), integrating from 0 to ∞ and solving the resulting expression for C, one can find that C is given by:

$$C = 1 - \sqrt{1 - \frac{C_T}{8\left(\frac{\sigma}{D_r}\right)^2}} \tag{2.35}$$

Then, assuming a linear expansion for the wake region similarly to the one considered by Jensen, σ/D_r can be written as:

$$\frac{\sigma}{D_r} = k^* \frac{x}{D_r} + \varepsilon_w \tag{2.36}$$

where $k^* = \partial\sigma/\partial x$ is the wake growth rate and ε_w is equivalent to the value of σ/D_r as x approaches zero. The value of ε_w was determined by equating the total mass flow deficit rates at $x = 0$ for this and the Frandsen wake model [44], yielding:

$$\varepsilon_w = 0.25\sqrt{\beta} \qquad where \qquad \beta = \frac{1}{2}\left(\frac{1 + \sqrt{1 - C_T}}{\sqrt{1 - C_T}}\right) \tag{2.37}$$

Lastly, combining the equations (2.35) and (2.36) with equation (2.34), the final analytical expression for the three-dimensional velocity deficit in the far wake behind a wind turbine is obtained:

$$U_w(x, y, z) = U_\infty \left(1 - C\, exp\left(-M\left\{\left(\frac{z - z_h}{D_r}\right)^2 + \left(\frac{y}{D_r}\right)^2\right\}\right)\right) \tag{2.38}$$

$$C = 1 - \sqrt{1 - 0.25MC_T} \tag{2.39}$$

$$M = \frac{1}{2\left(k^* \frac{x}{D_r} + 0.25\sqrt{\beta}\right)^2} \tag{2.40}$$

where y and z are spanwise and vertical coordinates, respectively, and z_h is the hub height. This model was further extended across several papers of F. Porté-Agel et al. to account for the atmospheric stability [45], operation in yaw [46] and rotor-added turbulence [47]. Introduction of these improvements to the description of wake velocity deficit modifies the previous equations (2.38), (2.39), (2.40) as follows:

$$U_w(x, y, z) = U_\infty \left(1 - C exp\left(-\frac{(y - \delta_w)^2}{2\sigma_y^2} - \frac{(z - z_h)^2}{2\sigma_z^2}\right)\right) \tag{2.41}$$

$$C = 1 - \sqrt{1 - \frac{(\sigma_{y0}\sigma_{z0})M_0}{\sigma_y \sigma_z}} \quad ; \quad M_0 = C_0(2 - C_0) \quad ; \quad C_0 = 1 - \sqrt{1 - C_T} \tag{2.42}$$

where δ_w is the wake deflection while σ_y and σ_z define the wake width in the y and z directions, respectively. Each of these parameters is defined for each turbine and the subscript "0" refers to the initial values at the beginning of the far wake. The wake grows differently in lateral and vertical direction, so the respective growth

rates σ_y *and* σ_z are defined as follows:

$$\frac{\sigma_z}{D} = k_z \frac{(x - x_0)}{D} + \frac{\sigma_{z0}}{D} \quad where \quad \frac{\sigma_{z0}}{D} = \frac{1}{2}\sqrt{\frac{U_r}{U_\infty + U_{br}}} \tag{2.43}$$

$$\frac{\sigma_y}{D} = k_y \frac{(x - x_0)}{D} + \frac{\sigma_{y0}}{D} \quad where \quad \frac{\sigma_{y0}}{D} = \frac{\sigma_{z0}}{D} cos\gamma \tag{2.44}$$

with x_0 being the downstream position at the beginning of far wake, D the rotor diameter, U_{br} the wind velocity just behind the rotor, and k_y and k_z define the wake expansion in the spanwise and vertical directions, respectively.

Despite the applied simplifications, this model represents a great improvement on the flow field description in the wake compared to top-hat wake models. Moreover, it conserves momentum unlike the Jensen model, though it's applicability is also limited to the far wake region only. The observed deficiencies of this model include its tendency to under-predict power gains of downstream turbines compared to high fidelity simulations and field test data.

2.2.2.3 Gauss – Curl Hybrid velocity deficit model

Recent studies have reported that the wake produced by a yawed wind turbine does not only deflects in the direction opposite to the yaw angle, but its cross-section deforms and becomes kidney-shaped in the far wake region. This phenomenon was first identified by M. F. Howland et al. [48] and described by a pair of counter-rotating vortices, which are shed from the top and bottom of the yawed rotor, shown in Figure 2.2.3. As the flow propagates downstream, these vortices move the wake to the side and create a curled wake shape. This behaviour was further observed in wake tunnel tests and elaborated by M. Bastankhah and F. Porté-Agel [46]. Large Eddy Simulation (LES) studies under various atmospheric stability conditions performed by L. Vollmer et al. [49] and T. Berdowski [50] also revealed such behaviour of the wake. Fleming et al. [51] investigated the influence of these counter-rotating vortices on yaw-based wake control and concluded that the inclusion of their impact in controls-oriented wake models is of critical importance, especially when considering arrays of multiple turbines.

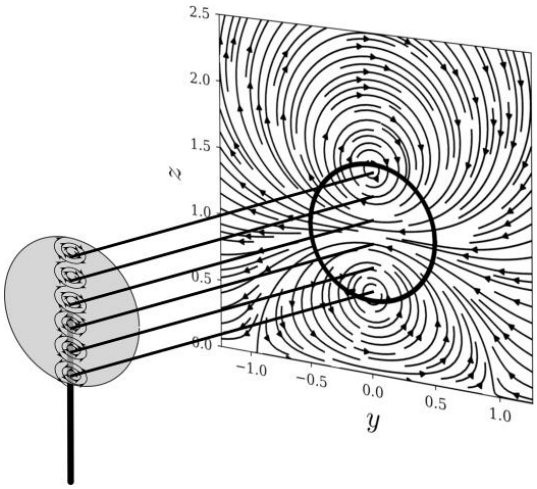

Figure 2.2.3 Collection of counter-rotating vortex pairs shed from a yawed rotor from [52]

The following Gauss-Curl Hybrid (GCH) model, presented in the work of King et al. [53], is a modification of the previously presented Gauss wake model [38, 45, 46, 47, 54] with the approximations made from the Curl model, proposed by L. A. Martínez-Tossas et al. [52] and modified in the work of C. Bay et al. [55]. In brief, the Curl model relies on the concept to capture steered wake behaviour (deflection and deformation) by direct modelling of the counter-rotating vortices pairs (CVP) shed from a yawed rotor. The reader is referred to the work of L. A. Martínez-Tossas et al. [52] for a detailed derivation and C. Bay et al. [55] for extension of the Curl model. The incorporation of the impact of CVP into the Gauss wake model starts from the determination of the spanwise V_{wr} and vertical W_{wr} wake velocity components due to wake rotation:

$$V_{wr} = \frac{\Gamma_{wr}(y - y_t)}{2\pi((y - y_t)^2 + (z - z_h)^2)}\left(1 - exp\left(\frac{-\left((y - y_t)^2 - (z - z_h)\right)^2}{\epsilon^2}\right)\right) \tag{2.45}$$

$$W_{wr} = \frac{\Gamma_{wr}(z - z_h)}{2\pi((y - y_t)^2 + (z - z_h)^2)}\left(1 - exp\left(\frac{-\left((y - y_t)^2 - (z - z_h)\right)^2}{\epsilon^2}\right)\right) \tag{2.46}$$

where y_t is the spanwise position of the machine, Γ_{wr} is the circulation strength of the wake rotation vortex computed as: $\Gamma_{wr} = \pi(a - a^2)U_\infty D\lambda^{-1}$ and ϵ represents the size of the vortex core ($\epsilon = 0.3D$ in their work).

When operating with the yaw angle offset, the counter-rotating vortices are released from the top and bottom of the rotor, contributing to the spanwise (V_{top} and V_{bottom}) and vertical (W_{top} and W_{bottom}) velocity components in the wake. The strength of these vortices is a function of the applied yaw angle γ, given by:

$$\Gamma(\gamma) = 0.125\pi\rho D U_\infty C_T sin\gamma cos\gamma^2 \tag{2.47}$$

and is used to find respective velocity components:

$$V_{top} = \frac{\Gamma(y - y_t)}{2\pi\left((y - y_t)^2 + \left(z - (z_h + R)\right)^2\right)}\left(1 - exp\left(\frac{-\left((y - y_t)^2 - \left(z - (z_h + R)\right)\right)^2}{\epsilon^2}\right)\right) \tag{2.48}$$

$$V_{bottom} = \frac{\Gamma(y - y_t)}{2\pi\left((y - y_t)^2 + \left(z - (z_h - R)\right)^2\right)}\left(1 - exp\left(\frac{-\left((y - y_t)^2 - \left(z - (z_h - R)\right)\right)^2}{\epsilon^2}\right)\right) \tag{2.49}$$

$$W_{top} = \frac{\Gamma(z - (z_h + R))}{2\pi\left((y - y_t)^2 + \left(z - (z_h + R)\right)^2\right)}\left(1 - exp\left(\frac{-\left((y - y_t)^2 - \left(z - (z_h + R)\right)\right)^2}{\epsilon^2}\right)\right) \tag{2.50}$$

$$W_{bottom} = \frac{\Gamma(z - (z_h - R))}{2\pi\left((y - y_t)^2 + \left(z - (z_h - R)\right)^2\right)}\left(1 - exp\left(\frac{-\left((y - y_t)^2 - \left(z - (z_h - R)\right)\right)^2}{\epsilon^2}\right)\right) \tag{2.51}$$

A linear combination is used to find the total spanwise and vertical velocities in the wake:

$$V_{wake} = V_{top} + V_{bottom} + V_{wr} \qquad and \qquad W_{wake} = W_{top} + W_{bottom} + W_{wr} \tag{2.52}$$

As the wake moves downstream, these rotor-generated vortices finally decay. The mechanism of their dissipation was described by C. Bay et al. [55] and is given by:

$$V = V_{wake}\left(\frac{\epsilon^2}{4v_T\,(x-x_0)/U_\infty + \epsilon^2}\right) \qquad and \qquad W = W_{wake}\left(\frac{\epsilon^2}{4v_T\,(x-x_0)/U_\infty + \epsilon^2}\right) \tag{2.53}$$

where v_T is the turbulent viscosity, defined with the use of a mixing length model: $v_T = l_m^2\left|\frac{\partial U}{\partial z}\right|$, where $l_m = \frac{\kappa z}{1+\kappa z/\lambda_T}$, $\kappa = 0.41$ and $\lambda_T = D/8$ and v_T is the value of the mixing length in the free atmosphere.

Due to the presence of streamwise and vertical velocity components in the wake of a yawed turbine, large-scale entrainment of the flow into the wind farm domain is observed. As a result, the wake recovers faster, and this yaw-induced added recovery is assumed to be caused primarily by the vertical velocity component, W, which is computed by adding a new element to the Gaussian model as given below:

$$U(x,y,z) = U_w(x,y,z) + \frac{W(x,y,z)(x-x_0)(y-y_0)}{\pi(\alpha_r(x-x_0)+0.5D)^2} \tag{2.54}$$

where U_w is computed with equation (2.41) and W is computed using equation (2.53), α_r is a dimensionless tuning parameter that defines how much the flow entrainment affects the wake recovery. The larger the α_r the weaker the effect of yaw induced wake recovery on the streamwise velocity component U ($\alpha_r = 0.03$ in the original work).

When an upstream turbine operates with yaw offset, counter-rotating vortices are released from its rotor. As a consequence, the incident wake deflects and deforms as it propagates downstream. The next non-yawed machine exposed to such flow field alteration produces a steered wake owing to the spanwise and vertical velocity flow components induced at the upstream machine. Such a phenomenon is termed secondary steering effect and could also be viewed as an "effective" yaw angle offset applied at the non-yawed downstream turbine. The magnitude of this hypothetical yaw angle is found using the spanwise velocity V, present at the downstream turbine rotor, which contributes to the effective circulation Γ_{eff}, calculated as:

$$\Gamma_{eff} = \frac{1}{N_r}\sum_{i}^{N_r}\left|\frac{2\pi V_i((y_i-y_0)^2+(z_i-z_0)^2)}{(y_i-y_0)(1-exp\left(\frac{-\left((y_i-y_0)^2-(z_i-z_h)\right)^2}{\epsilon^2}\right)}\right| \tag{2.55}$$

where V_i stands for spanwise velocities inside the rotor area and N_r is the number of points in the rotor area. The effective yaw angle γ_{eff} is computed using Γ_{eff} and solving for γ in equation (2.47). Then, the total deflection is computed using equation (2.59), where the total yaw angle is $\gamma = \gamma_t + \gamma_{eff}$ with γ_t being the factual yaw angle applied by the turbine.

The presented GCH model maintains many advantages of the Gauss wake model while introducing corrections to address the aerodynamic effects that have not been captured before. The four main important improvements account for the yaw-induced added wake recovery, the influence of the counter-rotating vortices on the wake deflection and deformation, and the secondary steering effect observed in multi-turbine arrays. Capturing these effects is especially imperative in terms of studying the feasibility of wake steering and wind farm optimization, which could still be done at relatively low computational cost with the use of the GCH model.

2.2.2.4 Jiménez deflection model

Á. Jiménez et al. [56] used LES to investigate the wake deflection of yawed wind turbines with different thrust coefficients, and proposed a simple analytical model to describe this phenomenon. The authors assumed a top-hat profile of the wake velocity deficit and performed an analysis based on the conservation of mass and momentum for a control volume around the turbine. In their consideration, the analytical expression for the wake skew angle χ was determined by equating cross-stream components of the force exerted on the wind by a yawed turbine, which reads:

$$\chi(x) = \frac{\chi_{init}}{\left(1 + 2k_d \frac{x}{D}\right)^2} \qquad with \qquad \chi_{init}(a,\gamma) = \frac{1}{2} cos^2\gamma sin\gamma C_T \tag{2.56}$$

where k_d is a tuneable model parameter that defines the sensitivity of the wake deflection to yaw and χ_{init} is the initial angle of the wake at the rotor. The thrust coefficient C_T in this equation is defined with respect to the induction factor a, as follows: $C_T(a) = 4a(1-a)$. Later, P. Gebraad et al. [14] integrated the tangent of the wake centreline angle χ over the downstream distance x to find the yaw-induced lateral offset δ_w (deflection) of the wake centre with respect to the hub of a turbine. The formulation was obtained by integrating a second-order Taylor series approximation of $\chi(x)$ and reads as follows:

$$\delta_w(x) \approx \frac{\chi_{init}\left[15\left[\frac{2k_d x}{D} + 1\right]^4 + \chi_{init}^2\right]}{\frac{30k_d}{D}\left[\frac{2k_d x}{D} + 1\right]^5} - \frac{\chi_{init} D[15 + \chi_{init}^2]}{30k_d} \tag{2.57}$$

2.2.2.5 Bastankhah deflection model

M. Bastankhah and F. Porté-Agel [46] carried out extensive wind tunnel studies to determine wake characteristics of a yawed wind turbine, immersed in a turbulent boundary layer. The researchers approached the deflection problem in a more in-depth theoretical way and used experimental data to perform a budget analysis on the steady-state continuity and Reynolds-averaged Navier-Stokes equations. This study allowed to develop approximate governing equations upon which a simple and computationally inexpensive analytical wake deflection model was built. The angle of wake deflection of a yawed turbine was defined as follows:

$$\chi = \frac{0.3cos\gamma}{cos\gamma}\left(1 - \sqrt{1 - C_T cos\gamma}\right) \tag{2.58}$$

The total deflection of the wake due to yaw misalignment can be computed as:

$$\delta_w = \delta_{w\_init} + \frac{\gamma E_0}{5.2}\sqrt{\frac{\sigma_{y0}\sigma_{z0}}{k_y k_z M_0}}\, ln\left[\frac{\left(1.6 + \sqrt{M_0}\right)\left(1.6\sqrt{\frac{\sigma_y\sigma_z}{\sigma_{y0}\sigma_{z0}}} - \sqrt{M_0}\right)}{\left(1.6 - \sqrt{M_0}\right)\left(1.6\sqrt{\frac{\sigma_y\sigma_z}{\sigma_{y0}\sigma_{z0}}} + \sqrt{M_0}\right)}\right] \tag{2.59}$$

The initial wake deflection δ_{w_init} was defined as $\delta_{w\_init} = x_{nw} tan\chi$, where x_{nw} indicates the length of the near wake (typically being the order of 3 rotor diameters according to the authors) and $E_0 = C_0^2 - 3e^{1/12}C_0 + 3e^{1/3}$.

In contrast to the Jiménez model, Bastankhah model assumes a self-similar Gaussian velocity profile in crosswise and vertical directions, and a constant wake growth rate, independent of the yaw error magnitude. It has also been shown that this model provides more consistent predictions of deflected wake trajectory when compared with the wind tunnel results, while the Jiménez model overestimates the deflection. In particular, the deflected wake predicted with Bastankhah model quickly tends to a turbulent free shear flow in a far wake region, whereas Jiménez model predicts the wake to deflect all the way along downwind direction.

2.2.2.6 Katic wake combination model

When several turbines are aligned with the wind direction, it has been experimentally observed that the first downstream machine suffers considerable power drop, while the subsequent devices experience relatively smaller further power losses. Widely used methods to analytically describe the effect of multiple overlapping wakes are superposition models, that include: geometric superposition model, linear superposition model, the sum of squares model and energy balance model. The sum of squares model was proposed by I. Katic et al. [36] in his classical literature about the Park model and will be used in the present Master's Thesis. Similarly to linear superposition and energy balance models, it is based on a principle that the flow characteristics in the superposition area is caused by the accumulation of all wakes from the upwind turbines. The model assumes the velocity deficit in the superposition area to be equal to the square root of the sum of squares of the velocity deficits from each upstream machine. The mathematical formulation to describe this phenomenon is:

$$U_i = U_\infty - \sqrt{\sum_k (U_\infty - U_{ki})^2} \tag{2.60}$$

where U_i is defined as velocity at the turbine i and U_{ki} is the wake velocity of turbine k at turbine i. In recent years, this model was found to be unsuitable for large wind farms as it does not account for deep array effects. This is due to the squared velocity deficits, which make the total velocity deficit to reach an equilibrium level, typically after 3 or 4 turbines in a row. Despite this little deficiency, Katic model is considered as very accurate and has well served in numerous wind farm studies for over 30 years.

Chapter 3

Wind farm control

This chapter intends to introduce the principles of an individual horizontal axis wind turbine (HAWT) control along with several possible concepts of controlling wind farm as a whole. The discussion begins with an overview of the most common wind turbine control systems and operation regions of a variable-speed variable-pitch machine. Then, the idea behind switching to collaborative control of individual turbines is brought up, followed by a brief description of power de-rating, wake steering and turbine repositioning control strategies. Finally, yaw-based wake redirection is addressed and a comprehensive review on the aerodynamics of a steered wake is presented.

3.1 Wind turbine control

From the perspective of wind energy engineering, the most striking characteristic of the wind resource is its variability. The changes in wind speed and direction can be observed over a wide range of scales, both in space and time. As the energy available in the wind varies with the cube of the wind speed, it is critical to understand the mechanisms that enable maximal wind energy exploitation. Therefore, wind turbine design should allow the machines to control the aerodynamic performance of the turbines, and adjust them to the experienced wind conditions, over the whole operational range of wind speeds. Besides the safe operation of the device, the two main objectives of wind turbine control include maximization of electrical power production and/or minimization of the structural loads, both of which eventually contribute to the decrease in the cost of generated electricity. Information provided in this section can be found in the book of J. F. Manwell et al. [2].

The resulting aerodynamic torque at the turbine's rotor is collectively influenced by the rotor tip speed ratio, blade geometry, wind speed, yaw error and any added rotor drag. Each of these components, except for wind speed, can be changed by a respective control system. Variable-speed turbines utilize power electronics systems to enable operation at different rotor speeds (and different tip speed ratios) via generator torque τ_g control, which gives control over the turbine's power. Pitch-regulated machines can change the rotor or blade geometry by manipulating the blade pitch angle θ to influence power capture [57] or experienced loads [58]. Yaw orientation systems enable a nacelle rotation about the axis of rotation aligned with the turbine tower to control the yaw error γ, also influencing the generated power. Some less common concepts include turbines with auxiliary drag devices that can modify rotor drag, or a mechanism enabling nacelle tilt. Implementing the yaw angle, blade pitch and generator torque controllers in a single turbine, illustrated in Figure 3.1.1 a), allows to obtain the ideal wind turbine power curve, as presented in Figure 3.1.1 b). This ideal power curve exhibits three main operating regions, defined with respect to cut-in, rated and cut-out wind speeds, each following a different control strategy.

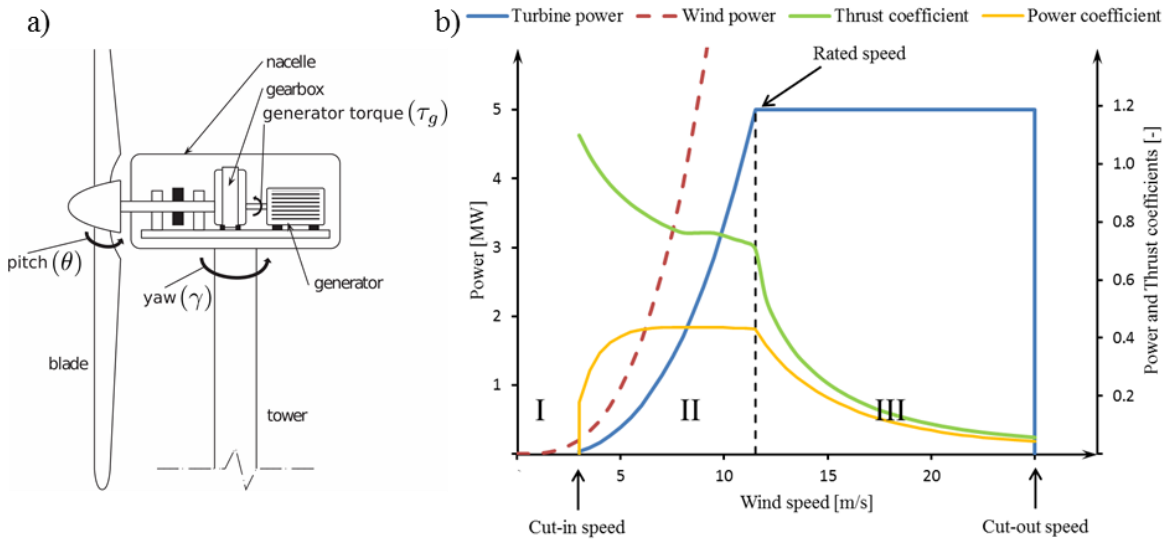

Figure 3.1.1 a) Main components of a HAWT and its degrees of freedom [6], b) power and thrust characteristics of a variable-speed variable-pitch HAWT, based on data available in [59]

Region I covers the wind speed range below cut-in wind speed, in which the available power in the wind is too small for a turbine to start operation. The cut-in wind speed varies among different designs of wind turbines. If a machine is meant to operate at a fixed rotational speed of the rotor, the higher designed rotor speeds will correspond to the higher cut-in wind speeds. The variable-speed turbines can decrease their rotational speed at low wind speeds, reducing the cut-in wind speed, and therefore, increasing their energy capture.

Region II begins at cut-in wind speed and ends at the wind speed for which the turbine power generation reaches the rated value. Within this region, it is desired that the machine extracts as much power as possible, meaning the operation at optimal power coefficient C_{Popt}, which is ensured by maintaining the optimal tip speed ratio λ_{opt}. To achieve this, the blades' pitch angle is kept constant, at the value which maximizes the aerodynamic torque produced by the blades, and the control over the generator torque τ plays a key role. As wind speed increases, the power electronics devices enable a proportional change of the rotor speed, such that λ_{opt} is maintained. A fixed-speed wind turbine would be able to operate with the optimal power coefficient only at one wind speed, significantly decreasing its energy capture. A common practice in wind turbine control is to start pitching the blades as the wind speed approaches the rated value in order to avoid excessive loads on the blades caused by high thrust force, at the expense of lower power generation. This procedure is known as peak shaving, and perfectly represents the concept that the wind turbine control aims at finding a compromise between power generation and loads mitigation.

Region III applies to the range of wind speeds, limited by the rated and cut-out speeds, within which a variable-pitch turbine operates at its rated power. The major contribution to the control actions in this region is the adjustment of the blades' pitch angles, aiming to limit the aerodynamic torque experienced by the rotor. Pitching to stall is one of the pitch control approaches that relies on applying variations of pitch angle that promote stalling. Though pitching to stall enables to regulate the power produced at the wind turbine, the blades experience the same aerodynamic damping and fatigue problems as those of fixed-pitch turbines. An alternative method is pitching to feather, in which the pitch angle settings increase progressively with wind speed, resulting in larger adjustments needed to maintain the rated power output compared to stall method. Pitching to feather ensures attached flow around the blade, provides good, positive damping and allows for a more accurate prediction of blade loads. Above the cut-out wind speed, the turbine operation is ceased to avoid excessive damage to the systems and components of the machine.

The current industrial wind farm standards still favour operation of each turbine with the control actions aiming to ensure their own maximum power capture. As a consequence, the downstream machines experience much smaller wind speeds and can extract significantly less energy than the upstream ones, especially in the cases of full wake overlap. However, the perception of an optimal plant-wise control strategy undergoes a paradigm shift, changing from optimal turbine – suboptimal plant to the suboptimal turbine – optimal farm performance.

3.2 Wind farm control

Wind Farm Control (WFC) is a term that refers to a wide range of actions aimed to ensure a safe and reliable operation of wind turbines while achieving on-going performance goals. WFC research can be divided into two large areas: (1) power electronics engineering, responsible for the quality of the electric current generated by wind turbines, and (2) mechanical/aerodynamic engineering, covering the wind energy extraction, fatigue and the wake effect. This study is focused on the latter area, and in particular, on the concept of intentional suboptimal operation of individual turbines that can collectively result in greater farm power output compared to what can be achieved with the greedy control settings. These potential power gains are associated with the alteration of the velocity field within a wind farm, which allows downstream turbines to extract more energy. This type of wind farm control is known as Active Wake Control (AWC).

AWC is an active field of research that attempts to improve wind plant performance by coordinating control of individual turbines to take into account turbine-wake interactions. The effectiveness of such plant-wise control methods depends on the quality of the local wind resource, farm spatial configuration and the operation of the controllers. Regardless of whether the control objective is to maximize the plant power or to decrease the loads experienced by the turbines, the control strategies can be classified into two groups: wake redirection and power de-rating. Simply put, the first one aims to redirect the wake of upstream machines away from the downstream ones, while the second intends to reduce the power of upstream turbines and thereby decrease the wind velocity deficit in their wakes.

While future wind farm planning will use the state-of-the-art design optimization techniques, considering the 28.3 GW global capacity of already operating offshore wind power built over the last 10 years [60], the only improvement in power generation, and therefore decrease in LCOE, can be achieved by the implementation of effective plant-wise control. Logically, a distinct advantage of such optimisation approach is that it is not in conflict with other plant design objectives, as it requires no adjustments in terms of turbine siting. As such, it can be tested and implemented in the existing and future wind farms regardless of their layout. An example of such venture is a €2.3 million demonstration project “Wind Farm Control Trials” carried out by Carbon Trust aiming to examine how effective implementation of wind farm control strategies can reduce the cost of offshore wind energy [61].

3.2.1 Power de-rating

Power de-rating method, proposed by Steinbuch et al. in 1988 [62], is the oldest and still widely researched concept of controlling the aerodynamic interaction between wind turbines, which relies on manipulating the axial induction factor of the turbines. The axial induction is directly related to the power and thrust coefficients of a wind turbine rotor and can be controlled by either changing the blade pitch angle [63] or operation at suboptimal tip speed ratio [64]. When an upstream turbine reduces its axial induction factor at the same time it decreases both its power output and the magnitude of the overall thrust force it exerts on the wind. Consequently, the velocity deficit within its wake is smaller. A downstream turbine operating in the wake of such a de-rated upstream turbine is exposed to higher wind speeds and generates more power. This approach is theoretically

valid in terms of total power increase since with the appropriate scale and turbine positioning the power loss of upstream machine can be outweighed by the power gain of the downstream one [13]. Many research attempts aimed to assess the benefits of power de-rating application were reviewed by Ali C. Kheirabadi et al. [65]. However, the merit of this method is still an open research question.

3.2.2 Wake steering

Wake steering approach consists of steering the wakes of upstream turbines away from the downstream ones, which can be achieved most effectively by operating the upstream machines with yaw angle offset [66]. Publications on this topic range from modelling the effects of yaw misalignment [46], through coupled power and loads optimization in a wind farm [67], simultaneous wind farm layout and power optimization [15], use of flow-measurements in a feedback control settings [68], to field tests in offshore wind farms [21]. Due to the misalignment of the rotor axis with the incoming wind, the blades experience variable aerodynamic loads as they rotate. At the same time, the thrust force exerted on the wind, which acts perpendicularly to the rotor plane, creates an angle with respect to the freestream wind direction. The resulting imbalance of loads and shifted direction of thrust impart an incident force that causes the wind to gain momentum in the crosswind direction and change its course of movement behind the turbine [26]. Further downstream the wake is influenced by a system of vortices released from the yawed rotor *i.e.* the wake rotation vortex and counter-rotating vortex pairs contributing to its deflection and deformation. As a result, the overlapping area between the deflected wake and a downstream turbine is reduced, leading to higher incident wind speed and consequently larger power output at the downstream machine. With the optimal yaw angle offset, the power output of a downstream turbine can exceed the yaw-induced losses of an upstream machine [69]. Besides yaw-based wake control, other, more holistic approaches for wake redirection are also being investigated, that include: rotor tilting, yaw-oriented and tilt-oriented individual pitch control (IPC) and wake avoidance via turbine repositioning [70, 69].

3.2.3 Turbine repositioning

The last noteworthy concept of wind farm control strategy is wake avoidance via turbine repositioning, as proposed by van Wingerden under the assumption of floating and repositionable machines [71]. Similarly to yaw-based wake redirection, it aims to reduce the overlap between the wake and a downstream turbine, however, to achieve this instead of manipulating the wake via yaw misalignment, the individual downstream turbine shifts its position. Regardless of the employed mechanism, by altering its location in the crosswind direction the downstream machine exposes itself to higher wind speeds resulting in increased power generation. Although viable in terms of aerodynamics, this concept receives limited attention from wind farm control communities mainly due to its narrow applicability in floating offshore wind sector at the current stage of development [6]. The technologies proposed for active position control of floating offshore wind turbines include under-water thrusters [72], winch mechanisms attached to a floating structure and anchored to the seabed [73], potentially thermally-actuated sewing thread artificial muscles [74] that alter tension within mooring lines, and alternatively, nacelle yaw angle and blade pitch angle control to manipulate turbine position with the use of aerodynamic forces [75].

3.3 Yaw-based wake redirection

Nowadays, wind farm control via yaw-based wake redirection is a broadly researched method, aimed to decrease the wake losses and/or influence loads experienced by the machines. When operating in yaw, a wind turbine causes its wake to deflect in the opposite direction to the implemented yaw angle offset, leading to a decreased overlap between the resulting wake and a downstream turbine rotor, as presented in Figure 3.3.1. The experience with yaw control shows that even when turbines are programmed to operate in non-yawed conditions, there is always some error in yaw alignment due to the limitations of the yaw controller. It fact, it has been demonstrated with LIght Detection And Ranging (LIDAR) measurements that wind turbines typically operate from 4° to 10° in yaw, when it attempts to track and align with the flow [76]. For a successful application of this operational control technique, precise knowledge about the dependency between inflow wind conditions, the aerodynamics of yawed rotor and the resulting wake characteristics is crucial.

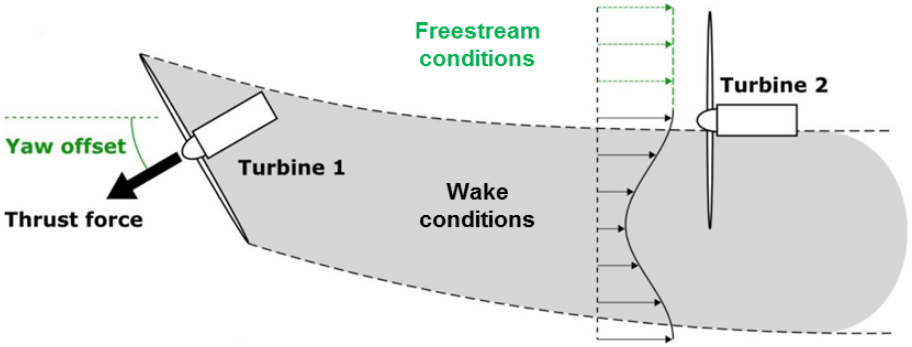

Figure 3.3.1 The concept of yaw-based wake steering [65]

High-fidelity numerical simulations, wind tunnel experiments and field campaigns have shown a large potential of yaw angle control. However, due to their high computational, measurement or monetary costs, they cannot be employed to fully explore the capability of this control method under the wide variety of conditions that have to be taken into account for an optimum operation of wind farms. The wind plant is continuously exposed to variations in mean wind velocity and direction, ambient turbulence, thermal stability and aerodynamic interaction between the machines. Thus, the development and validation of simple and computationally inexpensive wake models that could accurately predict the farm flow field over a wide range of operating conditions is crucial.

The next section provides state-of-the-art knowledge on the operation of a yawed turbine, deflected wake aerodynamics and potential for power improvement using yaw-based wake redirection technique. An important aspect of yaw control studies is the definition of yaw angle direction. In this Master's Thesis, the positive yaw angle refers to the counter-clockwise rotation of the nacelle, when looking at the turbine from the top, with the wind coming from the left-hand side. Following this concept, the upstream turbine from Figure 3.3.1 is operating with a positive yaw angle offset.

3.3.1 State-of-the-art

In some early studies of yawed turbines, Dahlberg and Medici [77], and later Medici and Alfredsson [78] measured the far-wake velocity distribution at some downwind distances from a turbine operating in yaw, located in a wind tunnel. Their measurements clearly showed that the wake rotates in the opposite direction to the rotation of the rotor, and more importantly, the misaligned rotor causes the wake to deflect to the side and deform as it propagates downstream. The wake position was dependent on the magnitude of the implemented yaw angle and the downstream distance. It was noticed that the wake recovery is substantially improved by the presence of freestream turbulence. Large scale vortex shedding from the turbine rotor was also observed, which was hypothesized to be the cause of meandering effect seen in the wakes of full-scale turbines.

Later, Jiménez et al. [56] used the LES technique to study the wake deflection for a range of yaw angles and thrust coefficients of the turbine. Their simulation revealed that as the yaw angle increases, the wake skew angle, and therefore wake deflection, becomes larger. However, the gains in skew angle tend to flatten off as the turbine approached relatively large yaw settings (around 30°). This lead to a conclusion that it is not beneficial to apply yaw offsets that exceed a certain threshold, as the turbine power decreases at the rate of cubed cosine of yaw angle while the achieved deflection shows a modest increase. They also pointed out that for a given yaw angle, the wake is deflected more for turbines with higher thrust coefficients, and its trajectory slowly becomes parallel to the main flow direction in the far-wake region. Assuming a top-hat shape wake profile, they proposed a simple analytical model to predict wake skew angle at a given downstream distance, as presented in section (2.2.2.4).

Further, the ability of a single turbine to redirect its wake was extensively studied by Fleming et al. [70] with the use of Simulator fOr Wind Farm Applications (SOWFA) – a high fidelity wind plant simulation tool. In their work, four different wake steering techniques were evaluated in terms of their impact on power generation, loads and wake deflection. These techniques included yaw and tilt induced wake redirection together with a novel IPC approach aiming to intentionally induce yaw or tilt moment. The results clearly indicated that yaw-based wake redirection is the most effective method for wake steering. The most important findings regarding this technique include:

- horizontal wake offset at 7D downstream distance is significantly (two- to three-fold) larger for a whole range of positive yaw angles (5° to 40°, 5° increment) than for the same range of negative ones
- vertical wake offset was observed, which also exhibits larger values for positive yaw settings
- power at the yawed turbine drops only slightly for small yaw misalignment settings while already achieving a considerable wake deflection
- measured loads (blade out-of-plane, drivetrain, tower and yaw bearing) are in general smaller for positive yaw settings than for negative yaw settings
- small horizontal wake deflection, in the same direction as for positive yaw error, could also be observed for the non-yawed baseline case, which was presumed to be due to the wake rotation

This contribution explains why many wind farm optimization studies constrain the yaw angle settings to only positive values and the maximum value of yaw angle to around 25°.

The later LES study of Fleming et al. [69] on a system of two turbines with 7D separation confirmed that yawing the upstream machine in the positive direction brings about overall gains in power up to 4.6% for $\gamma = 25°$, while applying any negative yaw angle results in overall power losses of the system. This means that power gains at a downstream turbine can overcome losses at the upstream one, however, at the expense of increased loads on the downwind machine (blade out-of-plane, drivetrain torsion and yaw bearing moment) due to partial wake overlap. It should be noted that in this study, the reference point for loads comparison was a full wake overlap condition. In a real wind farm, however, it would likely be a change from one partial overlap situation to another and it is hypothesised that the resulting change in loads could be negligible or even in the opposite direction.

In the work of Howland et al. [48], a porous disk was used to examine the deflection and morphology of a wake under yawed conditions in a uniform inflow. The flow measurements for a large yaw angle (30°) clearly showed a 3D asymmetry in the wake, with kidney-shaped cross-section, termed a curled wake. Such shape of the wake implies that the momentum deficit behind a yawed turbine is not fully deflected, as it was erroneously given by the horizontal plane measurements at the hub height. The resulting wake exhibits considerably less lateral deflection at the top and the bottom of the rotor area. The spanwise velocity components measured at certain downwind locations suggest the existence of CVP released from the top and bottom parts of a yawed disk. It was claimed that the curled wake shape has potential implication for the power optimization via yaw-based wake steering, as this phenomenon may cause a wake to miss more of a downstream turbine than previously believed.

Bastankhah and Porté-Agel [46] carried out extensive wind tunnel experiments to characterize a wake of a turbine under different yaw angles and proposed a new wake deflection model, presented in section (2.2.2.5). They confirmed that as the implemented yaw angle increases, the power output and thrust force decrease, the wake velocity deficit becomes smaller and the wake deflection becomes larger. For highly yawed turbines, CVP were observed in cross-sections of the wake at several downstream locations. These cross planes also showed that the wake becomes kidney-shaped and tends to move upward and downward for negative and positive yaw angles, respectively. Such vertical movement of the wake was found to be due to the interaction between the CVP, the ground and the wake rotation. It was observed that the wake growth rate is approximately the same for different yaw angle configurations, leading to roughly linear wake width variation along the downstream distance in the far-wake region. This is supported by the observation that the wake of a yawed turbine quickly aligns with the turbulent free shear flow as it leaves the near-wake region, where the wake recovery is mainly influenced by the incoming flow properties. The magnitude of the yaw angle, however, impacts the lateral width of the wake in a way that the wake width decreases with increasing yaw offset. Their analysis also revealed that in the far-wake region, the wake deflection increases with increasing thrust coefficient, which is consistent with the finding of Jiménez et al. [56]. Besides, the increasing level of ambient turbulence was deemed to improve the flow entrainment into the wake, leading to reduced achievable wake trajectory offsets. This finding may suggest that implementation of yaw-based wake redirection could be more promising in offshore wind farms, as their winds are characterized by lower turbulence levels.

Vollmer et al. [49] used LES to investigate the impact of the atmospheric boundary layer (ABL) conditions on

the effectiveness of wake deflection via yaw misalignment. The study clearly shows that the ambient flow parameters such as turbulence intensity, wind shear and veer strongly affect the resulting wake trajectory. Specifically, in stable ABL positive yawing is more favourable (30° against -30°) as it produces considerably larger wake offset, as measured at 6D downwind distance. A smaller magnitude of wake offset is observed in neutral ABL, while near-zero deflection is achieved in convective ABL. Additionally, the authors emphasize the importance to consider the uncertainty of the wake deflection estimation in wind farm control studies. Three sources of this uncertainty include atmospheric stability condition, the implemented method to derive wake position and the influence of time-averaging interval to find the wake deflection.

Schottler et al. [79] tested two different model wind turbines, both yawed at 30°, in a wind tunnel to observe how differences in size, geometry and blade design can impact wake deflection. Both models produced the same wake centre location measured at a 3D distance (0.19D offset) but gave different results at 6D (0.32D and 0.4D offsets). Due to significantly changed inflow conditions between the two experiments and the fact that one model turbine rotated clockwise and the other counter-clockwise, no conclusive information can be drawn with respect to the experiment's objective, however, the apparent wake location difference at 6D might indicate the contribution of the wake rotational effect to its trajectory.

A full-scale field test of wake steering was carried out by Fleming et al. [80], who used GE 1.5 SLE (1.5 MW) wind turbine and a nacelle-mounted LIDAR that scanned the wake at several ranges downwind (1D, 1.5D, 2D and 2.5D). The wake deflection was observed for both, 0° and 25° yaw offset settings, however, it was much more pronounced for the latter case. The measured wind velocity deficit was noticeably larger in the time of the turbine aligned with the freestream wind. The turbine power dropped insignificantly when operated in 12° yaw, and a minor drop could be seen for operation at 25° yaw. The standard rule that power is lost according to the cosine of yaw angle raised to a certain power (1.88 in this study) was found to reasonably well fit the mean values of turbine power for a range of wind speeds. A good agreement was achieved between the experimental data and predictions of a control-oriented wake model – FLORIS [14, 81] in terms of its key features: wake deflection, velocity deficit and recovery, power loss and wake skew.

Motivated by the earlier reports on the yawed-rotor-generated CVP, Fleming et al. [51] focused on investigating the impact of these flow structures on yaw-based wake steering. High-fidelity SOWFA simulations revealed that these vortices play an important role in (1) deforming the shape of the wake, (2) explaining the asymmetry of effectiveness in wake steering of oppositely signed yaw angles, and (3) understanding how a "steered" wake interacts with downstream and laterally adjacent wakes in a multi-turbine array. An important finding of their study was that, due to the presence of the CVP, a steered wake can deflect the wake of a downstream turbine, even if that downstream machine is not yawed, which was termed a "secondary steering".

As wind turbines constantly grow in size, Ciri et al. [82] used LES to examine the effect of two considerably different turbine scales on wind farm efficiency and effectiveness of the yaw-based wake control. Performance of two aligned NREL 5-MW reference turbines with rotor diameter D = 126 [m] was compared against two Vestas V27 300-kW machines with D = 27 [m], respecting the spacing in terms of rotor diameter. It was shown that the power loss at the yawed upstream turbine followed the same curve along the range of yaw angles for both models, while significantly larger gains at the downstream machine were observed for the NREL 5MW

model. This stems from the fact that for the same yaw angles at both turbine models, a larger wake deflection was achieved by the bigger turbine. It was speculated that due to the smaller length and time scales for V27 model, its wake is more affected by the surrounding flow and quickly realigns with the freestream flow, whereas the wake of NREL 5-MW turbine preserves its initial skew further downstream.

Qian and Ishihara [83] studied numerically and analytically the wake behaviour behind a yawed wind turbine and proposed a Gaussian-based wake model that accounts for ambient turbulence intensity, thrust coefficient and yaw angle effects. The model parameters are determined as a function of ambient turbulence and thrust coefficient, resulting in good applicability under various conditions, proven in comparison to a series of numerical simulations.

Bartl et al. [84] extensively studied the interaction of two aligned model wind turbines, where the upstream one was yawed at -30° and +30°, placed in a wind tunnel. They showed that Bastankhah deflection model [46] is in a better agreement with the measured wake trajectory than the model proposed by Jiménez [56]. The degree of wake redirection was observed to be only slightly dependent on the inflow turbulence level (0.23% and 10% turbulence intensities investigated), while Bastankhah and Porté-Agel [46] argued, that smaller inflow turbulence reduces the flow entrainment in the far-wake region and thus increases wake deflection. The study confirmed that a larger wake offset is achieved for a positively yawed machine, which is consistent with previous studies. A comparison of several methods to derive wake centre trajectory revealed that there is a significant difference in the calculated path of the wake, as previously reported by Vollmer et al. [49]. The power gains at the downstream turbine were found to be asymmetric with respect to the yaw direction at the upstream turbine (higher gains for positive yaw). They also increased as inter-turbine spacing was changed from 3D to 6D. A small wake deflection was observed for a non-yawed turbine, claimed to be due to the interaction of the rotating wake with the wake of a tower. The rotor-generated turbulence was found to be accumulated in the outermost peripheral region of the near-wake, being laterally deflected and deformed to the same degree as the velocity deficit profiles. This region of the wake corresponds to the locations of the highest gradients in mean streamwise velocity. As the wake evolves downstream from 3D to 6D distance, the magnitude of the wake cross-sectional turbulent kinetic energy (TKE) peak decreases, evening out as it is extending towards the centre of the wake. Their further analysis demonstrated that the peak turbulence levels decrease with the increasing yaw angle, at a similar rate to that of the rotor thrust.

Increasing interest in the curled shape of the wake encouraged Martínez-Tossas et al. [52] to develop a control-oriented analytical model that captures the curling effect, based on approximations to the Navier-Stokes equations. This model, named “curled wake model” is unique since it does not assume any shape of the wake, and additionally accounts for the effects due to yaw, wake rotation, atmospheric boundary layer profile and turbulence modelling. A good agreement was observed in terms of the predicted shape of the curled wake and flow parameters behind a yawed turbine when compared against LES simulations.

Bay et al. [55] improved the curled wake model to include vortex decay, validated its performance by conducting a series of multi-turbine array simulations, and compared its predictions against SOWFA results. The model was found to resemble well the wake shape obtained by SOWFA, accurately compute flow parameters and be very useful for wind farm optimization, as it takes into account the secondary steering effect.

Most recently, King et al. [53] proposed further improvements to modelling a wake of a yawed turbine by introducing analytical modifications to the Gaussian-based wake model to include added yaw-based wake recovery, the interaction of CVP with atmospheric boundary layer and secondary steering effects. The newly developed model significantly boosts the accuracy of predictions obtained by computationally inexpensive modelling of the yaw-based wake steering method.

Chapter 4

Methodology

This chapter covers the approach employed in the present study. First, the utilized modelling framework – FLORIS is introduced, followed by the simulation setup. The background information and characteristics of the NREL 5-MW reference turbine is brought up and the simulated wind conditions and farm configurations are presented. Later, the optimization setup is covered and the SLSQP optimization algorithm is discussed. Lastly, a study on the sensitivity of the optimization parameters is carried out and some preliminary conclusions are drawn.

4.1 FLORIS – controls oriented modelling utility

Flow Redirection and Induction in Steady State (FLORIS) [59] is a python-based software repository dedicated for studies of wind farm control, developed by researchers from the National Renewable Energy Laboratory (NREL) in the USA. FLORIS provides a suite of design and analysis tools, useful in wind farm control and co-designed layout optimization studies, such as optimization of turbine control set-points and farm layout, analysis of wind rose and annual energy production, flow field visualization as well as methods for coupling with other wind energy dedicated software. The steady-state wind farm aerodynamics is handled with the use of computationally inexpensive analytical engineering models while the power and thrust of each turbine are obtained from look-up tables included in the instantiation file. For the given wind conditions, spatial configuration and prescribed control settings, FLORIS enables to predict the flow characteristics inside the farm domain by modelling and combining multiple wakes. The wake models implemented in the utilized version of FLORIS (v2.2.0) include:

- wake velocity deficit models: Jensen [35], multi-zone [85, 14], Gauss [38, 45, 47, 86, 32, 83], Gauss-Curl Hybrid [53], Curl [52]
- wake deflection models: Jiménez [56], Bastankhah [46]
- wake combination model: Katic [36]

The available optimization modules allow for wind farm optimization in terms of layout, layout and hub-height, farm power density and yaw control set-points for single wind conditions or over a specified wind rose. The software comes with the implementation of NREL 5-MW reference wind turbine characteristics, however, any other turbine model can be added. The FLORIS modelling framework is open source and available for download and collaborative development (https://github.com/NREL/FLORIS/).

4.2 Simulation setup

4.2.1 NREL 5-MW reference HAWT

It was decided to investigate yaw-based wake control on a system consisting of the NREL offshore 5-MW baseline wind turbines, developed by researchers at NREL in the USA. This choice was motivated by the fact that this machine is a widely known representative of an utility-scale multimegawatt turbine that has been an object of many wind energy research projects and its specifications are publicly available. The most relevant information and data regarding this machine in terms of the present study will be provided in the current section while its full description is available in the paper of Jonkman et al. [87].

The NREL 5-MW machine is a conventional three-bladed upwind variable-speed variable blade-pitch-to-feather-controlled turbine. It was created with the use of publicly available properties from the conceptual models in the

WindPACT, RECOFF and DOWEC projects and some broad design information from the published documents of turbine manufacturers, with a heavy emphasis on the REpower 5MW machine. The basic size and power rating of the machine were chosen taking into consideration that for a deep-water wind system to be cost-effective, each turbine must be rated at 5-MW or higher. The basic gross properties of the NREL 5-MW baseline turbine were collected from the turbine documentation and data available in FLORIS and presented in *Table 4.2.1*.

Table 4.2.1 Gross properties of NREL 5-MW reference turbine

Rating	5 [MW]
Rotor Orientation, Configuration	Upwind, 3 Blades
Control	Variable Speed, Collective Pitch
Rotor, Hub Diameter	126 [m], 3 [m]
Hub Height	90 [m]
Cut-In, Rated, Cut-Out wind speed	3 [m/s], 11.4 [m/s], 25 [m/s]
Cut-In, Rated rotor speed	6.9 rpm, 12.1 rpm
Rated Tip Speed	80 [m/s]
Generator Efficiency	1
Mechanical Efficiency	1
The cosine exponent relating turbine power to its yaw settings "pP"	1.88

The turbine power control system is made of two subsystems: (1) generator-torque controller and (2) a full-span rotor-collective blade-pitch controller. These control subsystems are designed to work independently for most of the below-rated and above-rated wind-speed range and work together around the rated wind speed. The control over generator-torque aims to maximize the power capture below the rated operation point while controlling blade-pitch regulates the generator speed above the rated operation point. No control actions were specified for non-power production operations.

The implementation of this model turbine in FLORIS consist of the following set of data: rotor diameter, hub height, number of blades, cosine exponent for yawed and tilted turbine, generator efficiency and the look-up tables relating power and thrust coefficients to the wind speed. To obtain the power output of this turbine in FLORIS, the standard formula directly relating the power and yaw angle via cos(γ) raised to a certain power was instead applied to the wind speed used for power coefficient look-up table. Employing this approach gives more realistic power predictions for the wind speeds above the rated speed where pitch control would compensate for the yaw-induced losses. More information about this method is available in [88], while in FLORIS the following procedure applies. First, the rotor swept area average velocity U_{avg} is found as the cube root of the mean cubed velocity in the rotor area. However, when the machine operates in yaw, the average velocity is replaced with the following formula for the effective wind velocity:

$$U_{eff} = U_{avg} * cos^{\frac{pP}{3}}(\gamma) \tag{4.1}$$

where pP is the cosine exponent relating yawed and non-yawed properties. Such updated velocity is then used to

interpolate the corresponding effective power coefficient $C_{P,eff}$ from the look-up table. Then, the effective power is determined as:

$$P_{eff} = 0.5 * \rho * A * C_{P\_eff} * \eta_g * U_{eff}^3 \tag{4.2}$$

where η_g is generator efficiency.

The direction of yawing in FLORIS is defined in the same way as it was presented in the earlier chapter of this work. The positive yaw angle refers to the counter-clockwise rotation of the nacelle when looking at the turbine from the top, with the wind coming from the left-hand side.

4.2.2 Simulation matrix

This work aims to investigate the effectiveness of yaw-based wake steering method to maximize the total power output of a wind farm while neglecting the impact of yaw-induced loads. As yaw control technique strongly depends on the atmospheric conditions and plant spatial configuration, different values for wind speed, wind direction, turbulence intensity and spacing are tested. This section summarizes the scope of the tested operating conditions organized in the simulation matrix (*Table 4.2.2*) The abbreviations used in the respective columns of the simulation matrix have the following meaning: w_s (wind speed), w_d (wind direction), T_I (turbulence intensity) and spc (spacing) and each specified test is carried out using Jensen, Gauss and GCH wake models.

A very important test case is the one that serves as a baseline for all the other simulation scenarios, where the deviation in the test variables is made. This special test case is named “reference case” and has the values for wind conditions and spacing chosen based on the literature review, such that, on one hand, they are widely used in yaw control research and on the other, they represent well the situations with large wake losses. The remaining simulation scenarios assume the same values for test variables as in the reference case except for the one value that is changed in a particular test. To justify the choice of the magnitude of the deviations in test variables in subsequent simulation scenarios, a piece of explanation is provided:

- **Wind speed values**: while the reference value of 8 [m/s] is a commonly researched and highly occurring wind speed, it is of interest to examine the yaw-based wake steering when the wind farm is exposed to slower, but still frequently occurring wind velocities and also to those exceeding the rated wind speed of the machines. Therefore a choice of 5 [m/s] and 13 [m/s] is made.
- **Wind direction values**: the critical situation in terms wake losses takes place when the wind direction is aligned with a row of turbines, which would correspond to the reference value of 270° direction according to the convention used in FLORIS. Note that 0° corresponds to the direction of wind coming from the north and increases in the clockwise direction of rotation. The size of the deviation from the reference wind direction was chosen to be the half of the increase in the wind direction that is needed to create zero wake overlap situation, predicted with the Jensen wake model for the reference wind speed, turbulence intensity and spacing. The resulting values of the wind direction deviation were estimated to be of 5° and it is of interest to test such deviation in the positive direction (275°) and negative direction (265°).

- **Turbulence intensity values**: ambient turbulence intensity level affects the rate of wake recovery and in turn feasibility of yaw-based wake steering. In general, at offshore sites, the ambient turbulence intensity is lower than at onshore ones, which pleads in favour of employment of wake control away from land. Here, the idea is to pick a low, high and intermediate (reference) turbulence scenario. Based on the values encountered during the literature studies and the data from Horns Rev wind farm area presented in the article of H. E. Jørgensen et al. [89] (figure number 3, page 6), the appropriate values for testing low and high turbulence intensity scenarios should be 5 [%] and 10 [%], respectively, while the reference is set to 7.5 [%].

- **Spacing values**: spacing distance is the only test variable that is not an atmospheric condition in this study, however, its size is always determined based, among others, on the local wind climate of the considered offshore location. A typical value of spacing, widely used in the research of offshore wind farms is seven times the rotor diameter (7D), which is taken as a reference spacing. It is important to test how smaller and larger spacing distances would affect the power output when yaw control is employed. It is deemed appropriate to consider 5D and 9D spacing distances, for the respective test cases as they definitely affect the aerodynamics of the whole system and are also present in the industrial wind farms.

Table 4.2.2 Simulation matrix

Case Name	Test variables			
	w_s [m/s]	w_d [°]	T_I [%]	spc [m]
Reference case “RC”	8	270	7.5	7D
High wind speed “HWS”	13	270	7.5	7D
Low wind speed “LWS”	5	270	7.5	7D
Wind direction 275° “WD_275”	8	275	7.5	7D
Wind direction 265° “WD_265”	8	265	7.5	7D
High turbulence intensity “HTI”	8	270	10	7D
Low turbulence intensity “LTI”	8	270	5	7D
Small spacing “SS”	8	270	7.5	5D
Large spacing “LS”	8	270	7.5	9D

Further, it was decided that a row of eight NREL 5-MW reference wind turbines will be an appropriate size of the system for the present study due to several reasons. The plant-wise power losses are the largest when the wind direction is aligned with the rows of machines, especially in tightly packed rectilinear wind parks. As the economies of scale play a significant role in profitable harvesting of wind energy, a row composed of eight machines is nowadays common metrics. Taking into account the applicability conditions of yaw-based wake steering for park power maximization, the downstream machines should be largely exposed to the wakes of the upstream ones. Lastly, the secondary wake steering effects that are believed to have a great impact on yaw-based wind farm control should be well pronounced in such a system.

Except for the values presented in the simulation matrix, other atmospheric constants have to be set and the

tuneable parameters of the employed wake models must be specified. This study relies on the predictions of the wake models with their default settings, however, it is a common approach to tune the models so that they are aligned with the predictions of more credible modelling tools. The remaining relevant parameters are summarized in *Table A.1* and *Table A.2* of Annex A.

4.3 Optimization

4.3.1 Optimization setup

In this study, the cumulative power of wind turbines is being maximized with the yaw angle setting of each machine as the design variables. Since the present study does not take into account the yaw-induced loads, the bounds were set on the yaw angles so they would fall between $-50°$ and $+50°$. Although such yaw amplitude far exceeds the feasible operating region of industrial wind turbines, these numbers were chosen to ensure that the optimization solution is not affected by any imposed restrictions on the design space. However, a common approach applied in yaw-based wake steering studies is to allow only positive values of yaw misalignment with the lower and upper bound at $0°$ and around $+25°$, respectively. Such constrained design space is believed to provide the best trade-off between the achieved wake deflection and both power loss and load variations at the yawed turbine. The SciPy optimization package [90] was employed for the optimization, using the Sequential Least SQuares Programming (SLSQP) minimization method developed by D. Kraft [91]. This is the default optimization method set in FLORIS, which is suitable for solving nonlinear problems with multivariable objective functions and any combination of design space bounds, equality and inequality constraints. The optimization problem was defined as follows:

$$minimize\ P = -\sum_{i=1}^{N_t} P_i(\gamma_i) \tag{4.3}$$

$$subject\ to\ -50° < \gamma_i < +50° \tag{4.4}$$

where N_t is the number of turbines, P_i is the power and γ_i is the yaw angle setting of the *i-th* turbine. No equality or inequality constraints were prescribed in this formulation.

The SLSQP solver is the SciPy implementation of Sequential Quadratic Programming (SQP), a gradient-based iterative method, which consists of breaking down the original problem into a sequence of least squares optimization sub-problems and solving them in the course of finding the search direction. A prerequisite for SQP algorithms is that both the objective function and the constraints are twice continuously differentiable. The SLSQP algorithm requires the Jacobian matrices of the objective function and the constraints as an input. These matrices are numerically approximated at the design space points that correspond to the solution obtained in the current iteration using the forward differences method. The three main adjustable options of SLSQP optimization method include:

- maximum allowed number of iterations ($maxiter$),
- the precision goal of the value of the objective function in the stopping criterion (f_tol),
- the step size used for the numerical approximation of the Jacobian (ε)

The $maxiter$ option controls the termination of the optimization in case the solution is not found within the given number of iterations and it does not affect how well the SLSQP algorithm performs when searching for the solution. On the other hand, depending on the problem definition and the desired accuracy, the f_tol and ε settings may have a large impact on the effectiveness of the optimization algorithm and the final solution. Also, an inherent limitation of gradient-based methods is that they are local minimizers, which makes the initial vector of yaw angle settings, being the starting point in the optimization ($x0$), an important parameter to consider. Since every optimization problem is unique and no guidelines for selecting the appropriate values of f_tol, ε and $x0$ parameters were found, it was decided to first investigate their impact. This pre-optimization study relied on experimenting with the yaw settings to estimate a feasible initial guess of the vector of arguments ($x0\_G$) and then carrying out a sensitivity study on f_tol and ε. A more detailed description of this investigation is presented in section (4.3.3) of this chapter while the chosen optimization settings for each wake modelling approach are summarized in the table below.

Table 4.3.1 Summary of the optimization parameters for each wake model

Wake model	$maxiter$	f_tol	ε	$x0$
Jensen	100	10^{-13}	0.005	x0_G
Gauss	100	10^{-13}	0.005	x0_G
GCH	100	10^{-13}	0.02	x0_G

4.3.2 SLSQP optimization algorithm

A general nonlinear programming (NLP) problem, given by:

$$(NLP): \ min_{x \in R^n} \ f(x) \tag{4.5}$$

subject to

$$g_j(x) = 0, \quad j = 1, \dots, m_e \qquad and \qquad g_j(x) \geq 0, \quad j = m_e + 1, \dots, m_t \tag{4.6}$$

is solved iteratively, where m_e and $m - m_e$ are the numbers of equality and inequality constraints, respectively, starting with the initial guess of the vector of arguments $x0$, while the subsequent iterates x^{k+1} are obtained by the step:

$$x^{k+1} = x^k + \alpha^k d^k \tag{4.7}$$

where d^k is the search direction within the *k-th* step and α^k is the step length. The search direction is determined by a quadratic programming (QP) sub-problem, formulated as a quadratic approximation of the Lagrange function of (NLP): $\mathcal{L}(x, \lambda) = f(x) - \sum_{i=1}^{m} \lambda g_j(x)$ and a linear approximation of the constraints g_j:

$$(QP):\ \ min_{d\in R^n}\ \frac{1}{2}d^T B^k d + \nabla f(x^k)d \tag{4.8}$$

subject to

$$\nabla g_j(x^k)d + g_j(x^k) = 0,\quad j = 1,\dots,m_e \qquad and \qquad \nabla g_j(x^k)d + g_j(x^k) \geq 0,\quad j = m_e+1,\dots,m \tag{4.9}$$

where the B matrix is Hessian of the Lagrangian of NLP at the current iterate of the form: $B^k = \nabla^2_{xx}\mathcal{L}(x^k,\lambda^k)$ and λ is a vector of Lagrange multipliers. The step length is obtained using a backtracking line search scheme based on Armijo-Goldstein condition with bounds violation test. This procedure involves starting with a relatively large estimate of the step size along the search direction and iteratively shrinking the step size until a decrease of the objective function adequately corresponds to the expected value, based on the local gradient of the objective function. To maintain computational efficiency of the algorithm, the modification of the Broyden-Fletcher-Goldfarb-Shanno (BFGS) method, introduced by Han and Powell, is implemented to approximate the B matrix, instead of directly calculating all second partial derivatives of $\mathcal{L}(x,\lambda)$ in every iteration. The quadratic sub-problem QP is replaced by equality- and inequality-constrained linear least-squares (LSEI) problem, which is possible when the approximation of the B matrix is factorized using the LDL^T decomposition. The resulting LSEI problem is of the form:

$$(LSEI):\ \ min_{d\in R^n}\ \left\|(D^k)^{1/2}(L^k)^T d + (D^k)^{-1/2}(L^k)^{-1}\nabla f(x^k)\right\| \tag{4.10}$$

subject to

$$\nabla g_j(x^k)d + g_j(x^k) = 0,\quad j = 1,\dots,m_e \qquad and \qquad \nabla g_j(x^k)d + g_j(x^k) \geq 0,\quad j = m_e+1,\dots,m \tag{4.11}$$

The element $\|x\|$ denotes Euclidian vector norm of the form $\|x\| = \sqrt{\sum x_i^2}$ and $\|M\|$ is the corresponding induced matrix norm. Such LSEI problem is solved with the linear least squares methods of Lawson and Hanson [92].

4.3.3 Sensitivity study on the optimization parameters

It is a well-known fact that every optimization problem is unique and when gradient-based methods are concerned, the more elaborate the problem becomes, the more uncertain it is whether the achieved solution is global or local. Therefore, a good understanding of the impact of configurable parameters of SLSQP method on the algorithm performance and the achieved solution is imperative to draw credible conclusions. In this part, the procedure used to determine the initial guess of the starting point in the optimization (x0_G) and the results of the study on the optimization settings and their impact on the obtained solution will be discussed. The atmospheric conditions and wind farm layout correspond to the reference case conditions from *Table 4.2.2* for each simulation conducted within the present sensitivity study.

Starting with the estimation of the initial guess (x0_G), it was decided to utilize the wake modelling approach proposed by Jensen and to use the following procedure:

1) Set up the simulation domain in FLORIS with yaw angles at all turbines set to zero (x0_0)
2) Create the vector where the estimated initial guess of yaw angle set-points of each turbine will be stored

$x0\_G = [0, 0, 0, 0, 0, 0, 0, 0]$

3) Apply the yaw angles at each individual turbine according to the values in the current vector x0_G
4) Simulate the wind farm with the yaw settings at the i-th machine within the range $\gamma \in [-50° : +50°]$ with the step of 1° and record how each yaw set-point affects the power of the whole system (total of 101 simulations per turbine)
5) Take the yaw angle of the i-th machine for which there is the largest increase in power of the whole system and store it as the respective i-th entry of the initial guess of the vector of arguments (x0_G)
6) Repeat the steps 3 and 5 for all machines starting from the front one

Upon completion of this procedure, the vector x0_G containing the estimated yaw angle settings is:

$$x0\_G = [0,\ 27,\ 28,\ 28,\ 28,\ 28,\ 0,\ 0]$$

where each entry value is expressed in degrees. This vector of yaw angle settings will be used as an alternative starting point in the subsequent study on the sensitivity of the optimization options for all of the employed wake modelling approaches.

Further on, the impact of function tolerance *f_tol*, step size in gradient approximation ε and the guess of the initial yaw settings x0_G on the optimization solution was investigated. This study relied on performing a number of optimization runs for each considered wake modelling approach with different combinations of *f_tol* and ε values, and with the default (x0_0) and guessed (x0_G) vector of yaw angles as a starting point. The values of both parameters, *f_tol* and ε, are normalized before the actual optimization begins, which is done in the following way:

- Normalization of *f_tol*: the power of a given system of wind turbines with any yaw angle settings is divided by the power obtained for the same wind farm with all yaw angles set to zero. Supposing the starting point in the optimization is x0_0, then the normalized power of the system would be equal to 1 and any gains or losses due to a different yaw set-points distribution will cause a fractional increase or decrease of this value, respectively. Therefore, the value of *f_tol* indicates up to which decimal place of the normalized power should the solutions of two consecutive iterations be the same, which terminates the optimization algorithm.

- Normalization of ε: the amplitude of the allowable yaw angle settings, limited by the imposed bounds $\gamma\_\min = -50° \; and \; \gamma\_\max = +50°$ is linearly transformed such that it ranges from 0 to 1. Then, the value of ε stands for the fraction of this amplitude. This means that if the step size in gradient approximation was to be 1°, then the value of ε would have to be 0.01.

The investigated normalized values for *f_tol* were:

$$f\_tol\ [-] = 10^{-15},\ 10^{-14},\ 10^{-13},\ 10^{-12},\ 10^{-10},\ 10^{-8},\ 10^{-6},\ 10^{-4}$$

while the normalized and the corresponding absolute values for the step size were:

$$\varepsilon\,[-] = 0.0001,\ \ 0.0005,\ \ 0.001,\ \ 0.005,\ \ 0.01,\ \ 0.02,\ \ 0.05$$

$$\varepsilon_n\,[°] = 0.01,\ \ 0.05,\ \ 0.1,\ \ 0.5,\ \ 1,\ \ 2,\ \ 5$$

and the two vectors containing initial yaw angle settings:

$$x0\_0 = [0,\ \ 0,\ \ 0,\ \ 0,\ \ 0,\ \ 0,\ \ 0,\ \ 0]$$

$$x0\_G = [0,\ \ 27,\ \ 28,\ \ 28,\ \ 28,\ \ 28,\ \ 0,\ \ 0]$$

The figures below show the results from the conducted sensitivity studies for each wake modelling method. Each data point represents a solution of one optimization run, where the shape of the data point indicates whether x0_0 (circle) or x0_G (rhombus) was used as the initial vector of yaw angles, the colour differentiates between the applied ε (eps) settings and the horizontal order of the data points tells what function tolerance was set.

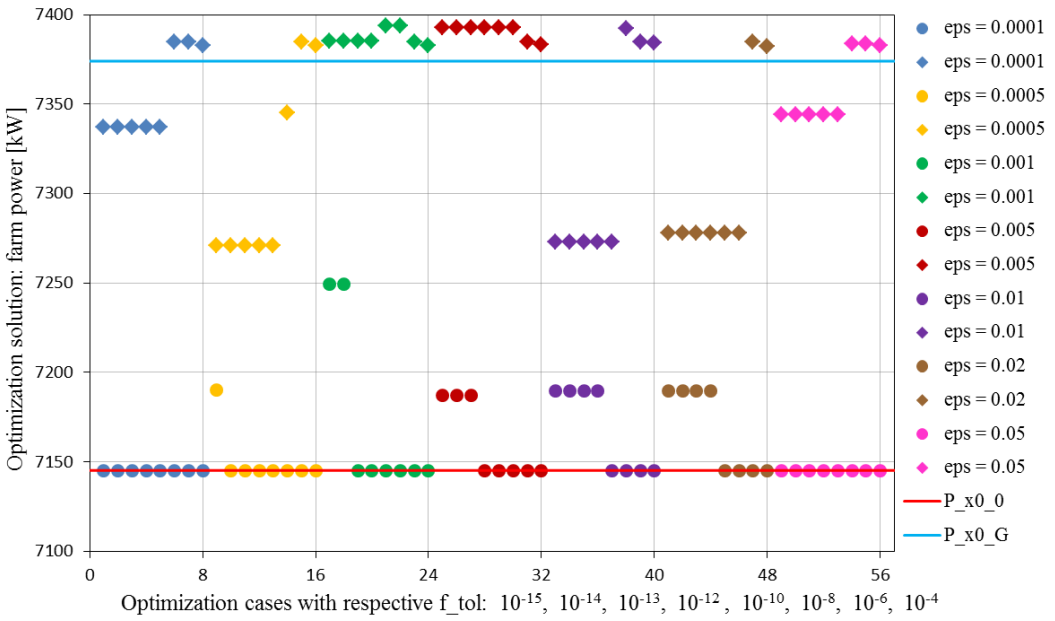

Figure 4.3.1 The results of the sensitivity study on f_tol, ε, and $x0$ for the Jensen wake model

Based on the above figure, when Jensen wake model is employed it appears that:

1) in general, there is a strong influence of the starting vector of yaw angles on the optimization solution in terms of the magnitude of the achieved power improvement
2) beyond that, $x0$ also considerably affects the ability of the optimizer to find an improvement since power gains were reported for 29 cases with $x0\_G$ with respect to P_x0_G (and 56 with respect to P_x0_0) and only for 14 cases with $x0\_0$ with respect to P_x0_0
3) when very small f_tol is used, the SLSQP algorithm finds a solution that brings power improvement for $x0\_0$ whereas for $x0\_G$ ends up at a solution that lowers the power

4) if the starting point *x0_G* is to be used, it is anticipated that a larger value of f_tol should give a better solution

5) with $x0\_0$ as a starting point a trend can be seen that the larger the ε and f_tol are, the more probable it is to find an improvement for yaw settings, however, with *x0_G* it can only be said that f_tol should not be smaller than 10^{-10}

6) the most suitable values for ε seem to be 0.001 and 0.005 with *x0_G*, or possibly 0.01 with *x0_0*

To summarize, the results show a lack of robustness of the SLSQP optimization method with respect to different simulation parameters when the Jensen wake model is employed. Jensen's wake modelling approach significantly simplifies the physics of the wake, which results in very abrupt changes in the flow field, especially when there is a transition from full to partial wake overlap. This causes difficulty for a gradient-based optimization method because it can interpret these sudden changes as a discontinuity in the objective function. Based on these results, it can be concluded that the Jensen wake model is not suitable for searching for the optimal yaw control settings with the SLSQP optimization method. Being aware of its limitations, it was decided to use the initial guess of the vector of yaw angles $x0\_G$ with f_tol equal to 10^{-13} and ε equal to 0.005 for further optimization studies in Chapter 5.

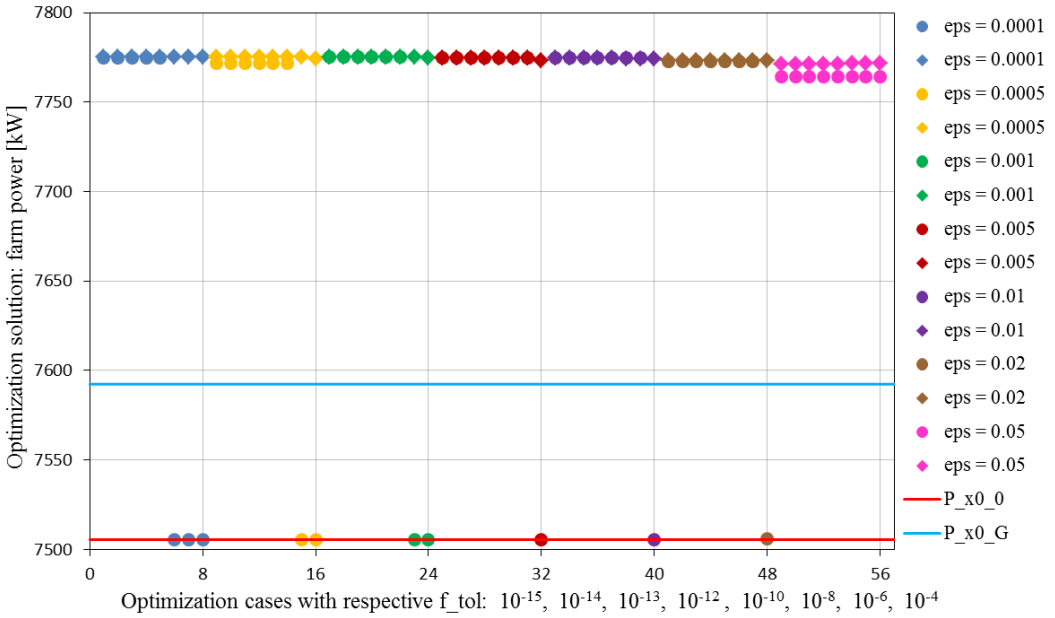

Figure 4.3.2 The results of the sensitivity study on f_tol, ε, and $x0$ for the Gauss wake model

The results obtained with the use of Gauss wake model are very promising, it can be seen that:

1) in general, there is very little impact of all investigated parameters on the optimization solution

2) with $x0\_0$ the optimization procedure terminates immediately when larger f_tol values are used, which is expected behaviour while employing $x0\_G$ completely eliminates the impact of f_tol

3) the magnitude of ε has virtually no influence on the optimization solution as nearly the same level of power improvement is found for all tested values regardless of the f_tol and $x0$

The wake modelling approach with Gaussian velocity profile is very well suited for studies on the yaw control optimization using SLSQP method. In the light of the above findings, it was decided to conduct further simulations with Gaussian wake model in Chapter 5 using the optimization parameters that correspond to these for the Jensen model. These are f_tol equal to 10^{-13}, ε equal to 0.005 and $x0\_G$ as a starting point.

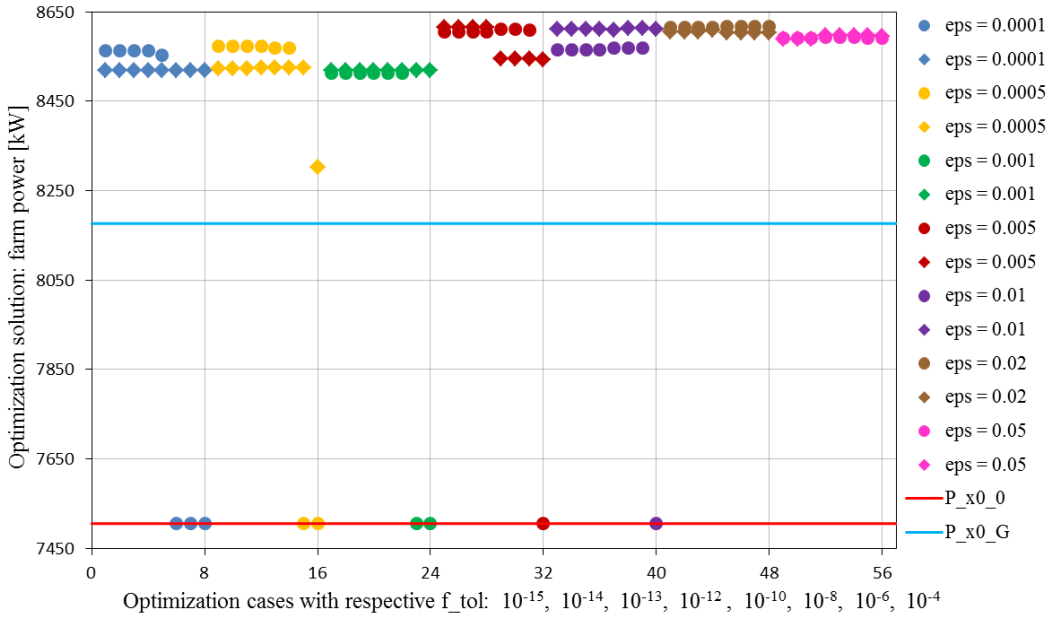

Figure 4.3.3 The results of the sensitivity study on f_tol, ε, and $x0$ for the GCH wake model

The results obtained for the GCH model to some extent resemble these obtained for the Gauss model, however, it clearly appears that:

1) f_tol, ε and $x0$ do have a non-negligible impact on the optimization results
2) similarly to the previous study, the use of $x0\_G$ as a starting point eliminates termination with a non-improved solution
3) different combinations of f_tol and ε result in different levels of optimized wind farm power and it can be observed that ε should not be less than 0.005

The variability of the final solution in terms of both, the total magnitude of power and the randomness of the sensitivity to the optimization parameters lead to a conclusion that GCH wake model is not as robust as the Gauss model. Based on this study, it is deemed appropriate to use ε equal to 0.02 as it ensures achieving satisfying solutions regardless of the values of other parameters while f_tol equal to 10^{-13} and $x0\_G$ as a starting point were set.

The whole sensitivity study also revealed that for each conducted optimization the solution was not affected by the imposed limit of maximum iterations, default to 100. Based on this observation it was decided to use this value for further optimization studies in Chapter 5.

Chapter 5

Results discussion

This chapter presents and discusses the plant-wise yaw control optimization results. Each following section is devoted to one simulation case of the simulation matrix. The discussion begins with the reference case, where a broader description of the apparent differences between the employed wake modelling approaches is provided, followed by the optimization results analysis. Then, the remaining simulation cases are addressed and partial conclusions are drawn.

5.1 Reference case

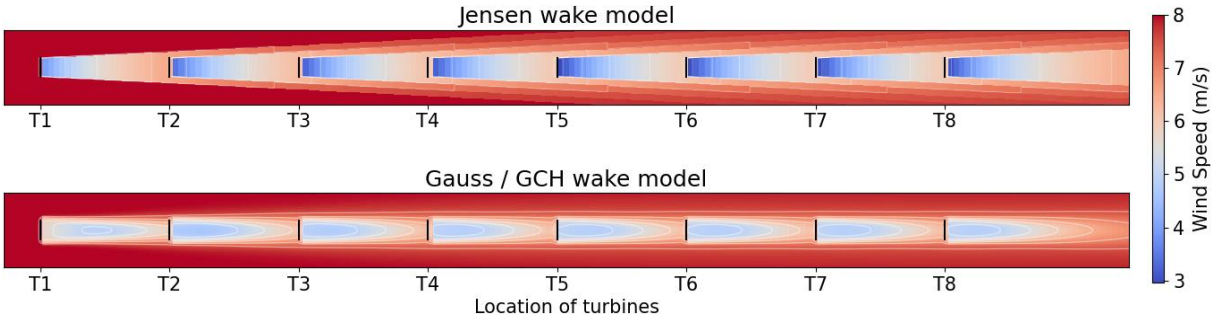

Figure 5.1.1 Hub height flow field with baseline yaw settings – RC

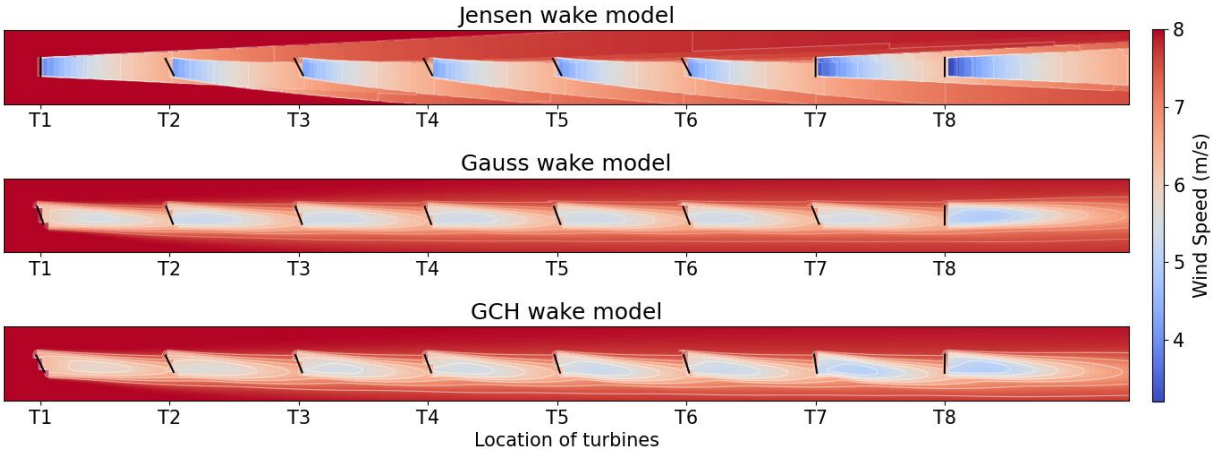

Figure 5.1.2 Hub height flow field with optimized yaw settings – RC

Table 5.1.1 Summary of the results for the RC simulation

Wake model	Baseline WF power [kW]	Optimized WF power [kW]	ΔP [%]	No. of iterations
Jensen	7 145	7 393	3.46	100
Gauss	7 506	7 775	3.59	24
GCH	7 506	8 606	14.66	100

Until the end of this report, a convention to refer to a specific machine in the row is applied, where "T" + "number" denotes a turbine and its position in the system (for example the 5th turbine will be denoted as T5). The reference case simulation parameters (w_s = 8 m/s, w_d = 270°, T_I = 0.075, spc = 7D) represent a situation when the park is exposed to moderate wind speed and turbulence intensity and unfavourable wind direction. The wake losses amount to as much as 47.3% (-6 418 kW *vs* the cumulative power of isolated turbines) for the Jensen and 44.7% (-6 057 kW *vs* the cumulative power of isolated turbines) for the Gauss / GCH wake models, creating a large room for improvement. The flow field within the wind farm with the baseline yaw settings (greedy control), meaning zero yaw angle misalignment applied at each machine, is presented in Figure 5.1.1. The impact of the wake characteristics on the incident velocity profile and its evolution can be observed and full wake overlap situations are clearly visible. In fact, the additional wake effects accounted for by the GCH wake model are only effective if a turbine operates in yaw misalignment. Thus, for the baseline yaw settings, there is no difference in the wind farm aerodynamics predicted by the Gauss and GCH wake models. The distribution of

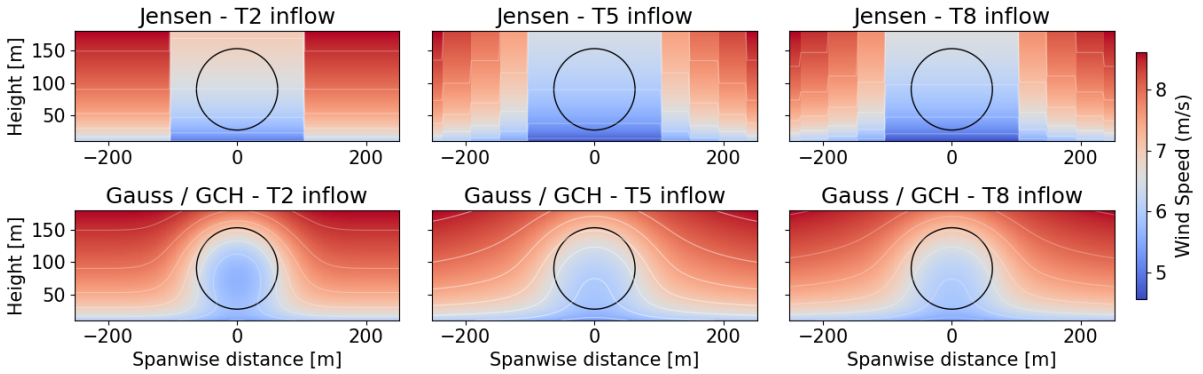

Figure 5.1.3 Velocity field 0.5D ahead of T2, T5 and T8 with baseline yaw settings – RC

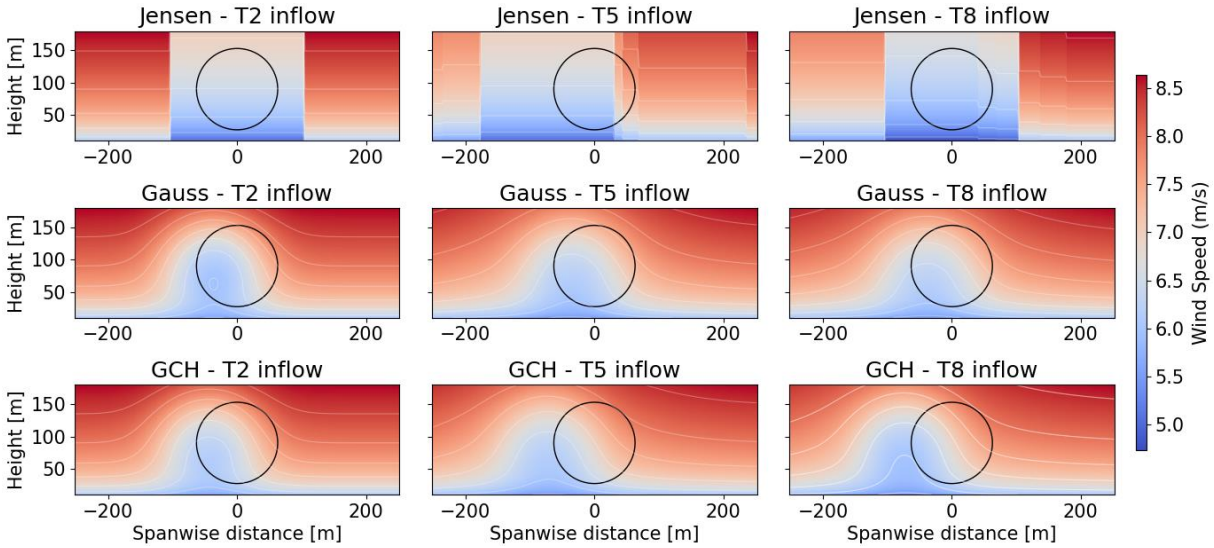

Figure 5.1.4 Velocity field 0.5D ahead of T2, T5 and T8 with optimized yaw settings – RC

the power output at individual turbines, illustrated in Figure 5.1.7, exhibits a noticeably different pattern between the Jensen and Gauss / GCH wake modelling approaches. In both cases, the front turbine extracts the largest portion of the energy carried by the undisturbed wind, being unaffected by any farm effects. However, starting from the second turbine, there is a considerable drop in the power generation, amounting to roughly 45% (-750 kW) of the power output at T1 when the Jensen wake model is employed. This power drop is gradually deepened at the subsequent machines to reach 58% (-970 kW) at T8. On the other hand, employing the Gauss / GCH wake modelling approach results in an even larger power loss at T2, which produces 56% (-950 kW) less power than T1. Then, the power loss due to the wake effect is reduced at each further downstream machine amounting to roughly 50% (-850 kW). Eventually, a larger total wind farm power is achieved compared to the predictions with the Jensen model, as summarized in *Table 5.1.1*. According to the FLORIS procedures, the effective wind velocity passing through the rotor swept area and the applied yaw setting at the specific turbine are the two values that directly affect the power output of the machine. Since the greedy control is used, a conclusion can be made that the wake recovery rate of the Jensen wake model is smaller than the one for the Gauss / GCH models with the default model-specific parameters. This is also very well depicted by the solid lines in Figure 5.1.5 that show the rotor area-averaged downstream wind velocity calculated at different downstream positions. It should be noted that the wake modelling method proposed by Jensen does not apply to the near wake region and the

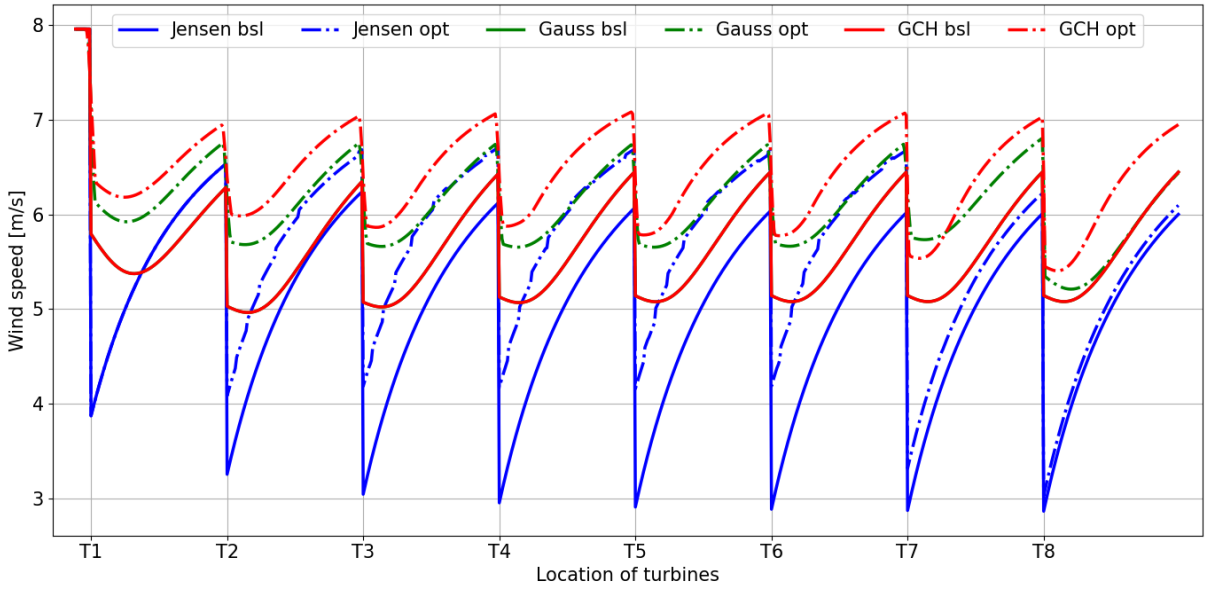

Figure 5.1.5 Evolution of rotor swept area-averaged wind velocity along the wind farm – RC

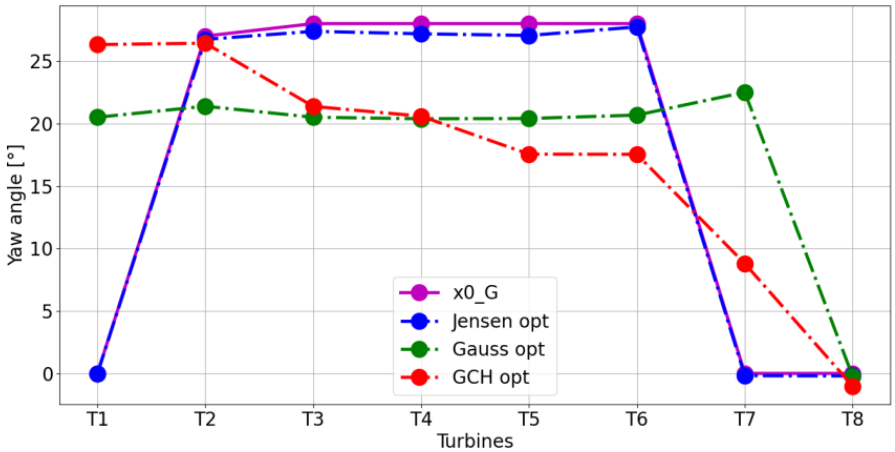

Figure 5.1.6 Yaw distribution in x0_G vector and the optimization solutions – RC

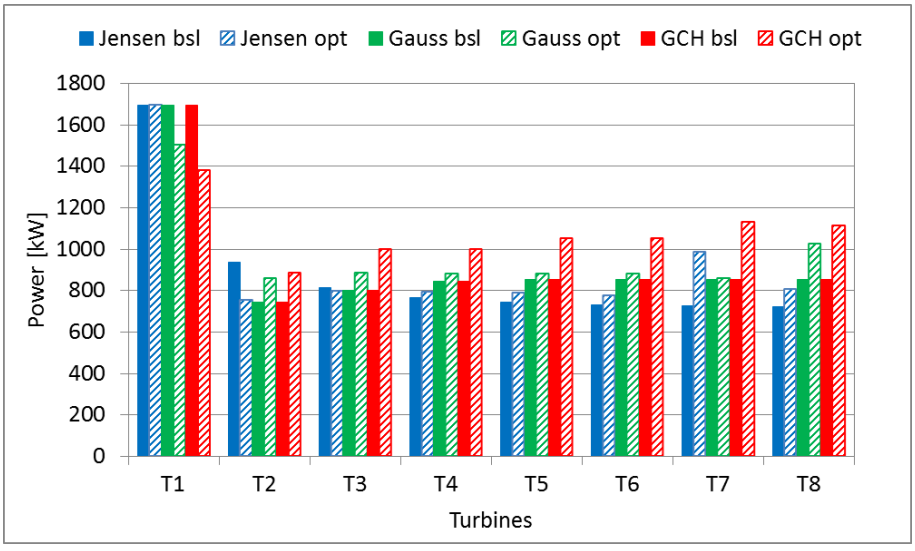

Figure 5.1.7 Power distribution with baseline and optimized yaw settings – RC

available corrections for the Gauss / GCH near-wake region modelling were not studied as they were considered not relevant for the present research. Thus, no conclusions should be made regarding the trajectory of the velocity evolution (Figure 5.1.5) in the close distance behind each turbine. An apparent difference in the resulting shape of the wake and the wind velocity deficit distribution is visible in the flow field cross-sections presented in Figure 5.1.3 with the black ring representing the rotor swept area of a non-yawed turbine. Because the turbines are immersed in the atmospheric boundary layer with a non-zero shear coefficient, the velocity profile changes along the vertical direction for each wake modelling approach both inside the wake region and in the freestream. As Jensen assumed a uniform distribution of velocity deficit, the incident vertical velocity profile in the wake follows the curvature of the wind profile power law. When using the Gauss / GCH models the distribution of the velocity deficit in the wake is very different. The incident cross-sectional wake velocity field is a superposition of the Gaussian distribution of velocity deficit in spanwise and vertical directions and the wind shear.

Moving forward to the optimization results for RC conditions, a power improvement is achieved for each of the wind farm aerodynamics' modelling approaches. The predicted plant-wise power gains with the optimized yaw control set-points are 3.46 %, 3.59 % and 14.66 % for the Jensen, Gauss and GCH models, respectively, as summarized in *Table 5.1.1*. The visible difference between these solutions comes from two sources, the applied wind farm modelling method and the effectiveness of the optimization algorithm to solve such defined optimization problems. The study on the optimization method was carried out in Chapter 4 while the optimization progress record for every simulation run is presented in Annex B. It should be noted that although in many optimization runs the algorithm is stopped by the *maxiter* termination condition, the acceptable convergence was often reached already within the first 10 iterations (see figures in Annex B). This behaviour is deemed to be due to such a small *f_tol* value applied with respect to the optimization problem resolution. The performance of the SLSQP algorithm will not be further investigated and the focus will now go to the main objective of this investigation. In this context, it is of interest to analyse how different wind farm aerodynamics models affect the resulting optimal distribution of the yaw settings in the wind park, the incident flow field modification, and consequently the power output of both the individual machines and the wind farm as a whole.

(1) Optimal yaw control with the Jensen wake model

The alteration of the flow field due to yaw control strategy optimization with the Jensen wake model can be observed in the top of the horizontal (Figure 5.1.2) and vertical (Figure 5.1.4) snapshots. Based on Figure 5.1.6 it can be seen that the distribution of the yaw settings is very similar to the one in x0_G vector. This correlation suggests that it is a good starting point in this optimization run. It is also very interesting to see that, although the largest power drop in relation to the nearest upstream turbine is present at T2, the algorithm does not suggest changing the yaw settings at T1. Presumably, the gains in power at T2 due to the partial wake overlap would not overcome the losses caused by yawing T1, which is slightly counter-intuitive. Taking into account that Jensen's wake is characterized by the uniform velocity deficit distribution, it most probably takes a large yaw angle at an upstream turbine to achieve a partial wake overlap situation at a downstream one. Therefore, yawing the front turbine might not be advantageous. The applied yaw misalignment at T2 – T6 yields approximately the value of 27° at each machine, which in turn leads to the increased effective wind velocity at the subsequent downstream

turbines as displayed by the blue dotted line in Figure 5.1.5. However, the incident power output of these interior machines is either smaller (T3) or slightly larger (T4 – T6) than the power obtained at the same machines for the baseline yaw settings. The power drop at T2 is solely caused by the operation in yaw while potential power gains due to the increased wind speed at T3-T6 are compensated to continuously redirect the wake. Judging further from Figure 5.1.7 it appears that the actual benefit from such yaw angles distribution is accumulated mainly at T7, which in fact is exposed to significantly higher wind speed (+0.6 m/s *vs* baseline) and does not lose the power due to yawing (+160 kW *vs* baseline). Similarly, the power gain at T8 is observed (+80 kW *vs* baseline) as it is aligned with the freestream wind direction and exposed to a slightly modified flow field (+0.2 m/s *vs* baseline) as a result of the combination of multiple redirected wakes.

(2) Optimal yaw control with the Gauss wake model

The visualization of the Gaussian-shaped wake velocity field with the optimized control strategy is depicted in the corresponding horizontal (Figure 5.1.2) and vertical (Figure 5.1.4) snapshots. In this case, the yaw control set-points distribution is different than the one in x0_G vector. The most favourable strategy turns out to be keeping all the upstream turbines up to T7 yawed by around 20° and T8 aligned with the undisturbed wind. With such configuration, the major gains in power are at T2, T3 and T8 (+115 kW, +80 kW, +175 kW) while nearly the same effective wind speed increase of roughly 0.4 m/s is observed at each machine. In contrast to the Jensen wake model, yawing T1 is found to be beneficial in terms of total farm power and it also appears to be the only turbine that reports a power drop (-200 kW *vs* baseline). Such an outcome of the yaw control strategy supports the idea to sacrifice the power at the upstream machines to increase the power at the downstream ones. The Gaussian shape of the wake profile is considered to have the largest influence on the resulting yaw distribution. Thanks to such wake characteristics less power has to be sacrificed, as yawing any upstream machine even by a small angle immediately affects the inflow at the next downstream turbine.

(3) Optimal yaw control with the GCH wake model

The flow field predicted with the GCH wake modelling approach and the optimal yaw control strategy is presented in the bottom snapshots of Figure 5.1.2 and Figure 5.1.4. A considerably larger total power gain is achieved (+1 100 kW *vs* baseline) compared to the previous simulation cases. The distribution of the optimal yaw settings in Figure 5.1.6 illustrates well the impact of the yaw-induced effects. The largest yaw offset is applied at the first two machines and it gradually falls down at the subsequent downstream ones. Moreover, the partial wake overlap observed at T5 and T8 in Figure 5.1.4 is noticeably larger when compared to the Gauss wake model. The effective wind speed increase at each downstream turbine is of approximately 0.65 m/s compared to the baseline control. This, in turn, results in significant power gains at T2 – T8 (+1410 kW cumulatively *vs* baseline) that largely exceed the power loss due to yawing at T1 (-310 kW *vs* baseline). It is very apparent that although subsequent turbines apply smaller yaw offset, the effective wind velocity at the machines remains nearly constant (7 m/s). Thus, the differences in power gains between the turbines are due to the different magnitude of the yaw setting. Interestingly, the optimal yaw angle at T8 is found to be -1° instead of the intuitive 0°. Besides, the impact of the secondary steering effect can be observed in the flow field behind T8 in Figure 5.1.2 and Figure 5.1.5, as its wake is still being redirected and the effective wind speed increases even though the turbine is nearly aligned with the freestream wind.

To sum up, based on the RC simulation results, it is apparent that the use of different approaches of wind farm aerodynamics modelling substantially impacts the solution of yaw control optimization. The discrepancies are observed for the interrelated yaw offsets distribution, alteration of the flow field within the farm, and magnitude of resulting power changes at individual machines. For a broader understanding of this impact, it is important to further examine the effectiveness of yaw-based wake control under different wind conditions and plant layouts.

5.2 High wind speed

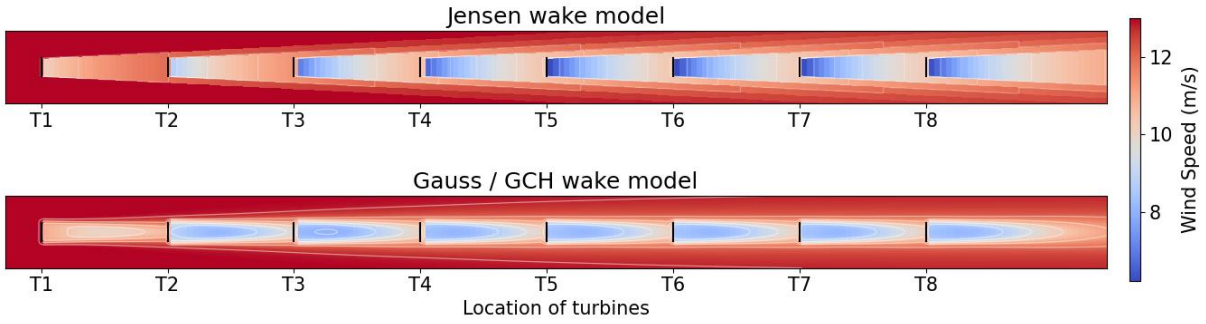

Figure 5.2.1 Hub height flow field with baseline yaw settings – HWS

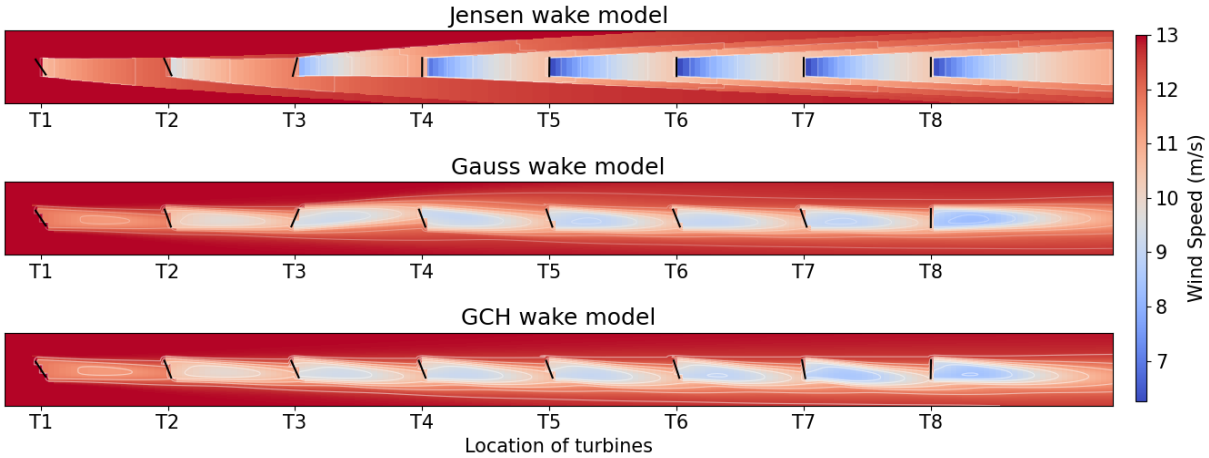

Figure 5.2.2 Hub height flow field with optimized yaw settings – HWS

Table 5.2.1 Summary of the results for the HWS simulation

Wake model	**Baseline WF power [kW]**	**Optimized WF power [kW]**	**ΔP [%]**	**No. of iterations**
Jensen	33 934	34 799	2.55	100
Gauss	31 303	33 580	7.27	32
GCH	31 303	36 442	16.42	100

The high wind speed simulation case parameters (w_s = 13 m/s, w_d = 270°, T_I = 0.075, spc = 7D) represent wind conditions for which the freestream wind velocity exceeds the rated wind speed (11.4 m/s) of NREL 5-MW turbines. As a result, the wind farm power output is large and the wake losses are moderate, yielding 14.9% and 21.5% (-5 927 kW and -8 558 kW *vs* the cumulative power of isolated turbines) for the Jensen and Gauss / GCH wake models, respectively. Also, the front machine, being exposed to the undisturbed wind, operates in the third control region (at rated power) while the downstream ones remain in the second control region (working at maximum C_P). The sensitivity of power change due to an increase in effective velocity is high for the wind velocities close to the rated wind speed. Therefore, exposing the downstream turbines to higher wind speeds and switching to the third control region should have a meaningful impact on the plant power output.

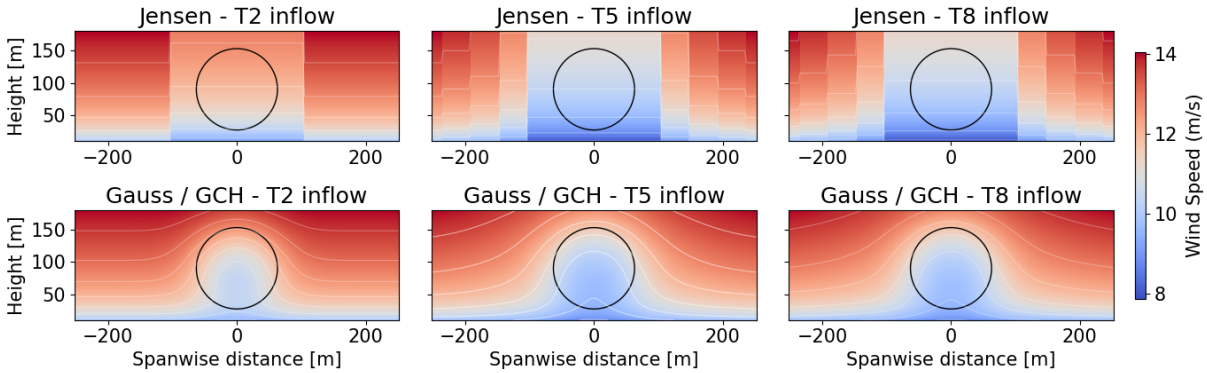

Figure 5.2.3 Velocity field 0.5D ahead of T2, T5 and T8 with baseline yaw settings – HWS

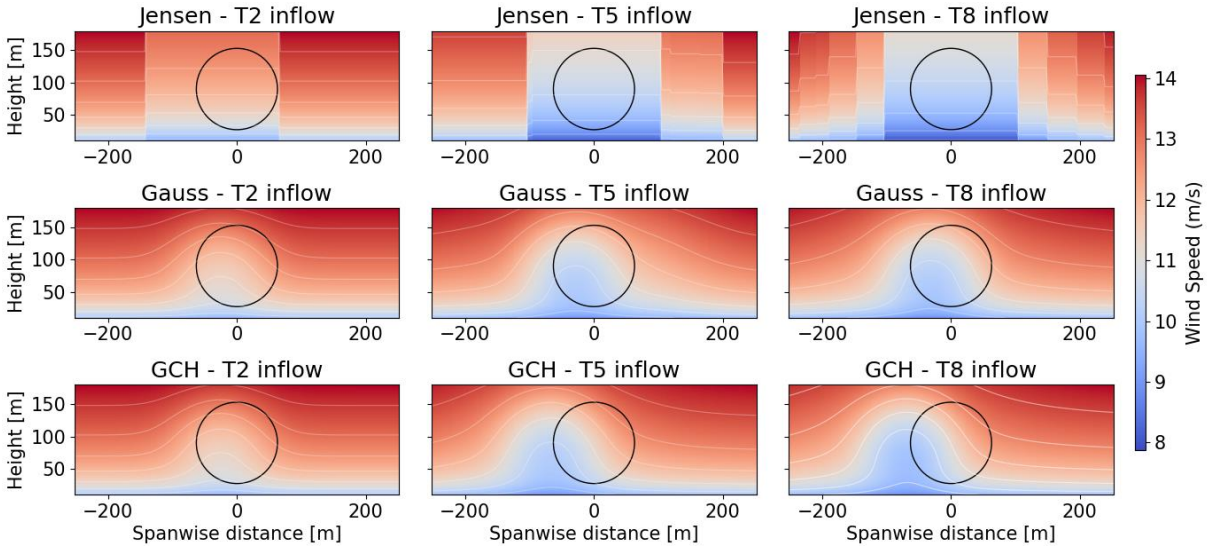

Figure 5.2.4 Velocity field 0.5D ahead of T2, T5 and T8 with optimized yaw settings – HWS

The park performance under high wind speed for baseline and optimized yaw settings is summarized in *Table 5.2.1*. Unlike in the RC simulation, here the total power generation with greedy control is larger for the Jensen model, which predicts significantly higher wind speeds, and consequently the power output at T2 – T4, as observed in Figure 5.2.5 an Figure 5.2.7. The results of yaw control optimization are discussed below.

(1) Optimal yaw control with the Jensen wake model

The plant-wise power gain of 2.55 % (+865 kW *vs* baseline) is reported for the optimization with the Jensen wake model. Interestingly, a large yaw offset (+34°) was suggested at T1 (Figure 5.2.6), which is on the verge of causing a partial wake overlap situation at T2 (Figure 5.2.4). This is consistent with the engineering intuition and supports the earlier assumption regarding the advantage of yawing the first turbine with the Jensen model employed. Additionally, T1 does not experience any yaw-induced power loss as it still operates above the rated wind speed. In general, it shows that the optimization algorithm correctly "understood" the farm behaviour under HWS conditions and proposed a reasonable solution. The second turbine also applies large yaw offset and ensures operation at rated power while the distribution of yaw misalignments at further machines is not intuitive. For some reason, it is better to yaw T3 in the negative direction and keep the remaining turbines nearly aligned with the freestream wind (yaw magnitude up to -0.5°). Thanks to such wake redirection strategy, T2 and T3

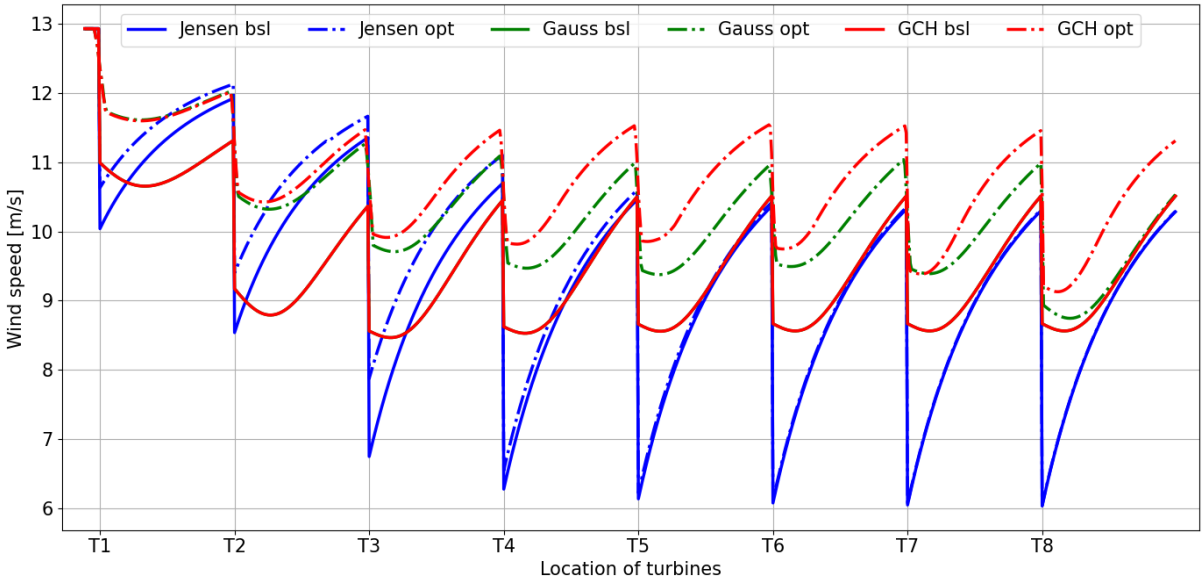

Figure 5.2.5 Evolution of rotor swept area-averaged wind velocity along the wind farm – HWS

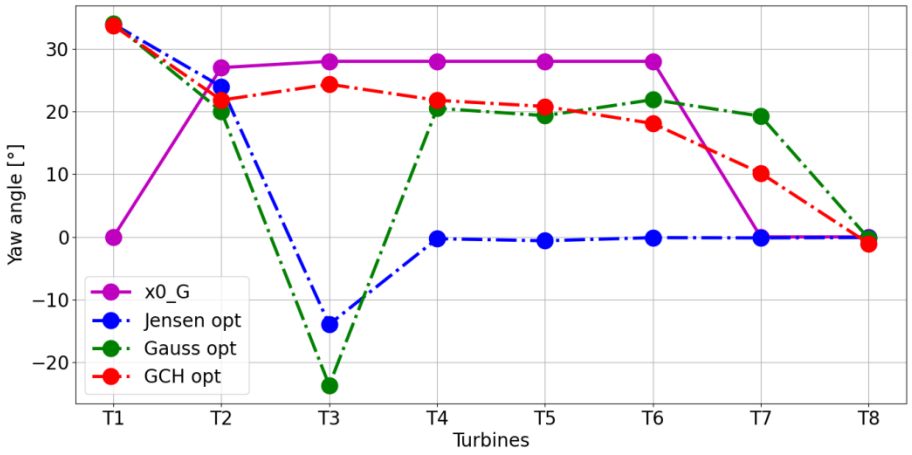

Figure 5.2.6 Yaw distribution in x0_G vector and the optimization solutions – HWS

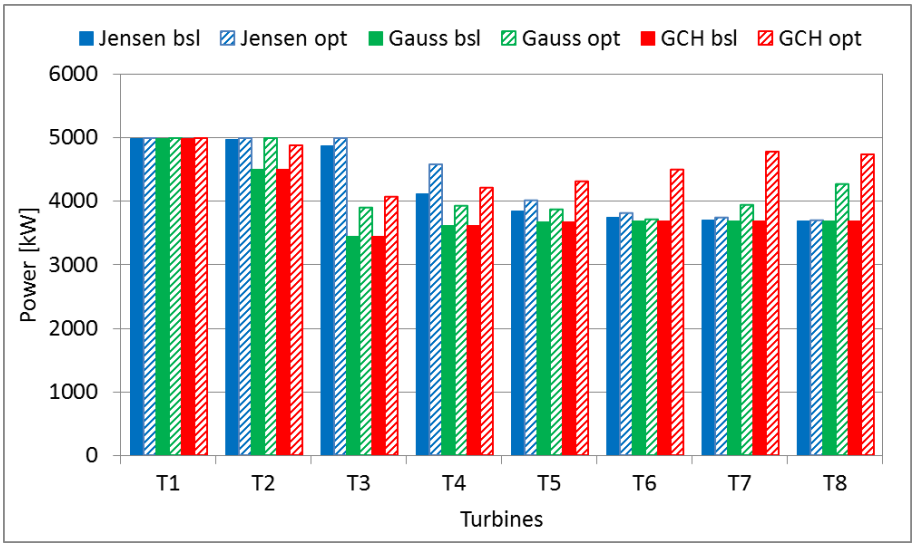

Figure 5.2.7 Power distribution with baseline and optimized yaw settings – HWS

switched to operation at rated power, T4 experiences significant power gain (+467 kW *vs* baseline) while T5 reports a minor increase (+156 kW *vs* baseline). The apparent wind velocity slowly evens out starting from T6 and so does the power output of the remaining machines. It is also observed that the incident distribution of yaw angles deviates significantly from the starting vector $x0\_G$.

(2) Optimal yaw control with the Gauss wake model

Employing the Gauss wake model for yaw control optimization results in the total wind farm power increase of 7.27% (+2 277 kW *vs* baseline). Again, the largest yaw angle is applied at T1, with magnitude corresponding to the value suggested for the Jensen wake model. In fact, as T1 is exposed to the undisturbed wind it is expected that this particular machine will apply the same yaw offset regardless of the utilized wake modelling approach. Despite applying a +20° yaw angle misalignment, T2 operates at rated power (+500 kW *vs* baseline), leading to a substantial wind speed increase at T3 (+1 m/s *vs* baseline). It is not understandable why T3 applies a large negative yaw offset (-24°) resulting in deflection of the wake in the opposite direction with associated power gain of +445 kW *vs* baseline. It appears that it is the best setting in terms of plant-wise benefits that the optimization algorithm could find. As opposed to the predictions using the Jensen wake model, the further downstream turbines apply a yaw angle misalignment of around +20°, while the last one is aligned with the freestream. The resulting power gains are distributed among T4, T5, T7 and T8, with the latter one contributing the most to the power gain due to lack of yaw-induced power losses.

(3) Optimal yaw control with the GCH wake model

The total power gain reported with GCH model amounts to as much as 16.42% (+5 139 kW *vs* baseline), considerably exceeding the two previous results. Consistently with the other models, T1 is yawed at +34° and produces rated power. The yaw misalignment at T2 yields +22° and increases to 24° at T3. Then, a gradual drop in yaw offset is seen at the subsequent turbines till the end of the row. The flow field modification due to such yaw distribution is significant, as depicted in Figure 5.2.5. It appears that the wind velocity recovers to the rated speed before reaching each machine, however, due to yaw-induced power losses the rated power cannot be achieved. Nevertheless, the incident power gains at individual turbines range between +400 kW to nearly 1.1 MW across the wind farm. The impact of the secondary steering effect is very noticeable, especially at the rear turbines, which effectively redirect the wake with successively smaller applied yaw errors while showing increasing power gains.

To summarize, yaw-based wake steering is also recommended for higher wind speeds conditions. The predictions of yaw distribution and the resulting power gains are very different between the investigated models. It is not clear why no change in yaw settings is obtained for the rear turbines when the Jensen wake model is employed. Presumably, the wake recovery is efficient enough so that the yaw-induced power losses would not be overcome by the gains at the successive downstream machines. Also, it is doubtful whether T3 should operate with a negative yaw setting, as predicted with the Jensen and Gauss models. Unquestionably, the results obtained for the GCH wake modelling approach indicate there is a very large potential for wind farm power improvement event at high wind speeds.

5.3 Low wind speed

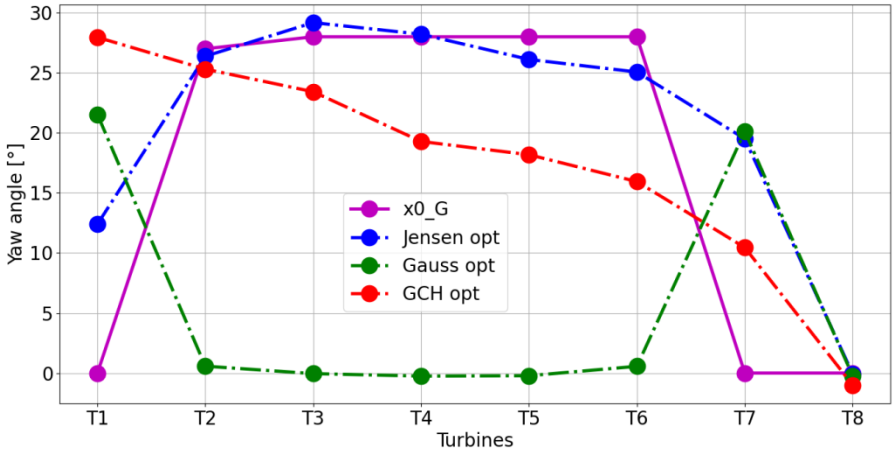

Figure 5.3.1 Yaw distribution in x0_G vector and the optimization solutions – LWS

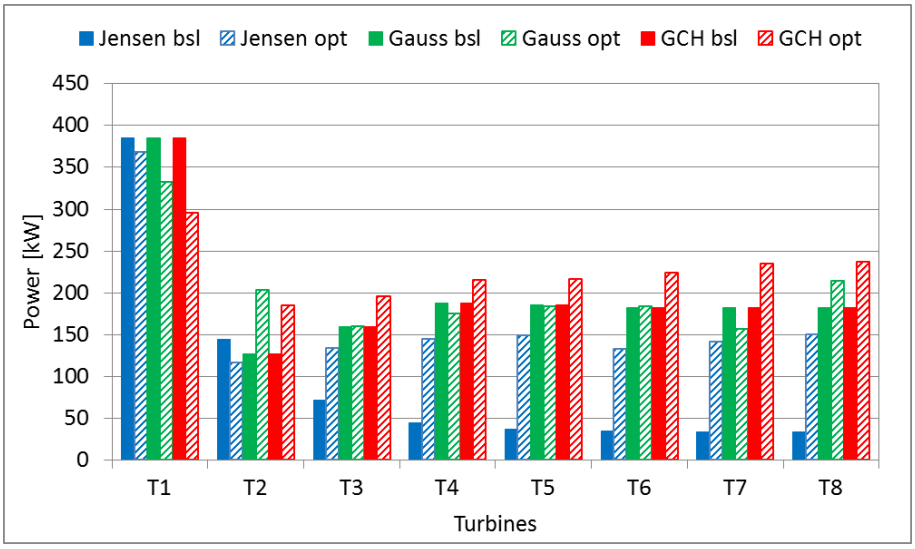

Figure 5.3.2 Power distribution with baseline and optimized yaw settings – LWS

Table 5.3.1 Summary of the results for the LWS simulation

Wake model	Baseline WF power [kW]	Optimized WF power [kW]	ΔP [%]	No. of iterations
Jensen	785	1 332	69.61	97
Gauss	1 591	1 606	0.95	100
GCH	1 591	1 799	13.11	98

The low wind speed simulation case (w_s = 5 m/s, w_d = 270°, T_I = 0.075, spc = 7D) is the opposite scenario to the HWS simulation, which intends to assess the applicability of yaw control in a wind farm exposed to wind resource of low energy and unfavourable direction. Since the present scenario is considered less relevant than its HWS counterpart, it was decided to limit the number of figures only to these presenting the distribution of yaw set-points and power output of individual turbines. The flow field visualization and rotor swept area wind velocity evolution throughout the park are shown in Annex C.1. The same measure was applied to WD_265°,

LTI and LS simulation cases.

For the greedy yaw control, a large discrepancy in wind farm power between the models is reported, as visible in Figure 5.3.2. The wake losses under low wind speed are 74.5% and 48.3% (-2 292 kW and -1 487 kW *vs* the cumulative power of isolated turbines) for the Jensen and Gauss / GCH wake models, respectively. It appears that the velocity deficit predicted with the Jensen model is significantly deeper, resulting in low effective wind speeds at the downstream machines. The results of the yaw control optimization are summarized in *Table 5.3.1*.

(1) Optimal yaw control with the Jensen wake model

The magnitude of power improvement achieved with the Jensen wake model is relatively large (+547 kW *vs* baseline). The resulting yaw settings indeed effectively redirect the wake creating partial wake overlap at the downstream machines, which in turn brings about large power gains at the successive machines. However, in the light of such small baseline farm yield and the limitations of the Jensen model, the credibility of such an outcome in a real wind farm is doubtful.

(2) Optimal yaw control with the Gauss wake model

Based on the results obtained for the Gauss wake model in terms of both the total power gain (+15 kW *vs* baseline) and the yaw angles distribution, it appears that the application of yaw control is not beneficial at low wind speeds.

(3) Optimal yaw control with the GCH wake model

The results obtained for the GCH wake model are to some degree consistent with the previous observations of its impact on yaw control optimization. The power gain of 13.11% (+108 kW *vs* baseline) is reported caused by a gradually decreasing yaw offset applied at subsequent turbines.

In conclusion, even though the obtained numbers plead in favour of the potential to improve the farm power using yaw-based wake redirection, the advantage of its application is not evident. Under low wind speed conditions, considerable discrepancies between the predictions of the employed models are observed for both the baseline and optimized yaw control. It is assumed that the Jensen wake model underpredicts the total power when the machines are aligned with the flow and promises significant power gains with optimized yaw settings. The Gauss wake model, which is believed to be more credible, predicts much larger baseline farm power but optimization results in very modest yield improvement. Owing to the inclusion of yaw-induced effects, the GCH model proposes a promising solution in terms of power gains. However, taking into account the level of achieved power gains and the magnitude of the required yaw angle offsets, the actual viability of yaw control is questionable. A more in-depth study on this method including its impact on the loads should be carried out to credibly assess the potential benefits of its application under low wind speed conditions.

5.4 Wind direction 275°

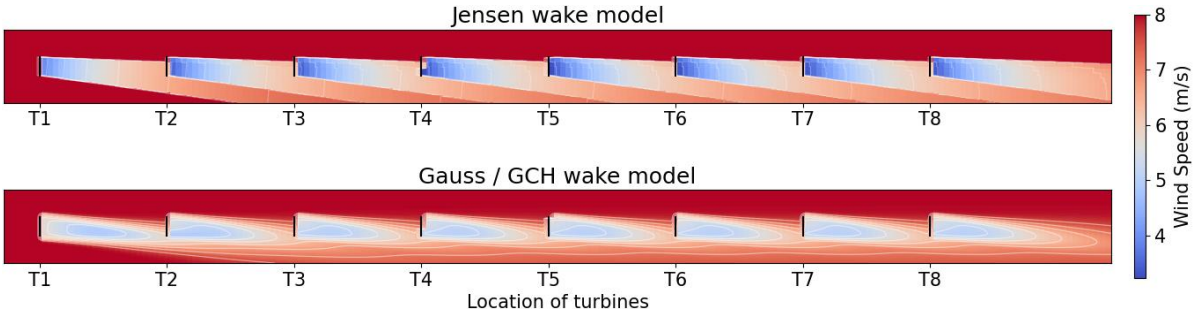

Figure 5.4.1 Hub height flow field with baseline yaw settings – WD_275°

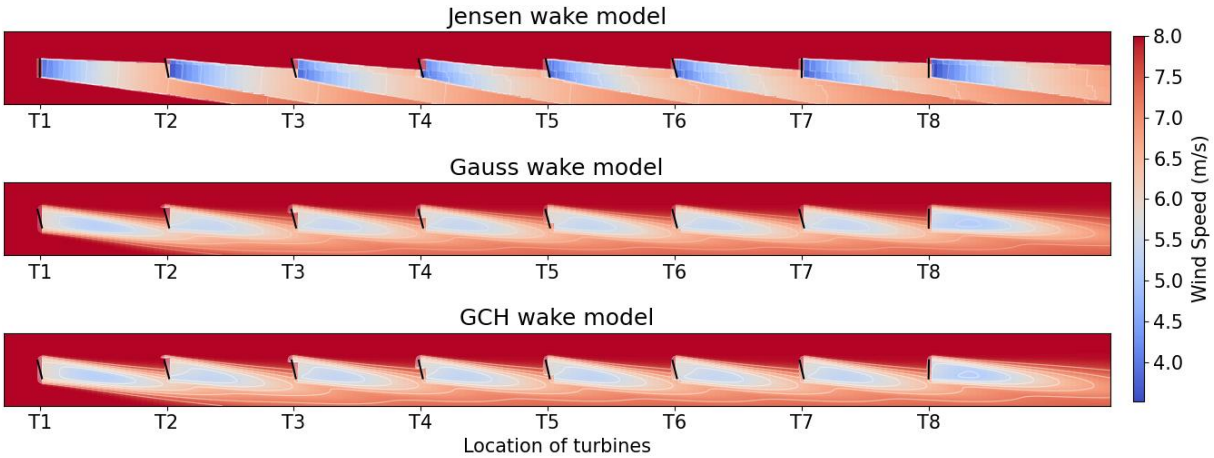

Figure 5.4.2 Hub height flow field with optimized yaw settings – WD_275°

Table 5.4.1 Summary of the results for the WD_275° simulation case

Wake model	Baseline WF power [kW]	Optimized WF power [kW]	ΔP [%]	No. of iterations
Jensen	8 937	10 941	22.42	99
Gauss	10 228	11 084	8.37	100
GCH	10 228	11 291	10.40	100

The wind direction 275° simulation case parameters (w_s = 8 m/s, w_d = 275°, T_I = 0.075, spc = 7D) represent a situation when partial wake overlap is naturally achieved, as observed in Figure 5.4.1 and Figure 5.4.3. As a consequence, the turbines operating with greedy yaw control generate more power (+1 792 kW for Jensen and +2 722 kW for Gauss / GCH) compared to the RC baseline yaw control simulation. However, the farm power loss due to the wake effect is still present and amounts to 34.1% and 24.6% (-4 626 kW and -3 335 kW *vs* the power of isolated turbines) for the Jensen and Gauss / GCH wake models, respectively.

The plant-wise power prediction for the baseline and optimized yaw control strategies is summarized in *Table 5.4.1*. Similarly to the RC simulation, the baseline wind farm power obtained for the Jensen's wake modelling approach is smaller than the one predicted with the Gauss / GCH models. In the WD_275° simulation case, the reason behind it is due to the very different wake characteristics of these models. Based on Figure 5.4.3, it is apparent that the area of the wake overlap at the downstream machines is significantly larger for the Jensen

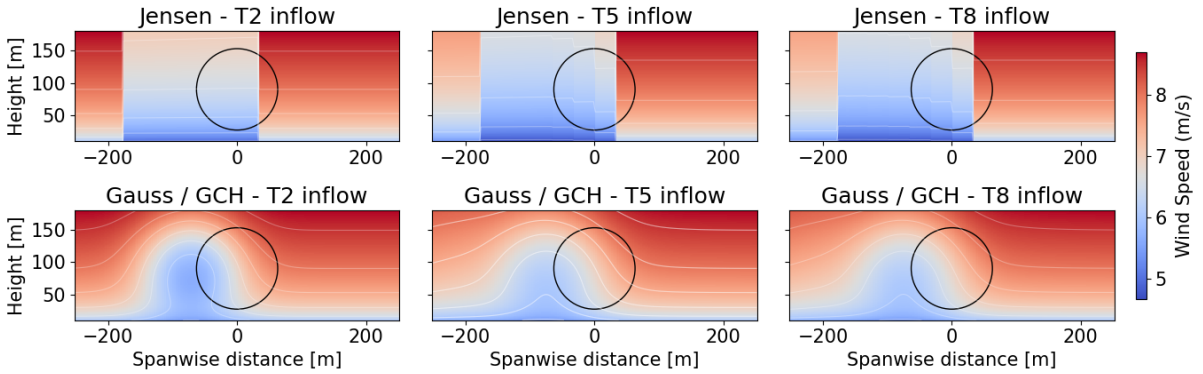

Figure 5.4.3 Velocity field 0.5D ahead of T2, T5 and T8 with baseline yaw settings – WD_275°

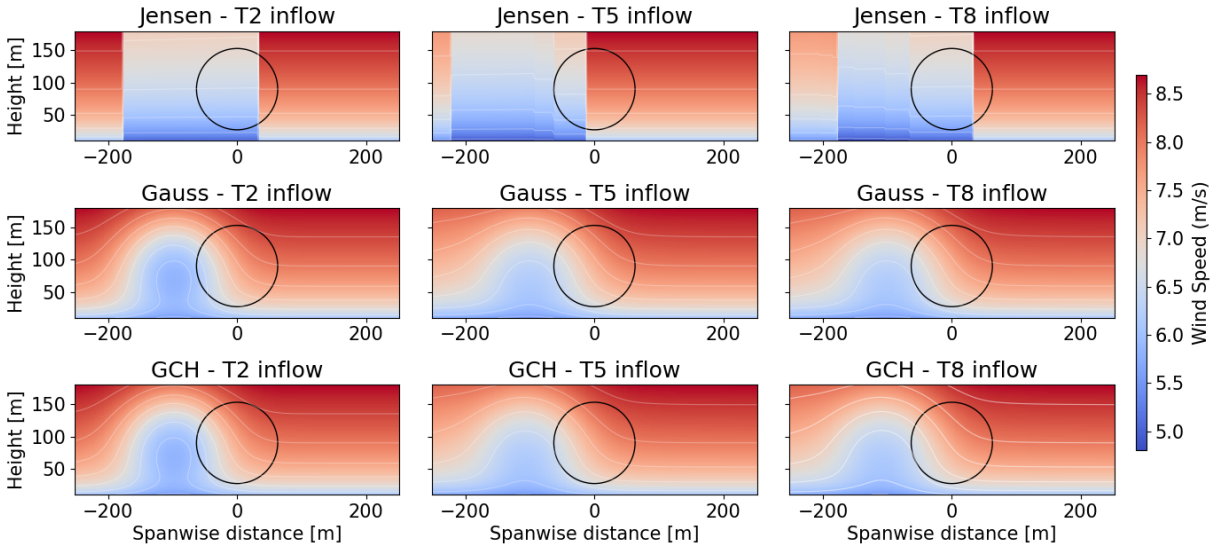

Figure 5.4.4 Velocity field 0.5D ahead of T2, T5 and T8 with optimized yaw settings – WD_275°

model, resulting in lower effective wind velocities affecting the rotors. This is also confirmed by the evolution of the rotor swept area wind velocity along the wind farm for the baseline yaw control in Figure 5.4.5. Moreover, this figure allows to observe the wiggles in the velocity evolution obtained with the Jensen model due to its "binary", non-smooth wake boundary.

(1) Optimal yaw control with the Jensen wake model

The reported total power gain with the optimal yaw control settings yields 22.42 % (+2 004 kW *vs* baseline) and is the largest improvement among the considered wake models under present wind conditions. A noticeable change in the inflow conditions at T5 can be observed in Figure 5.4.4. Similarly to the RC simulation results, T1, T7 and T8 are selected to remain aligned with the freestream wind. However, the interior machines T2 – T6 are yawed by the angle between 10° and 15°. Such yaw settings distribution results in a modification in the effective wind flow at T2 (+0.65 m/s *vs* baseline) and T3 – T7 (+1 m/s *vs* baseline), which in turn brings about significant power gains at these turbines, as displayed in Figure 5.4.7. In this scenario, only a small fraction of power at T2 is sacrificed (-35 kW *vs* baseline). Understandably, the present wind direction is favourable for the yaw control using Jensen's wake characteristics as the region of inconsequent yawing that is required before a partial wake overlap situation at a downstream rotor is achieved is completely omitted.

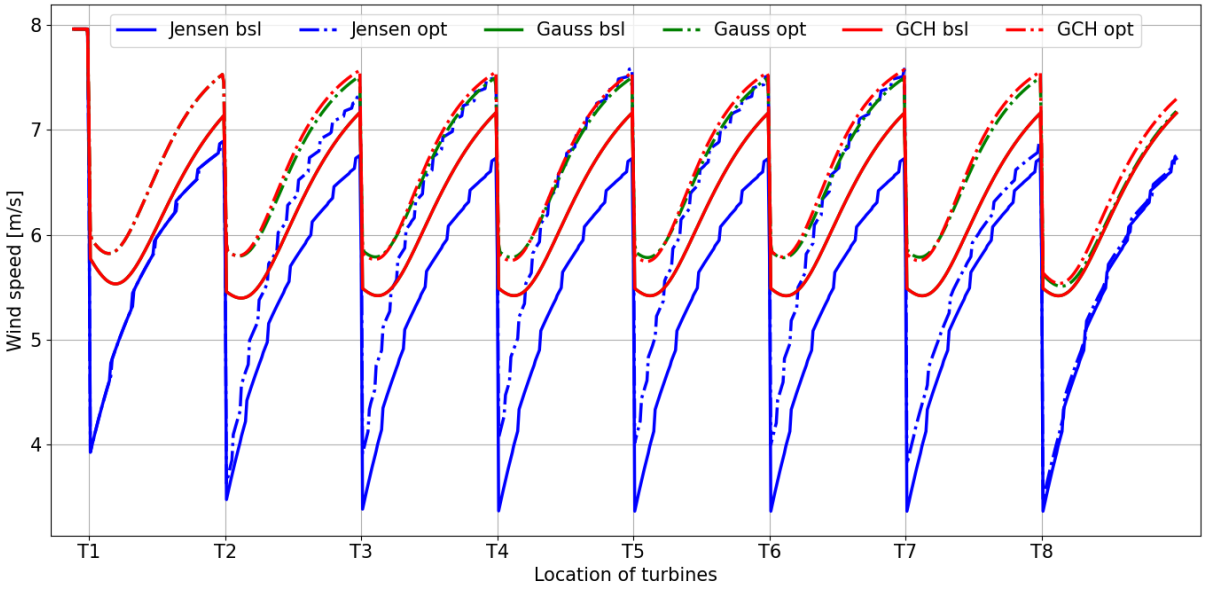

Figure 5.4.5 Evolution of rotor swept area-averaged wind velocity along the wind farm – WD_275°

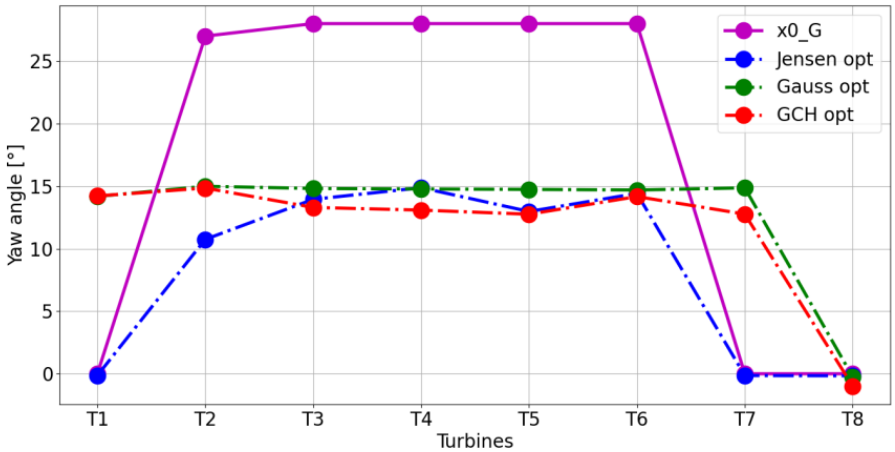

Figure 5.4.6 Yaw distribution in x0_G vector and the optimization solutions – WD_275°

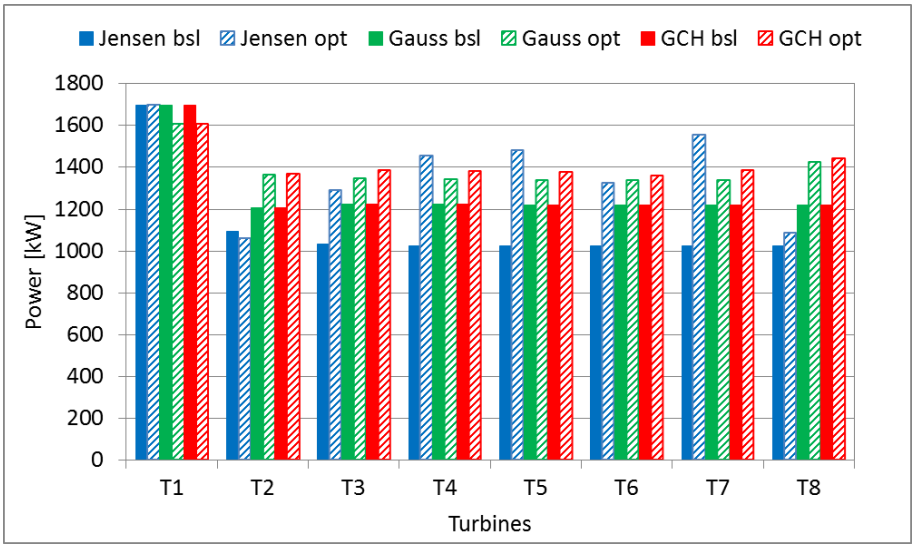

Figure 5.4.7 Power distribution with baseline and optimized yaw settings – WD_275°

(2) Optimal yaw control with the Gauss wake model

The predicted plant-wise power improvement due to the optimized yaw control using the Gauss wake modelling method yields 8.37 % (+856 kW *vs* baseline). The overall pattern of the yaw angles distribution closely resembles the one obtained in the RC simulation, however, the magnitude of yaw offsets is smaller. The optimized yaw settings applied at T1 – T7 are approximately 15° at each machine whereas the last one is aligned with the undisturbed wind direction. Consequently, the downstream machines T2 – T8 are exposed to higher effective wind velocity (+0.5 m/s *vs* baseline), which in turn results in the evenly distributed power gains presented in Figure 5.4.7. The achieved power improvement is significantly larger compared to the RC simulation with the Gauss wake model. The reason behind it lies in the fact that velocity deficit is accumulated in the centre of the Gaussian wake. Due to the wake redirection, its centre avoids passing through the rotor area at all inflow conditions captured in Figure 5.4.4.

(3) Optimal yaw control with the GCH wake model

Employing the GCH wake model for the optimization of yaw set-points results in the total power improvement of 10.4 % (+1 063 kW *vs* baseline). For the simulations with both Gauss and GCH wake models, a power drop at T2 (-90 kW *vs* baseline) is observed. Also, the obtained distributions of the optimized yaw angles are similar, however, with a modest decrease in the magnitude at T3 – T5 and T7. Due to the secondary steering effect, the same effective wind velocity at the downstream turbines is achieved, as given in Figure 5.4.5. This in turn makes the power gains at individual machines larger than those achieved with the Gauss model. It is important to notice that the impact of the secondary steering is not as considerable as it was in the RC simulation with full wake overlap at each downstream rotor.

To sum up, it appears that although under present wind conditions the wake loses are naturally reduced compared to RC conditions, the potential for power improvement is still great. Despite some minor discrepancies, all three models are in a relatively good agreement and support that statement. When the wind direction slightly deviates from the direction of turbines alignment, as seen in this example, the downstream machines naturally operate with the increased cyclic loads due to partial wake overlap situations. Presumably, in such cases, wake redirection could not only enable a significant power improvement but also reduce these adverse loads. It is recommended that the investigation of this matter receives more attention in future works. In addition, according to the consecutive optimization solutions history presented in Figure B.4 of Annex B, incorrect behaviour of the optimization algorithm is observed when the Jensen wake model was employed. For some reason, the algorithm chooses to start the 27-th and 46-th iterations with a solution that lowers the already achieved wind farm power improvement and terminated with a sub-optimal solution.

5.5 Wind direction 265°

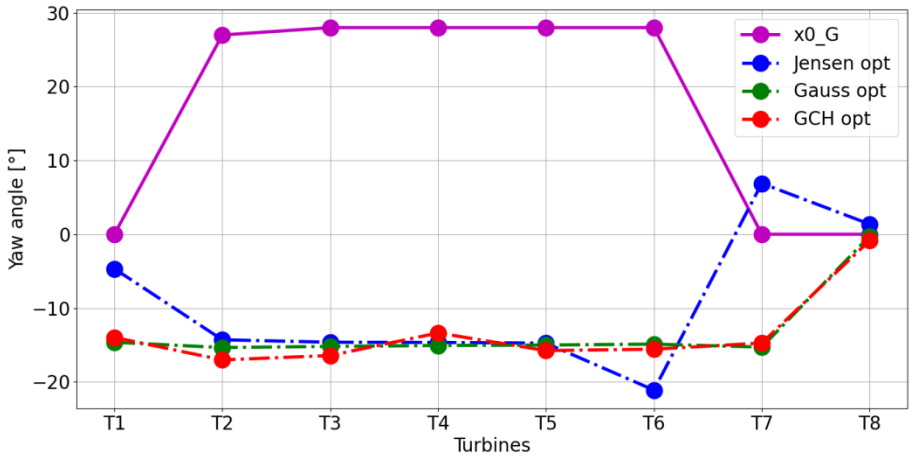

Figure 5.5.1 Yaw distribution in x0_G vector and the optimization solutions – WD_265°

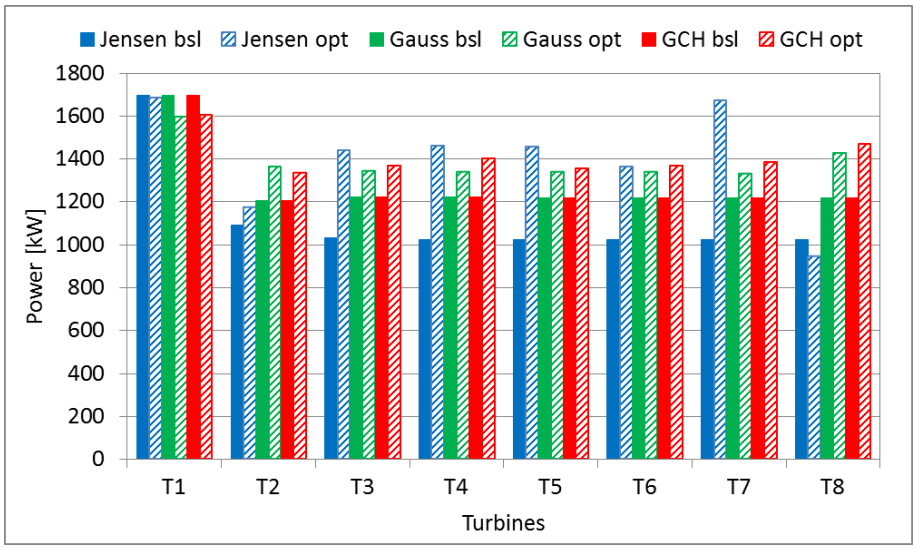

Figure 5.5.2 Power distribution with baseline and optimized yaw settings – WD_265°

Table 5.5.1 Summary of the results for the WD_265° simulation case

Wake model	Baseline WF power [kW]	Optimized WF power [kW]	ΔP [%]	No. of iterations
Jensen	8 937	11 204	25.37	100
Gauss	10 228	11 084	8.37	100
GCH	10 228	11 300	10.48	100

The wind direction 265° simulation (w_s = 8 m/s, w_d = 265°, T_I = 0.075, spc = 7D) intends to examine the applicability of yaw control when the wind deviation is in the opposite direction to that of WD_275° conditions. In the present scenario with the baseline yaw settings, the downstream turbines naturally operate in partial wake overlap as presented in Figure 5.4.3 but the wake is shifted to the right. The predicted baseline power and the associated wake losses are exactly the same as they were in WD_275° simulation. However, it is of interest to observe how the change of wind direction impacts the predictions of the models and the optimization of yaw

control, which results were summarized in *Table 5.5.1*. The flow field visualization and rotor swept area wind velocity evolution throughout the park are shown in Annex C.2.

(1) Optimal yaw control with the Jensen wake model

The achieved farm power gain of as much as 25.37% (+2 267 kW *vs* baseline) is reported using the Jensen wake model, which is larger than the one obtained in the corresponding WD_275° simulation. This finding is very interesting given that both the Jensen and Jiménez models do not account for any effects that could lead to a different velocity field predictions depending on the direction of yaw misalignment. The suggested optimal yaw settings are noticeably different compared to WD_275° simulation. Here, the first turbine is yawed at -5°, the latter T2 – T5 yaw approximately -15°, T6 is yawed at -21°, T7 at +7° and lastly T8 at +1.5°. The power gains are accumulated in the interior turbines, with the largest at T7. However, it is not clear why T7 and T8 apply positive yaw angles as it is certain to cause power losses.

(2) Optimal yaw control with the Gauss wake model

The magnitude of wind farm power improvement obtained with the Gauss wake modelling approach corresponds to that achieved in WD_275° simulation. The yaw angles distribution in the park is the same but with the opposite sign while the resulting power gains at individual turbines are identical as for WD_275° conditions. Based on the knowledge of the model, this is expected behaviour since this wake modelling method does not account for any effects related to the direction of yawing.

(3) Optimal yaw control with the GCH wake model

Although the achieved level of farm power improvement is nearly the same as in WD_275° simulation, the incident distribution of the yaw settings is a bit different for the GCH wake model. As expected, the yaw angles at T1 – T7 become negative, however, the magnitude of yaw errors applied at T2, T3, T5-T7 increases by 1.5° to 3°. This suggests that larger yaw misalignment had to be set to achieve nearly the same power as for WD_275° conditions. In other words, it appears that yawing in the negative direction is less effective, which is attributed to the impact of wake rotation vortex.

To sum up, negative yaw offsets were proposed for each wake modelling approach except for some inconsistencies reported for the Jensen wake model. The reason behind these deviations is not known but it is presumed to be purely due to the intricacies of the optimization algorithm. The robustness of yaw control optimization with the Jensen wake model was already shown to be doubtful and the present results support this statement. Nevertheless, a promising level of power gains was reported in each optimization and the Gauss-profile-based models behaved according to expectations.

5.6 High turbulence intensity

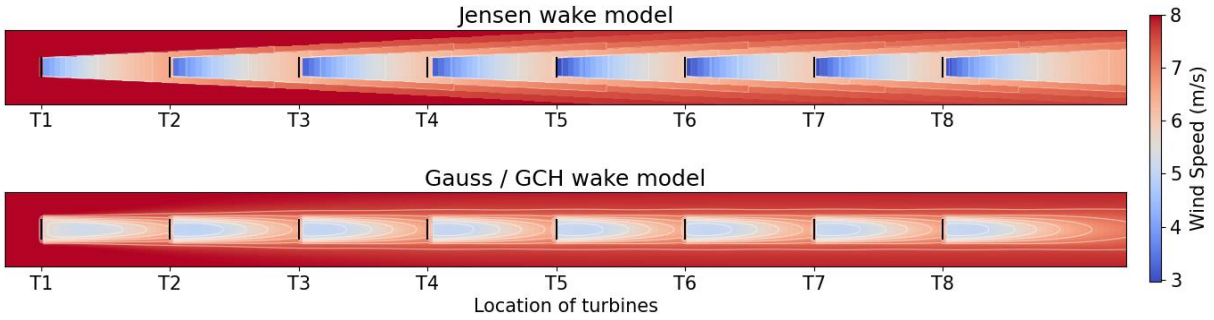

Figure 5.6.1 Hub height flow field with baseline yaw settings – HTI

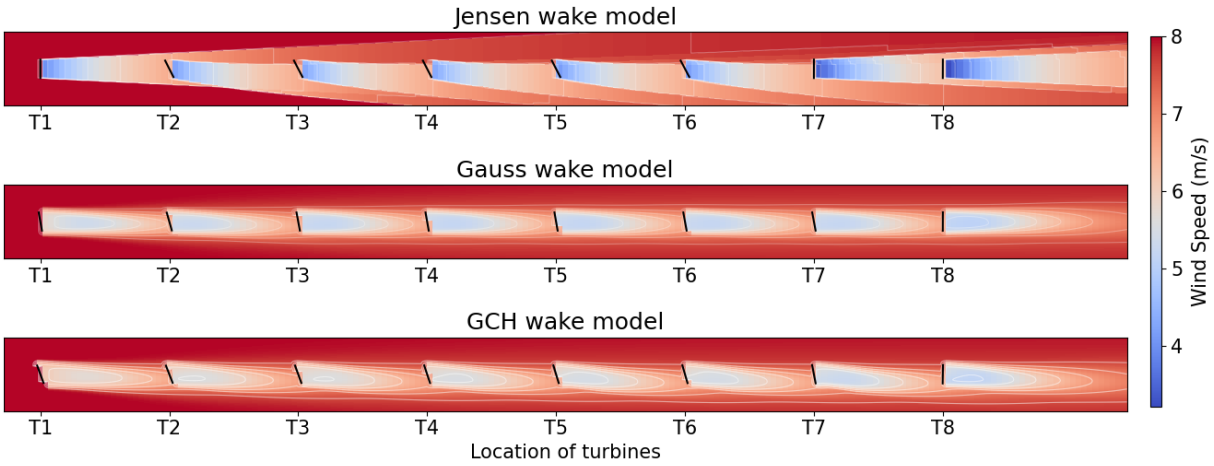

Figure 5.6.2 Hub height flow field with optimized yaw settings – HTI

Table 5.6.1 Summary of the results for the HTI simulation case

Wake model	Baseline WF power [kW]	Optimized WF power [kW]	ΔP [%]	No. of iterations
Jensen	7 145	7 393	3.46	100
Gauss	8 407	8 430	0.27	100
GCH	8 407	8 884	5.67	100

The high turbulence intensity simulation case parameters (w_s = 8 m/s, w_d = 270°, T_I = 0.1, spc = 7D) represent wind conditions characterized by moderate speed, unfavourable wind direction and increased free stream turbulence. It is known that higher turbulence levels positively affect the wake recovery rate due to better turbulent mixing of the flow of the wake with the undisturbed wind. However, many old and strongly simplified wake models, like the one proposed by Jensen, do not directly account for the effect of the turbulence intensity. A common practice is to adjust the wake recovery constant so that the predicted wake resembles better the behaviour of the factual wake under given turbulence intensity level. On the other hand, the Gauss and GCH wake models account for both the turbulence intensity in the freestream and the added turbulence coming from the nearest upstream rotor. The incident turbulence level is then used to determine the local wake growth rate, which eventually affects the width of the Gaussian shape in spanwise and vertical directions as well as the magnitude of the velocity deficit inside the wake at a given downstream distance.

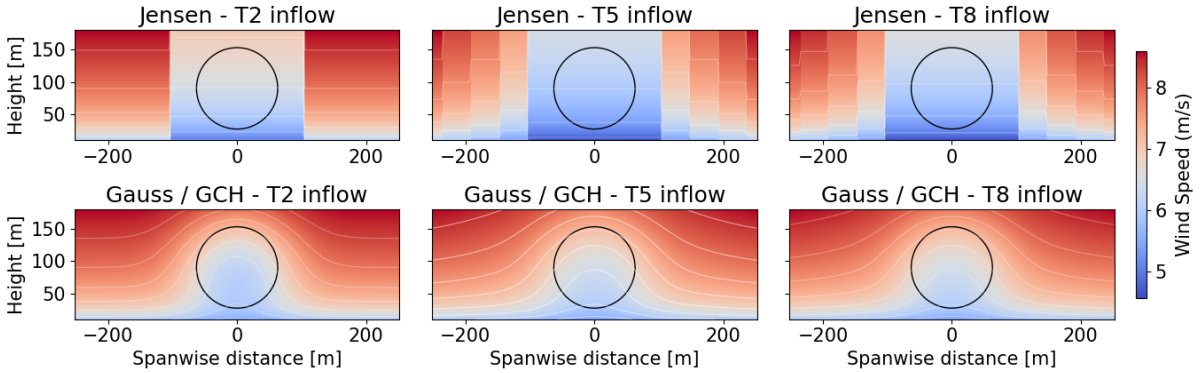

Figure 5.6.3 Velocity field 0.5D ahead of T2, T5 and T8 with baseline yaw settings – HTI

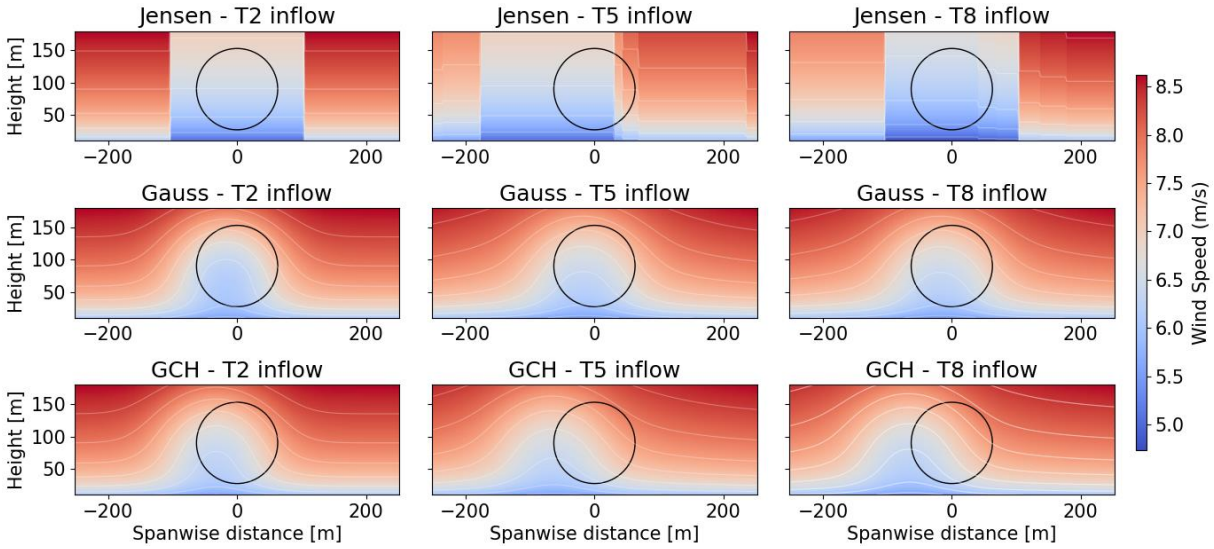

Figure 5.6.4 Velocity field 0.5D ahead of T2, T5 and T8 with optimized yaw settings – HTI

The wind farm power prediction for baseline and optimized yaw control set-points is summarized in *Table 5.6.1*. The present wake losses amount to 47.3% and 38% (-6 418 kW and -5 156 kW *vs* the cumulative power of isolated turbines) for the Jensen and Gauss / GCH wake models, respectively. An apparent farm power gain (+901 kW) due to increased turbulence level can be observed for the greedy yaw control using Gauss / GCH wake models versus the respective scenarios from RC simulation.

(1) Optimal yaw control with the Jensen wake model

Since the Jensen wake model does not directly account for the impact of turbulence within the flow, the optimization results are identical as those reported in the RC simulation. The assumption of the constant wake growth rate is likely unrealistic in the light of the present knowledge on the wake aerodynamics. This example shows the evident limitation of the Jensen wake model in terms of its application in studying yaw-based wake redirection wind farm control.

(2) Optimal yaw control with the Gauss wake model

A modest power improvement of 0.27 % (+23 kW *vs* baseline) is achieved for the Gauss wake modelling method. Due to the increased wake recovery rate, the effective wind speeds at the downstream turbines are

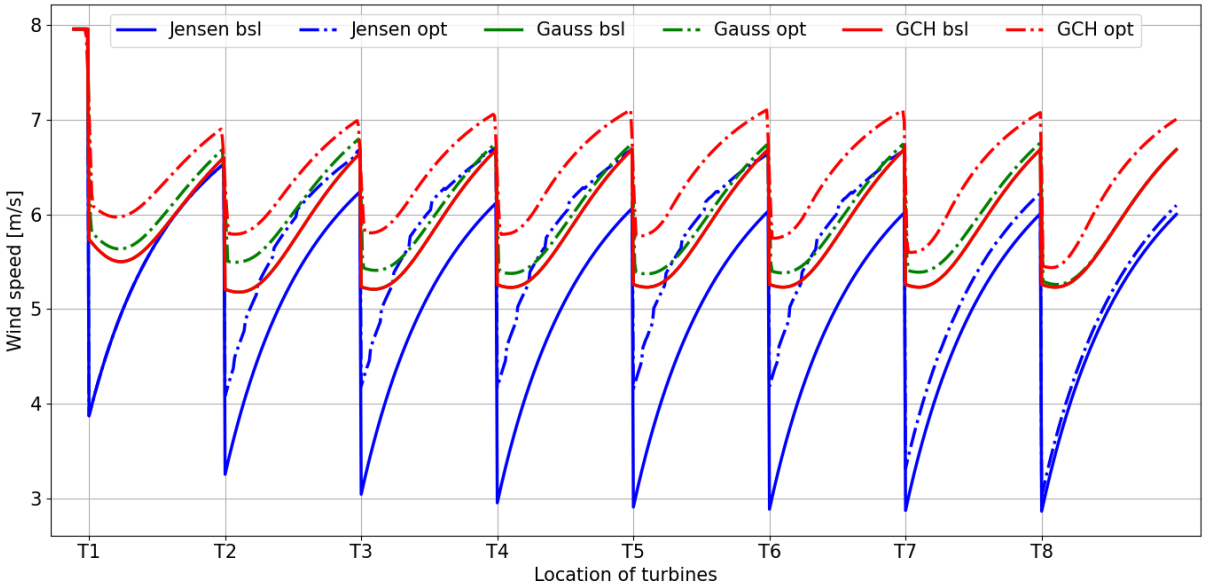

Figure 5.6.5 Evolution of rotor swept area-averaged wind velocity along the wind farm – HTI

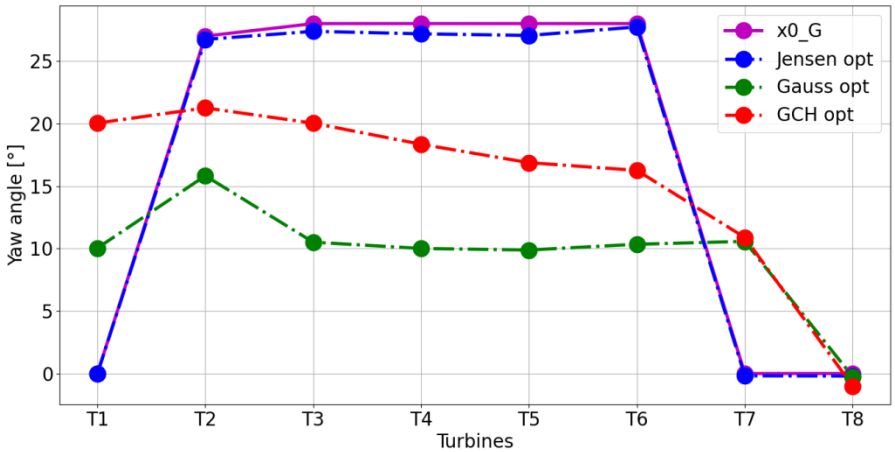

Figure 5.6.6 Yaw distribution in x0_G vector and the optimization solutions – HTI

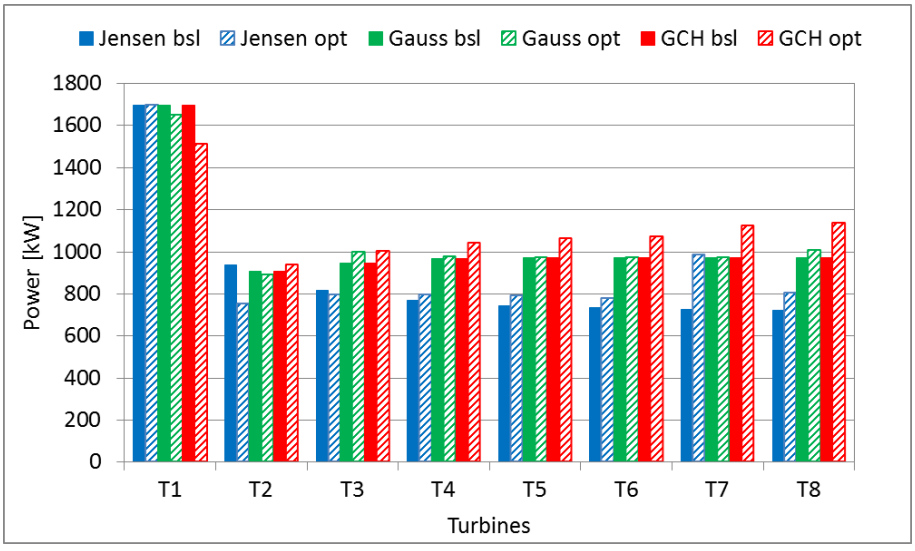

Figure 5.6.7 Power distribution with baseline and optimized yaw settings – HTI

substantially larger with the baseline yaw control when compared to the RC simulation. In fact, the values of rotor inflow wind velocity obtained with zero yaw misalignment shown in Figure 5.6.5 achieve the magnitude of the incident wind velocities with the optimized yaw settings in the respective RC scenario. The distribution of the optimal yaw angles in Figure 5.6.6 indicates that smaller yaw offsets are preferred, resulting in a small wake deflection as observed in Figure 5.6.4. Taking into account the resulting distribution of power output achieved at individual turbines in Figure 5.6.7. and the magnitude of the total power improvement, it is questionable whether the use of yaw-based wake redirection method is beneficial under highly turbulent winds. It appears that due to higher wake recovery the potential gains in power caused by redirecting the wake are compensated by the yaw-induced power losses.

(3) Optimal yaw control with the GCH wake model

Incorporation of the yaw-added wake recovery and secondary steering effect significantly changes the prediction of the wind farm performance with the optimized yaw control strategy. The total power gain of 5.67 % (+477 kW *vs* baseline) is achieved. The overall pattern of the optimized yaw settings distribution resembles the one obtained in the RC simulation. Larger yaw offsets are preferred at T1 – T3, which are reduced at the subsequent turbines to arrive at -1° at T8. The combined impact of the applied yaw errors and the secondary steering effect results in a substantial wake redirection as observed in Figure 5.6.2 and Figure 5.6.4. This in turn changes the rotor averaged wind velocity by approximately +0.4 m/s at each downstream machine. The distribution of power output along the turbines follows the opposite trend to one of the yaw angles. Power at T1 is sacrificed (-183 kW *vs* baseline) but is more than compensated by the gains at the remaining machines (+660 kW in total *vs* baseline).

To sum up, the high turbulence intensity simulation scenario revealed very insightful findings in terms of assessing the potential of yaw-based wake control. Depending on the fidelity of the applied model, substantially different yaw distributions are proposed by the optimization algorithm, which results in different levels of achieved power improvement. More specifically, it is impossible to examine the farm behaviour under changing turbulence intensities without manually adjusting the Jensen wake model. This wake modelling approach was again proven to be unsuitable for yaw control optimization. According to the predictions with the Gauss wake model, the magnitude of improvement is quite small and it is questionable whether yaw control should be employed. On the other hand, due to the secondary steering effect, the predictions of the GCH wake model give promising results and plead in favour of the potential of collaborative yaw control even for highly turbulent winds.

5.7 Low turbulence intensity

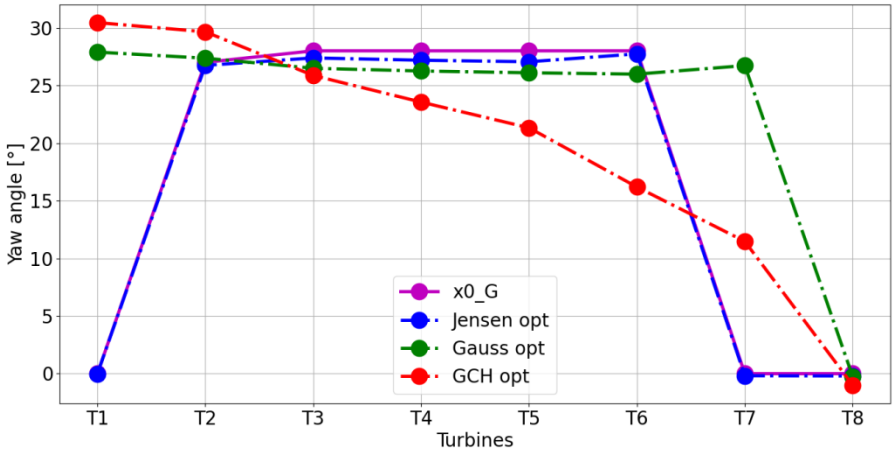

Figure 5.7.1 Yaw distribution in x0_G vector and the optimization solutions – LTI

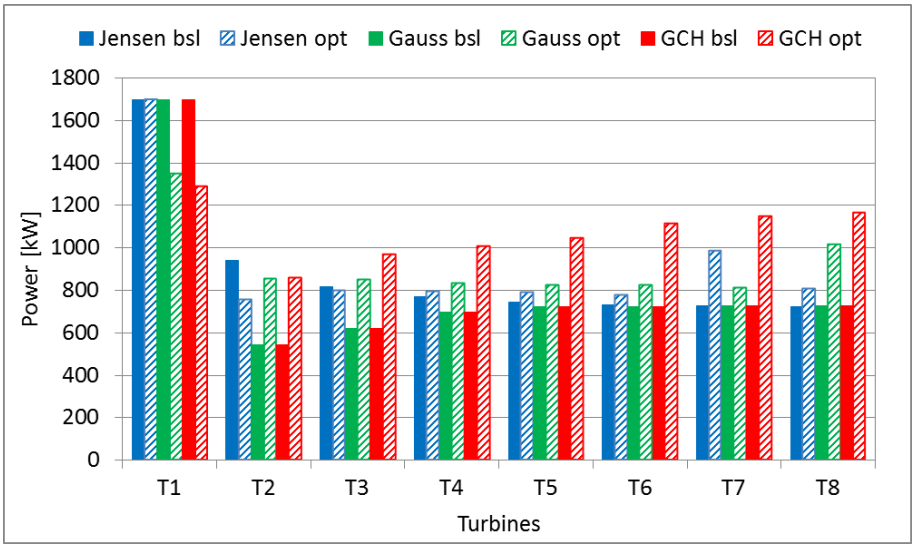

Figure 5.7.2 Power distribution with baseline and optimized yaw settings – LTI

Table 5.7.1 Summary of the results for the LTI simulation case

Wake model	Baseline WF power [kW]	Optimized WF power [kW]	ΔP [%]	No. of iterations
Jensen	7 145	7 393	3.46	100
Gauss	6 459	7 343	13.69	17
GCH	6 459	8 584	32.89	100

The low turbulence intensity simulation case parameters (w_s = 8 m/s, w_d = 270°, T_I = 0.05, spc = 7D) characterize wind of moderate speed, unfavourable direction and low freestream turbulence intensity. Such operating conditions are especially adverse in a real wind farm since in addition to the full wake overlap situations at the downstream rotors the wake recovery rate is reduced. In the present simulation, the wake losses amount to 47.3% and 52.4% (-6 418 kW and -7 104 kW *vs* the cumulative power of isolated turbines) for the Jensen and Gauss / GCH wake models, respectively. In contrast to HTI simulation case, here an apparent farm

power loss (-1 047 kW) due to reduced turbulence level can be observed for the greedy yaw control using Gauss / GCH wake models versus the respective scenarios from RC simulation. The flow field visualization and rotor swept area wind velocity evolution throughout the park are shown in Annex C.3.

(1) Optimal yaw control with the Jensen wake model

The findings regarding the yaw control optimization using the Jensen wake modelling method, under different turbulence levels, elaborated in the HTI simulation case, equally apply to the present LTI test. No further comments on this matter will be made.

(2) Optimal yaw control with the Gauss wake model

In contrast to what is observed in the HTI simulation case, a satisfying power improvement of 13.69% (+884 kW *vs* baseline) is achieved with the Gauss wake model employed. Relatively large yaw angle offsets, exceeding +25°, were proposed for T1 – T7 while T8 remained aligned with the freestream. Such increased magnitude stems from the fact that the velocity deficit at downstream turbines' rotors is enlarged. More specifically, the incident wind speeds are lower and the wake region where these velocity deficits are accumulated is wider. Therefore, yawing the machines by larger yaw angles is still advantageous in terms of overall power gains. A significant yaw-induced power drop at T1 is reported (-350 kW *vs* baseline), which is almost completely compensated already at T2 (+305 kW *vs* baseline).

(3) Optimal yaw control with the GCH wake model

An outstanding power improvement is obtained when yaw optimization is conducted using the GCH wake model. The total power gain reached as much as 32.89% (+2 125 kW *vs* baseline) with large yaw angle offset applied at T1, which was gradually reduced at the consecutive machines. The resulting overall pattern of the yaw angles distribution closely resembles one obtained in LWS simulation case, where the magnitude of the wake loss within the park was also significant. The impact of the yaw-induced features captured by this model is substantial in the present scenario.

To summarize, it is seen that under low turbulence intensity the wake losses are increased, which creates a large potential for power improvement via yaw-based wake steering. While the Jensen wake model is oblivious to this change in wind conditions, the Gauss and GCH models capture its impact and suggest reasonable yaw angles configurations. Based on the results, it is evident that the wake characteristics substantially affects the outcome of yaw control optimization with the differences especially pronounced when wake losses are large.

5.8 Small spacing

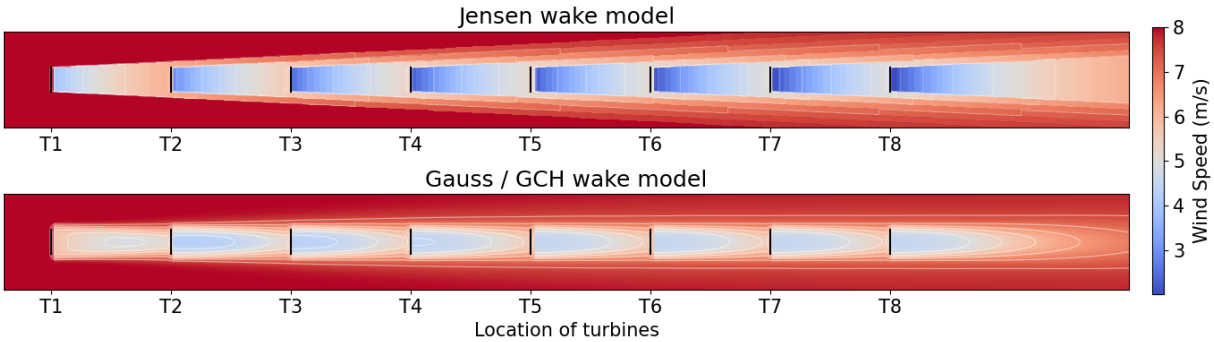

Figure 5.8.1 Hub height flow field with baseline yaw settings – SS

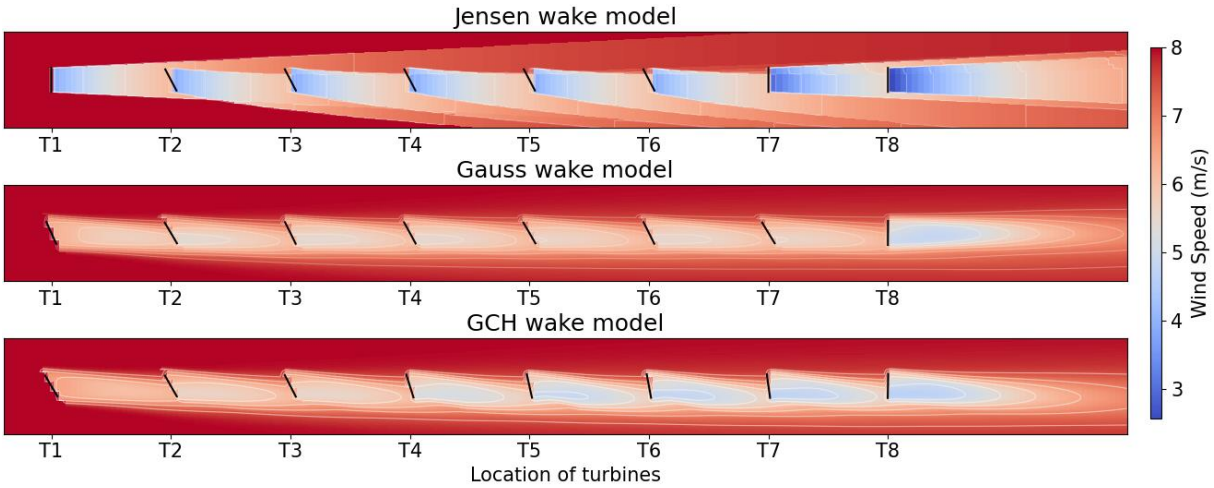

Figure 5.8.2 Hub height flow field with optimized yaw settings – SS

Table 5.8.1 Summary of the results for the SS simulation case

Wake model	Baseline WF power [kW]	Optimized WF power [kW]	ΔP [%]	No. of iterations
Jensen	5 302	6 249	17.86	98
Gauss	5 893	6 569	11.48	13
GCH	5 893	7 590	28.80	75

The small spacing simulation case parameters (w_s = 8 m/s, w_d = 270°, T_I = 0.075, spc = 5D) represent the same wind conditions as in the RC simulation, however, the aerodynamics of the wind farm is affected by a smaller spacing distance between the machines. Due to such configuration, the wake travels a shorter distance before it hits the consecutive turbine, which limits its level of recovery. Based on the results summarized in *Table 5.8.1* it is evident that the total power output of the wind farm with 5D spacing and greedy settings is reduced compared to the respective RC simulations. This magnitude of power drop yields 25% (-1 843 kW) for the Jensen and 21.5% (-1 613 kW) for the Gauss / GCH wake models. In the present scenario, the wake losses with baseline yaw settings are significant, amounting to 61% and 56.6% (-8 261 kW and -7 670 kW *vs* the cumulative power of isolated turbines) for the Jensen and Gauss / GCH wake models, respectively. It is believed that a successful implementation of yaw-based wake redirection could enable tighter wind farm layouts, leading

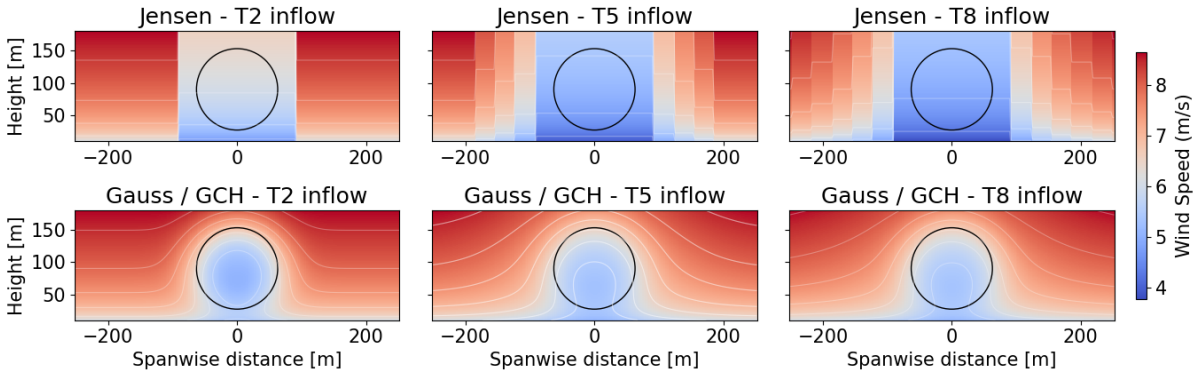

Figure 5.8.3 Velocity field 0.5D ahead of T2, T5 and T8 with baseline yaw settings – SS

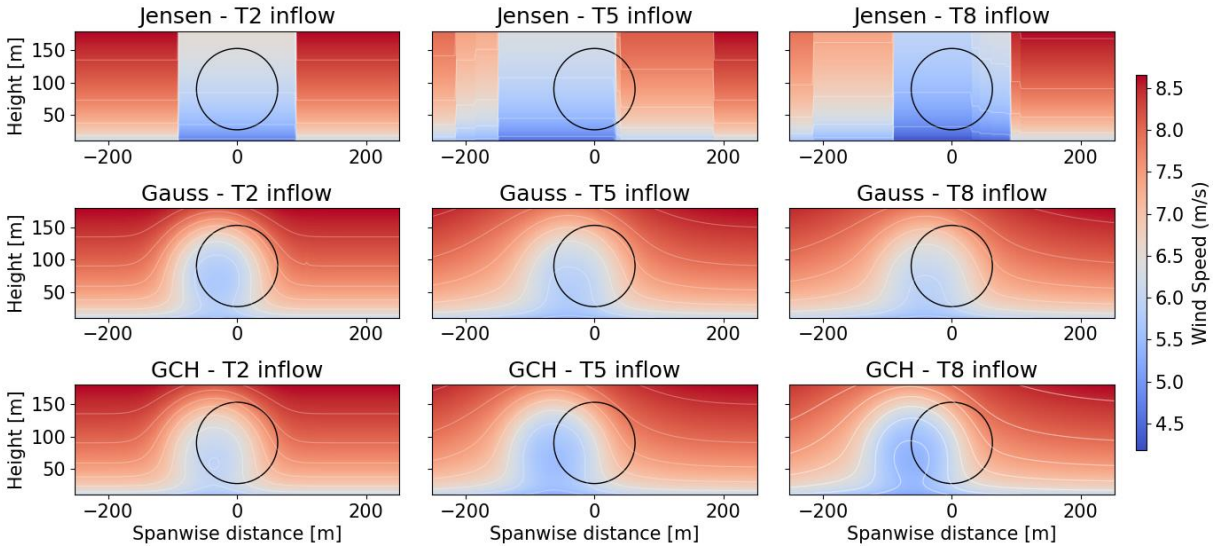

Figure 5.8.4 Velocity field 0.5D ahead of T2, T5 and T8 with optimized yaw settings – SS

to an increase in farm power density. In the present simulation scenario, an attempt will be made to validate this hypothesis.

(1) Optimal yaw control with the Jensen wake model

Employment of the wake model proposed by Jensen results in an increase of total power generation by 17.86% (+947 kW *vs* baseline) when the yaw control set-points are optimized. The incident distribution of yaw angles very closely follows the pattern of the initial guess of the vector x0_G, as seen in Figure 5.8.6. Again, zero yaw offset is proposed for T1, T7 and T8 while the interior T2 – T6 are all yawed by an angle of approximately 28°. Thanks to such yaw configuration wind speed gains of 0.6 m/s are achieved at T3 and T8 while T4 – T7 are exposed to 1 m/s higher velocity. Similarly to the RC simulation, the power drop due to operation in yaw is reported at T2 (-168 kW *vs* baseline) whereas growing gains were obtained at further downstream machines as depicted in Figure 5.8.7. It appears that either the x0_G was a good guess of the optimization starting point or the optimization algorithm was trapped around the initially imposed solution.

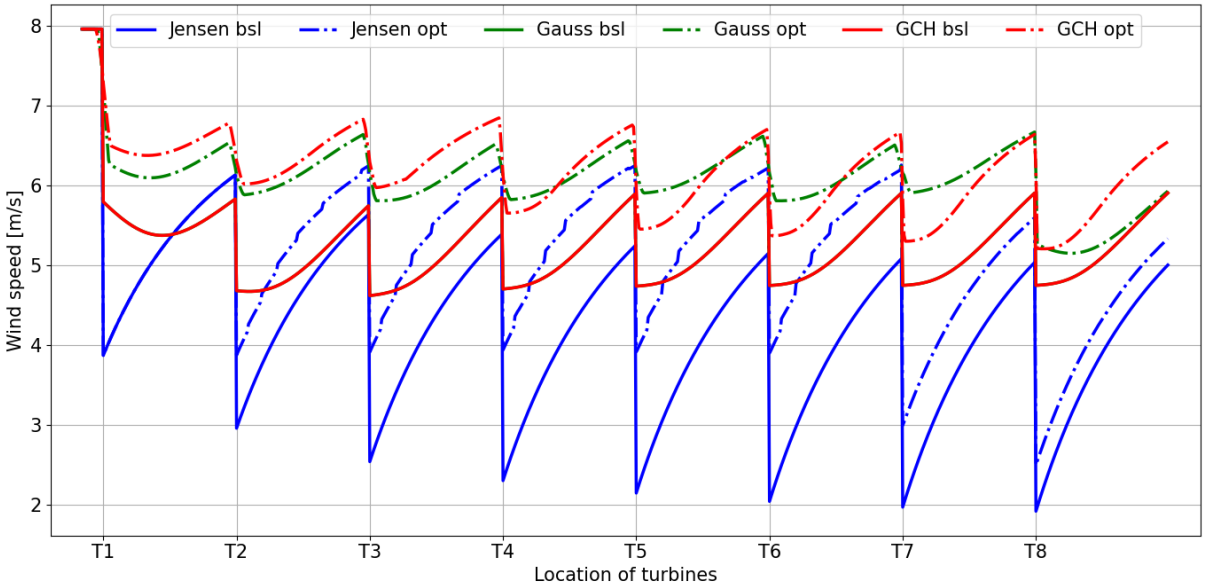

Figure 5.8.5 Evolution of rotor swept area-averaged wind velocity along the wind farm – SS

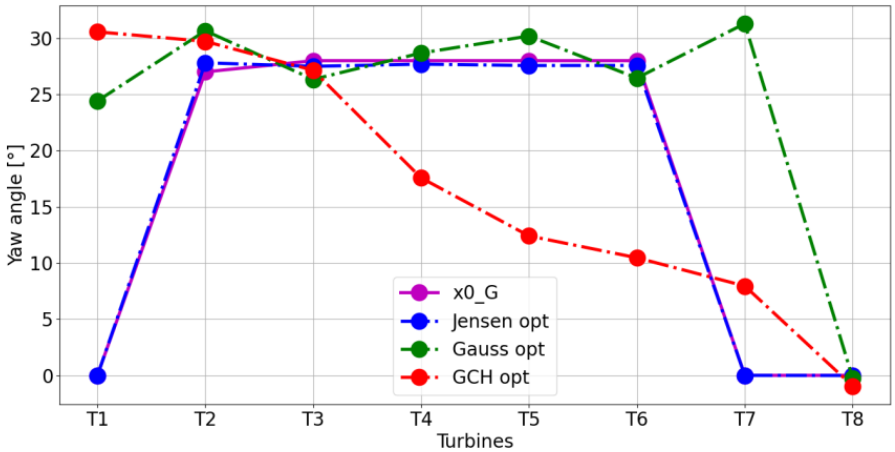

Figure 5.8.6 Yaw distribution in x0_G vector and the optimization solutions – SS

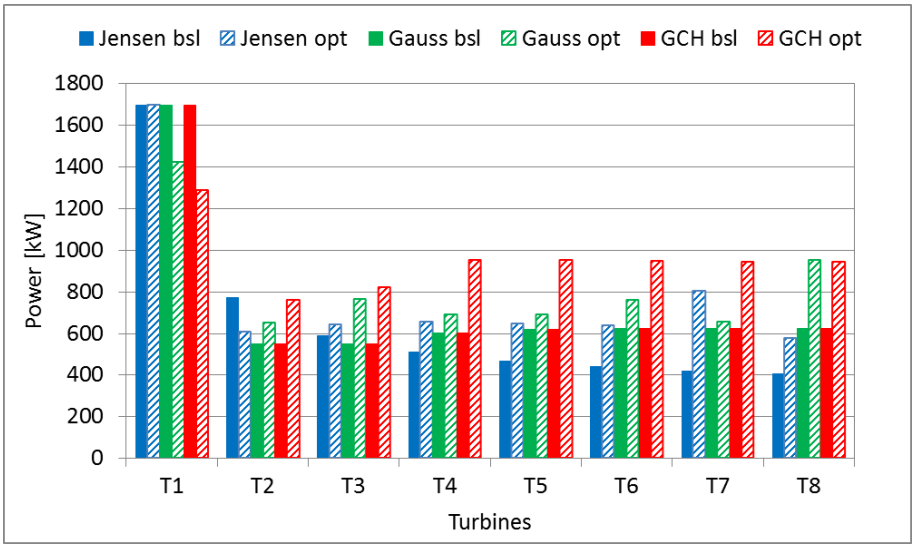

Figure 5.8.7 Power distribution with baseline and optimized yaw settings – SS

(2) Optimal yaw control with the Gauss wake model

Wind farm power improvement by 11.48% (+676 kW *vs* baseline) is achieved when the yaw optimization was run with the Gauss wake model. Unlike for the Jensen wake model, the resultant yaw angle distribution is noticeably different than the one obtained in the RC simulation. The yaw angle settings fall between 24.5° and 31° for T1 – T7, creating a saw shape, and remain 0° at T8. The incident effective wind velocity at each downstream turbine is increased by roughly 0.8 m/s. A clear correlation can be observed between the distribution of yaw settings and distribution of power output at individual machines. The largest power gains are reported at T3, T6, and T8, being the nearest downstream machines behind T2, T5 and T7, which operate with yaw error of over 30°. As a result of the smaller spacing distance and the associated larger velocity deficits experienced by the downstream machines, greater yaw angle offsets are proposed, which is consistent with the engineering intuition.

(3) Optimal yaw control with the GCH wake model

The plant-wise power gain of 28.8% (+2 697 kW *vs* baseline) is obtained with the GCH wake modelling method employed. It is also the only scenario in which the optimized wind farm power reaches the magnitude of the baseline total power in the RC simulation. The yaw distribution starts with large, slowly decreasing yaw errors applied at the front turbines, T1 – T3. Then, a more pronounced reduction in yaw is observed at T4, which decreases at the subsequent turbines, T5 – T7, to again become significant at T8. Such yaw configuration together with the impact of the counter-rotating vortices causes substantial wake deflection as seen in Figure 5.8.4. This way the downstream machines are exposed to significantly higher wind speeds with the velocity gain ranging from +0.8 m/s to even 1.2 m/s, observed in Figure 5.8.5. Consequently, considerable power gains at individual turbines, especially T4 – T8, are achieved. According to the predictions with GCH wake model, the reduced spacing distance created a great potential for improving the power of the system via collaborative yaw control strategy.

In conclusion, the results of yaw control optimization in terms of power gains are encouraging for all of the employed wake models. Although the aerodynamics of the wind farm is highly affected by the reduction in spacing, the solution obtained for the Jensen wake model was very similar to the initial guess x0_G. Further, the Gauss wake model promotes large magnitudes of yaw errors at all turbines except for the last one, which is an understandable behaviour. Lastly, the GCH wake model suggests gradually decreasing yaw offsets that enable the wind farm to reach the level of power achieved for 7D spacing with greedy control.

The distance between T1 and T8 with 7D spacing is 6.2 km while for 5D spacing it is only 4.4 km, which is a 28.5% reduction. This creates a space that could fit two additional machines without exceeding the original layout length, increasing the total power per unit length. Alternatively, wind farm size-dependent costs could be decreased, maintaining the original power output, according to the GCH wake model predictions. Although promising, these are only rough estimates and a closer look into this matter using more sophisticated tools and taking into account other relevant aspects should be made.

5.9 Large spacing

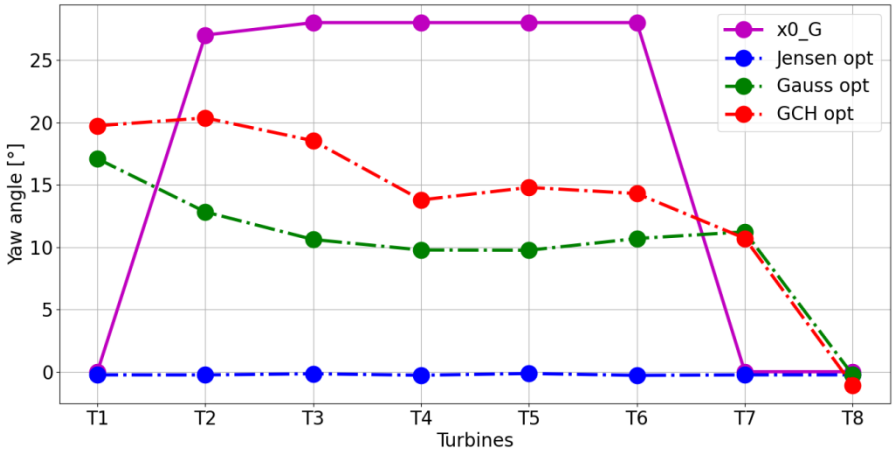

Figure 5.9.1 Yaw distribution in x0_G vector and the optimization solutions – LS

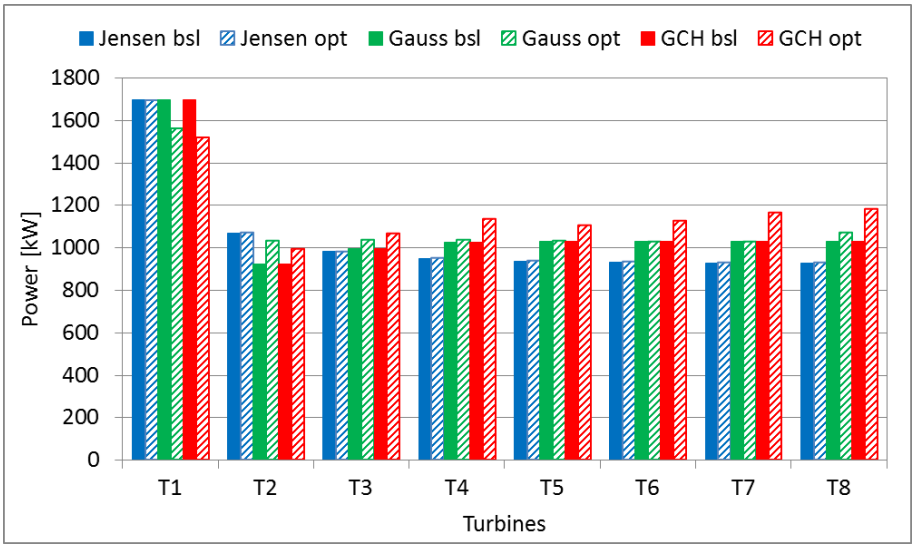

Figure 5.9.2 Power distribution with baseline and optimized yaw settings – LS

Table 5.9.1 Summary of the results for the LS simulation case

Wake model	Baseline WF power [kW]	Optimized WF power [kW]	ΔP [%]	No. of iterations
Jensen	8 427	8 427	0.00	100
Gauss	8 764	8 818	0.61	100
GCH	8 764	9 277	5.85	100

The large spacing simulation (w_s = 8 m/s, w_d = 270°, T_I = 0.075, spc = 9D) intends to evaluate the applicability of yaw-based wake redirection when the turbines are spaced further apart than in the RC simulation. In contrast to SS simulation, now the wake travels a longer distance before it hits the consecutive turbine, which enhances its level of recovery. The results summarized in *Table 5.9.1* show that the total power output of the wind farm with 9D spacing and greedy settings is improved compared to the respective RC simulations. The magnitude of improvement amounts to 18% (+1 282 kW) for the Jensen and 17% (+1 258 kW) for the Gauss /

GCH wake models. Consequently, the wake losses experienced with baseline yaw control are reduced and yield 37.9% and 35.4% (-5 136 kW and -4 799 kW *vs* the cumulative power of isolated turbines) for the Jensen and Gauss / GCH wake models, respectively. The flow field visualization and rotor swept area wind velocity evolution throughout the park are shown in Annex C.4.

(1) Optimal yaw control with the Jensen wake model

No change in the yaw settings, and consequently no power improvement is suggested when the Jensen model is used. It appears that the wake recovers enough so that it is not beneficial to sacrifice the power by yawing the machines to create partial wake overlap situations at the downstream rotors. Knowing the characteristics of Jensen's wake, it is an understandable behaviour.

(2) Optimal yaw control with the Gauss wake model

For the simulation with the Gauss wake modelling approach, a small total power improvement is achieved, amounting to 0.61% (+54 kW *vs* baseline). The suggested yaw settings start with 17° misalignment at T1 that is gradually reduced at further turbines until T4 and T5, which both yaw by 10°. Then, the magnitude of yaw offset rises insignificantly at T6 and T7 and remains 0° at T8. The yaw-induced power loss of -133 kW at T1 is reported, which is barely compensated with the power gains at the remaining downstream turbines. Given the level of achieved improvement in this test, the benefit of plant-wise yaw control for further spaced turbines is questionable.

(3) Optimal yaw control with the GCH wake model

A satisfying level of total power gain, amounting to 5.85% (+513 kW *vs* baseline) is obtained for the simulation with the GCH wake model. Although the wake is more recovered, due to the impact of the secondary steering it is still advantageous to implement yaw-based wake redirection.

To summarize, depending on the fidelity of the applied wake modelling approach, different solutions of the yaw control optimization are obtained with various levels of power improvement. More specifically, the application of yaw control examined with the Jensen wake model is not beneficial, with the Gauss model there is a modest advantage and with the GCH model is recommended. The observed discrepancy in the results is directly related to the wake characteristics of each model. It is known that for wind farms with a large spacing distance the potential of wake loss reduction is minor. Given that, the outcomes of the present tests are aligned with what was expected.

5.10 Overview of the optimization results

In order to summarize the optimization results obtained throughout the study, yaw angle distributions sorted by wake modelling approach are presented below.

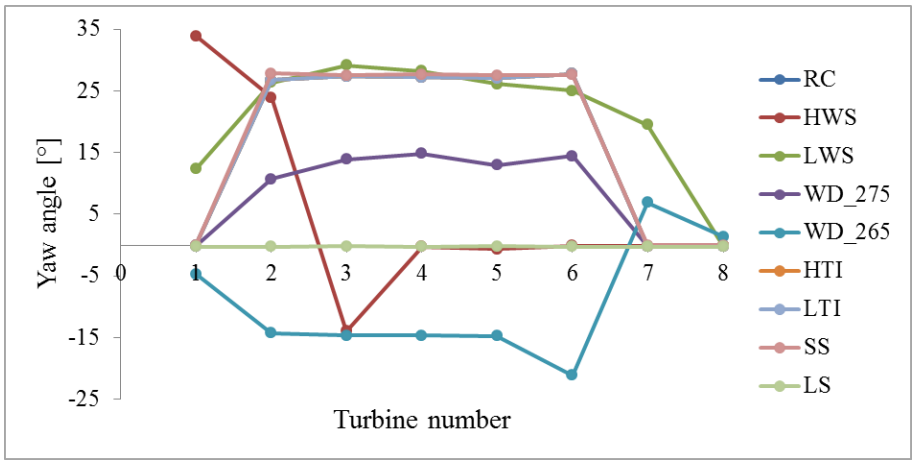

Figure 5.10.1 Collection of yaw angle distributions obtained with the Jensen model

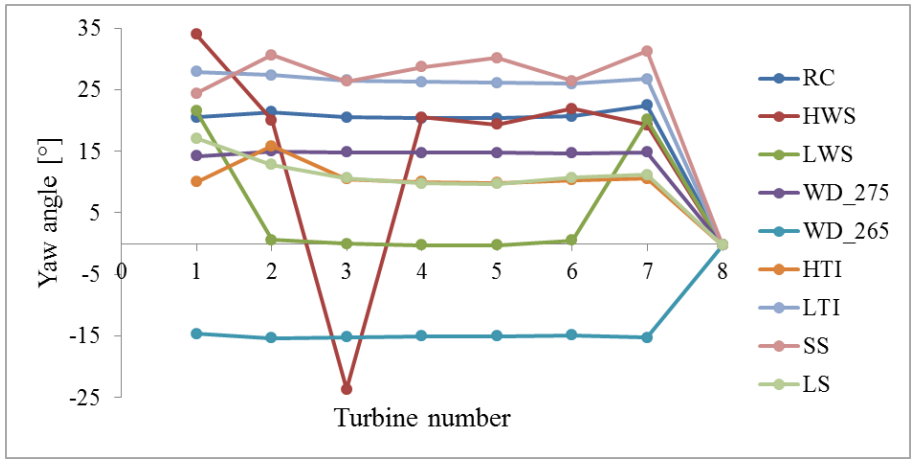

Figure 5.10.2 Collection of yaw angle distributions obtained with the Gauss model

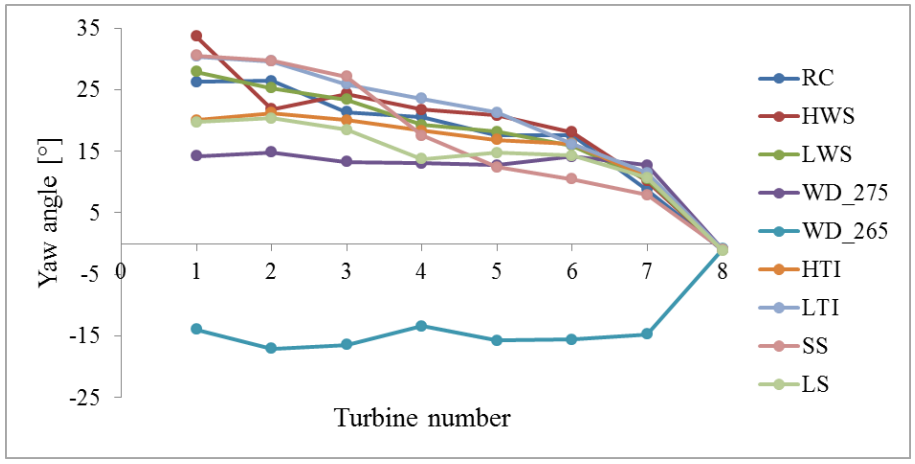

Figure 5.10.3 Collection of yaw angle distributions obtained with the GCH model

Chapter 6

Conclusions and Recommendations

The present chapter provides a summary of the conducted research, states the most important conclusions and gives suggestions for the direction of further investigations.

6.1 Conclusions

In this work, a collaborative yaw-based wake steering approach to control a wind farm under various wind conditions and layouts was investigated. Three wake modelling approaches of different level of fidelity (Jensen, Gauss, Gauss-Curl Hybrid) were employed to account for the aerodynamic interference between the machines. The objective of the study was to investigate the impact of the applied wake modelling method on the solution of yaw control optimization with the purpose of maximizing power generation of a wind park. The most important conclusions drawn from this study are stated below.

1) Though not the main goal of this work, it was shown that the wake characteristics, in particular the assumed velocity deficit profile, has a significant influence on the ability of the SLSQP optimizer to find an improved solution. Also, an appropriate choice of the relevant optimization parameters (*f_tol*, ε and x0) is crucial to ensure achieving the best solution within the bounds of the defined problem. More specifically, due to the uniformly distributed velocity deficit in the Jensen's wake, the optimization algorithm generally exhibited random behaviour for the whole range of tested *f_tol*, ε and x0 values. On the other hand, when the models assuming a Gaussian-shaped velocity deficit were tested, the optimization algorithm showed negligible dependence on the prescribed ε and x0 values. However, an immediate termination was observed if the *f_tol* value was too large (10^{-8}) for such defined problem, which is expected behaviour.

2) Regarding the application of the Jensen wake model in the present work, several deficiencies of this simple model were found. First, it was observed that in situations when the wind direction is aligned with the turbines, there is always a certain scope of "idle" yawing an upstream turbine that is needed to reach the transition point between full and partial wake overlap condition at a nearest downstream rotor. As a consequence, the upstream machine loses power according to the $\cos^2\gamma$ rule of thumb while the downstream one experiences meaninglessly low gains only because the upstream machine extracted less energy. This range of unproductive yawing was checked for RC simulation conditions and amounted to 14° with the associated power loss of 5.3% at the upstream turbine. Due to such behaviour, the Jensen model gives a very unrealistic flow field prediction, which is especially unacceptable when the objective is to achieve power improvement by manipulating yaw angles. In contrast, in WD_275° and WD_265° simulations, the impact of "idle" yawing was naturally mitigated resulting in very large power gains predicted with the Jensen model, which supports the above statements. Secondly, this simple model doesn't directly account for the turbulence intensity level, which was proven to have a significant impact on the applicability of yaw control. Overall, plant-wise power gains were reported for 8 out of 9 simulations, however, in four (RC, HTI, LTI, SS) the resulting yaw distribution is nearly the same as in *x0_G* vector. Moreover, in the LS case, the greedy control is suggested while in another three cases (HWS, LWS, WD_265°) the credibility of the optimization results is doubtful. Taking into account the limitations of Jensen's model, the yaw control proposed in WD_275° simulation is to some extent satisfying. Besides, the only consistency in the prediction of optimal yaw settings distribution was that the last turbine should remain aligned with the freestream. In light of the above findings, it is concluded that the Jensen wake model is not suitable for wind farm optimization studies that rely on yaw control.

3) The Bastankhah model assuming the Gaussian profile of the wake velocity deficit was found to be much more suitable for yaw control optimization than the Jensen model. Due to its higher fidelity level, the improvement was seen in terms of both the performance of the optimization algorithm and robustness in wind farm aerodynamics predictions under varied atmospheric conditions and park layouts. The yaw angles adjustments proposed by the optimizer were consistent and sensible throughout the whole study. According to the predictions made with this model, encouraging power improvement was observed for six tests (RC, HWS, WD_275°, WD_265°, LTI, SS) while for the remaining three (LWS, HTI, LS) the benefits of yaw-based wake steering implementation were doubtful. These results are aligned with the common conjecture that yaw control is applicable only when the wake losses are significant. With few exceptions, it was noticed that a nearly constant yaw distribution was proposed for T1 – T7, with the magnitude dependent on the simulation parameters, while the last machine was always aligned with the freestream. In the reference wind farm considered, a power gain of 3.59% (+270 kW) was achieved with the following yaw angle misalignments distribution [20.5 21.5 20.5 20.5 20.5 20.5 22.5 0] compared to operation with the greedy turbine-level control strategy.

4) Regarding the application of the Gauss-Curl Hybrid model, good performance of the optimization algorithm was observed together with robust wind farm aerodynamics predictions. The incorporation of the yaw-induced features of this model resulted in very promising farm power gains for all of the conducted yaw optimization cases. In general, due to the enhanced wake deflection and recovery, this wake modelling approach promotes larger yaw offset at the front turbine, which is being gradually reduced at the consecutive machines. Such behaviour is aligned with the engineering intuition, with an exception that it is not clear why the last turbine is always yawed by -1° angle instead of being aligned with the undisturbed wind. In the reference wind farm considered, a power gain of 14.66% (+1 100 kW) was achieved with the following yaw set-points distribution [26.5 26.5 21.5 20.5 17.5 17.5 9 -1] compared to operation with the greedy turbine-level control strategy. Based on the results obtained with this model, it appears that the inclusion of the secondary steering effect has a game-changing impact in terms of the potential for yield increase and yaw misalignment distribution of collaborative WF control.

6.2 Recommendations

Yaw-based wake redirection is a very broad and complex research topic, which has to be comprehensively examined before its implementation takes place in industrial wind farms. In the course of developing this work, several ideas for improvement and extension of the present investigation appeared, which could not be incorporated due to the limited time and availability of resources. The most important are listed below:

1) As mentioned in the very beginning of this work, wind farm control is about seeking the compromise between the generated power and experienced loads at the turbines. Therefore, evaluation of the yaw-induced loads is considered to be a very important and relevant direction for further studies.

2) The present industrial wind farms consist of dozens or even hundreds of wind turbines that are

configured in either rectilinear or some less conventional layouts. Naturally, one could think of assessing the impact of applied wake modelling method on the feasibility of yaw-based wake steering technique in a large array of turbines and over a complete wind rose.

3) Since yaw-based wake steering can be coupled with wind farm layout optimization, the combined impact of these two measures for plant performance improvement could be investigated, like it was done in the work of P. Gebraad [15] and P. Fleming [93].

4) With the possession of relevant data from high fidelity simulations, model-specific parameters could be tuned to increase the accuracy and credibility of their predictions.

5) The secondary steering effect was shown to have a significant influence on the yaw angles distribution and the associated power improvements. In fact, this phenomenon is receiving growing attention of the wind energy researchers and validation of its real impact is still an open research question. Given that the GCH wake model is one of the first analytical models that capture this wake behaviour, the fidelity of its predictions could be investigated with the use of more sophisticated modelling tools.

6) This work was limited to take into account only the steady-state phenomena and wind farm behaviour. In order to investigate the full impact and potential of WF yaw control, it is important to account for the unsteady aerodynamic phenomena, such as wake meandering, in further studies on this topic.

References

[1] IRENA, "Future of wind: Deployment, investment, technology, grid integration and socio-economic aspects (a global energy transformation paper)," International Renewable Energy Agency, Abu Dhabi, Tech. Rep., 2019.

[2] J. F. Manwell, J. G. McGowan, and A. L. Rogers, *Wind energy explained: theory, design and application*. John Wiley & Sons, 2010.

[3] O. Anaya-Lara, J. O. Tande, K. Uhlen, and K. Merz, *Offshore Wind Energy Technology*. Wiley Online Library, 2018.

[4] IRENA, "Renewable power generation costs in 2018," International Renewable Energy Agency, Abu Dhabi, Tech. Rep., 2019.

[5] S. Krohn, P.-E. Morthorst, S. Awerbuch *et al.*, "The economics of wind energy," *European Wind Energy Association*, pp. 28–29, 2009.

[6] S. Boersma, B. Doekemeijer, P. M. Gebraad, P. A. Fleming, J. Annoni, A. K. Scholbrock, J. Frederik, and J.-W. van Wingerden, "A tutorial on control-oriented modeling and control of wind farms," in *2017 American Control Conference (ACC)*. IEEE, 2017, pp. 1–18.

[7] J. F. Herbert-Acero, O. Probst, P.-E. Réthoré, G. C. Larsen, and K. K. Castillo-Villar, "A review of methodological approaches for the design and optimization of wind farms," *Energies*, vol. 7, no. 11, pp. 6930–7016, 2014.

[8] B. Sanderse, "Aerodynamics of wind turbine wakes," Technical Report ECN-E-09-016, Energy Centre of the Netherlands, Tech. Rep., 2009.

[9] L. Vermeer, J. N. Sørensen, and A. Crespo, "Wind turbine wake aerodynamics," *Progress in aerospace sciences*, vol. 39, no. 6-7, pp. 467–510, 2003.

[10] C. B. Hasager, L. Rasmussen, A. Peña, L. E. Jensen, and P.-E. Réthoré, "Wind farm wake: The horns rev photo case," *Energies*, vol. 6, no. 2, pp. 696–716, 2013.

[11] C. Kjaer, B. Douglas, and D. Luga, "Ewea wind energy - the facts," *Earthscan, London*, 2009.

[12] R. J. Barthelmie, O. Rathmann, S. T. Frandsen, K. Hansen, E. Politis, J. Prospathopoulos, K. Rados, D. Cabezón, W. Schlez, J. Phillips *et al.*, "Modelling and measurements of wakes in large wind farms," in *Journal of Physics: Conference Series*, vol. 75, no. 1. IOP Publishing, 2007, p. 012049.

[13] K. E. Johnson and N. Thomas, "Wind farm control: Addressing the aerodynamic interaction among wind turbines," in *2009 American Control Conference*. IEEE, 2009, pp. 2104–2109.

[14] P. M. Gebraad, F. Teeuwisse, J. Van Wingerden, P. A. Fleming, S. Ruben, J. Marden, and L. Pao,

"Wind plant power optimization through yaw control using a parametric model for wake effects - a cfd simulation study," *Wind Energy*, vol. 19, no. 1, pp. 95–114, 2016.

[15] P. Gebraad, J. J. Thomas, A. Ning, P. Fleming, and K. Dykes, "Maximization of the annual energy production of wind power plants by optimization of layout and yaw-based wake control," *Wind Energy*, vol. 20, no. 1, pp. 97–107, 2017.

[16] C. L. Archer and A. Vasel-Be-Hagh, "Wake steering via yaw control in multi-turbine wind farms: Recommendations based on large-eddy simulation," *Sustainable Energy Technologies and Assessments*, vol. 33, pp. 34–43, 2019.

[17] D. Medici, "Experimental studies of wind turbine wakes: power optimisation and meandering," Ph.D. dissertation, KTH, 2005.

[18] F. Campagnolo, V. Petrovic, C. L. Bottasso, and A. Croce, "Wind tunnel testing of wake control strategies," in *2016 American Control Conference (ACC)*. ÍEEE, 2016, pp. 513–518.

[19] J. Schottler, A. Hölling, J. Peinke, and M. Hölling, "Wind tunnel tests on controllable model wind turbines in yaw," in *34th wind energy symposium*, 2016, p. 1523.

[20] J. Wagenaar, L. Machielse, and J. Schepers, "Controlling wind in ecn's scaled wind farm," *Proc. Europe Premier Wind Energy Event*, pp. 685–694, 2012.

[21] P. Fleming, J. Annoni, J. J. Shah, L. Wang, S. Ananthan, Z. Zhang, K. Hutchings, P. Wang, W. Chen, and L. Chen, "Field test of wake steering at an offshore wind farm," *Wind Energy Science Discussions*, vol. 2, no. NREL/JA-5000-67623, 2017.

[22] P. Fleming, J. King, K. Dykes, E. Simley, J. Roadman, A. Scholbrock, P. Murphy, J. K. Lundquist, P. Moriarty, K. Fleming *et al.*, "Initial results from a field campaign of wake steering applied at a commercial wind farm–part 1," *Wind Energy Science (Online)*, vol. 4, no. NREL/JA-5000-73991, 2019.

[23] J. R. Marden, S. D. Ruben, and L. Y. Pao, "A model-free approach to wind farm control using game theoretic methods," *IEEE Transactions on Control Systems Technology*, vol. 21, no. 4, pp. 1207–1214, 2013.

[24] J. G. Schepers, "Engineering models in wind energy aerodynamics: Development, implementation and analysis using dedicated aerodynamic measurements," PhD Thesis, Delft University of Technology, Delft, Netherlands, retrieved from database: repository.tudelft.nl, 2012.

[25] B. Sanderse, S. Van der Pijl, and B. Koren, "Review of computational fluid dynamics for wind turbine wake aerodynamics," *Wind energy*, vol. 14, no. 7, pp. 799–819, 2011.

[26] T. Burton, N. Jenkins, D. Sharpe, and E. Bossanyi, *Wind energy handbook*. John Wiley & Sons, 2011.

[27] NREL's S819 Airfoil (s819-nr) data, URL:http://airfoiltools.com/polar/details?polar=xf-s819-nr-1000000, accessed online December 2020.

[28] R. E. Wilson and P. B. Lissaman, "Applied aerodynamics of wind power machines," *National Science Foundation*, 1974.

[29] S. Chowdhury, J. Zhang, A. Messac, and L. Castillo, "Characterizing the influence of land area and nameplate capacity on the optimal wind farm performance," in *ASME 2012 6th International Conference on Energy Sustainability collocated with the ASME 2012 10th International Conference on Fuel Cell Science, Engineering and Technology*. American Society of Mechanical Engineers Digital Collection, 2012, pp. 1349–1359.

[30] R. J. Barthelmie, S. T. Frandsen, O. Rathmann, K. S. Hansen, E. S. Politis, J. Prospathopoulos, D. Cabezón Martnez, K. Rados, S. Van Der Pijl, J. Schepers *ét al.*, "Flow and wakes in large wind farms in complex terrain and offshore," 2008.

[31] R. Barthelmie, S. Frandsen, K. Hansen, J. Schepers, K. Rados, W. Schlez, A. Neubert, L. Jensen, and S. Neckelmann, "Modelling the impact of wakes on power output at nysted and horns rev," in *European Wind Energy Conference*, 2009.

[32] F. Blondel and M. Cathelain, "An alternative form of the super-gaussian wind turbine wake model," *Wind. Energy Sci. Discuss*, vol. 2020, pp. 1–16, 2020.

[33] G. España, S. Aubrun-Sanches, and P. Devinant, "The meandering phenomenon of a wind turbine wake," in *European Wind Energy Conference and Exhibition*, 2009.

[34] C. L. Archer, A. Vasel-Be-Hagh, C. Yan, S. Wu, Y. Pan, J. F. Brodie, and A. E. Maguire, "Review and evaluation of wake loss models for wind energy applications," *Applied Energy*, vol. 226, pp. 1187–1207, 2018.

[35] N. O. Jensen, *A note on wind generator interaction*. Risø National Laboratory, 1983.

[36] I. Katic, J. Højstrup, and N. O. Jensen, "A simple model for cluster efficiency," in *European wind energy association conference and exhibition*. A. Raguzzi, 1987, pp. 407–410.

[37] F. González-Longatt, P. Wall, and V. Terzija, "Wake effect in wind farm performance: Steady-state and dynamic behavior," *Renewable Energy*, vol. 39, no. 1, pp. 329–338, 2012.

[38] M. Bastankhah and F. Porté-Agel, "A new analytical model for wind-turbine wakes," *Renewable Energy*, vol. 70, pp. 116–123, 2014.

[39] P. Vermeulen, *A Wind Tunnel Study of the Wake of a Horizontal Axis Wind Turbine: Report*. TNO, 1978.

[40] G. Taylor, "Wake and performance measurements on the lawson-tancred 17 m horizontal-axis windmill," *IEE Proceedings A (Physical Science, Measurement and Instrumentation, Management and Education, Reviews)*, vol. 130, no. 9, pp. 604–612, 1983.

[41] Y.-T. Wu and F. Porté-Agel, "Atmospheric turbulence effects on wind-turbine wakes: An les study," *energies*, vol. 5, no. 12, pp. 5340–5362, 2012.

[42] L. P. Chamorro and F. Porté-Agel, "A wind-tunnel investigation of wind-turbine wakes: boundary-layer turbulence effects," *Boundary-layer meteorology*, vol. 132, no. 1, pp. 129–149, 2009.

[43] N. Nygaard, L. Jensen, R. Downey, and M. Méchali, "Construction and validation of a new offshore wake model," in *Proceedings of the International Conference on Aerodynamics of Offshore Wind*

Energy Systems and Wakes (ICOWES) Conference, Lyngby, Danmark, vol. 1719, 2013.

[44] S. Frandsen, R. Barthelmie, S. Pryor, O. Rathmann, S. Larsen, J. Højstrup, and M. Thøgersen, "Analytical modelling of wind speed deficit in large offshore wind farms," *Wind Energy: An International Journal for Progress and Applications in Wind Power Conversion Technology*, vol. 9, no. 1-2, pp. 39–53, 2006.

[45] M. Abkar and F. Porté-Agel, "Influence of atmospheric stability on wind-turbine wakes: A large-eddy simulation study," *Physics of fluids*, vol. 27, no. 3, p. 035104, 2015.

[46] M. Bastankhah and F. Porté-Agel, "Experimental and theoretical study of wind turbine wakes in yawed conditions," *Journal of Fluid Mechanics*, vol. 806, pp. 506–541, 2016.

[47] A. Niayifar and F. Porté-Agel, "Analytical modeling of wind farms: A new approach for power prediction," *Energies*, vol. 9, no. 9, p. 741, 2016.

[48] M. F. Howland, J. Bossuyt, L. A. Martnez-Tossas, J. Meyers, and C. Meneveau, "Wake structure in actuator disk models of wind turbines in yaw under uniform inflow conditions," *Journal of Renewable and Sustainable Energy*, vol. 8, no. 4, p. 043301, 2016.

[49] L. Vollmer, G. Steinfeld, D. Heinemann, and M. Kühn, "Estimating the wake deflection downstream of a wind turbine in different atmospheric stabilities: an les study," *Wind Energ. Sci*, vol. 1, pp. 129–141, 2016.

[50] T. Berdowski, "Three-dimensional free-wake vortex simulations of an actuator disc in yaw and tilt," in *2018 Wind Energy Symposium*, 2018, p. 0513.

[51] P. Fleming, J. Annoni, M. Churchfield, L. A. Martinez-Tossas, K. Gruchalla, M. Lawson, and P. Moriarty, "A simulation study demonstrating the importance of large-scale trailing vortices in wake steering," *Wind Energy Science Discussions*, vol. 3, no. NREL/JA-5000-70521, 2018.

[52] L. A. Martnez-Tossas, J. Annoni, P. A. Fleming, and M. J. Churchfield, "The aerodynamics of the curled wake: A simplified model in view of flow control," *Wind Energy Science (Online)*, vol. 4, no. NREL/JA-5000-73451, 2019.

[53] J. King, P. Fleming, R. King, L. A. Martnez-Tossas, C. J. Bay, R. Mudafort, and E. Simley, "Controls-oriented model for secondary effects of wake steering," *Wind Energy Science Discussions*, vol. 2020, pp. 1–22, 2020. [Online]. Available: https://www.wind-energ-sci-discuss.net/wes-2020-3/

[54] M. Abkar and F. Porté-Agel, "The effect of atmospheric stability on wind-turbine wakes: A large-eddy simulation study," in *Journal of Physics: Conference Series*, vol. 524, no. 1. IOP Publishing, 2014, p. 012138.

[55] C. Bay, J. King, P. Fleming, R. Mudafort, and L. Martinez, "Unlocking the full potential of wake steering: implementation and assessment of a controls-oriented model," National Renewable Energy Lab.(NREL), Golden, CO (United States), Tech. Rep., 2019.

[56] Á. Jiménez, A. Crespo, and E. Migoya, "Application of a les technique to characterize the wake deflection of a wind turbine in yaw," *Wind energy*, vol. 13, no. 6, pp. 559–572, 2010.

[57] M. M. Hand and M. J. Balas, “Systematic controller design methodology for variable-speed wind turbines,” *Wind Engineering*, vol. 24, no. 3, pp. 169–187, 2000.

[58] E. A. Bossanyi, “Individual blade pitch control for load reduction,” *Wind Energy: An International Journal for Progress and Applications in Wind Power Conversion Technology*, vol. 6, no. 2, pp. 119–128, 2003.

[59] NREL, “FLORIS. Version 2.2.0,” 2020. [Online]. Available: https://github.com/NREL/floris

[60] IRENA, “Renewable capacity statistics 2019,” International Renewable Energy Agency, Abu Dhabi, Tech. Rep., 2019.

[61] Carbon Trust staff, “Holistic offshore wind farm control strategies to be put to the test,” 2017. [Online]. Available: https://www.carbontrust.com/news/2017/12/wind-farm-control-trials/

[62] M. Steinbuch, W. De Boer, O. Bosgra, S. Peeters, and J. Ploeg, “Optimal control of wind power plants,” *Journal of Wind Engineering and Industrial Aerodynamics*, vol. 27, no. 1-3, pp. 237–246, 1988.

[63] G. Corten and P. Schaak, “Heat and flux: Increase of wind farm production by reduction of the axial induction,” in *Proceedings of the European Wind Energy Conference*, 2003.

[64] D. van der Hoek, S. Kanev, and W. Engels, “Comparison of down-regulation strategies for wind farm control and their effects on fatigue loads,” in *2018 Annual American Control Conference (ACC)*. IEEE, 2018, pp. 3116–3121.

[65] A. C. Kheirabadi and R. Nagamune, “A quantitative review of wind farm control with the objective of wind farm power maximization,” *Journal of Wind Engineering and Industrial Aerodynamics*, vol. 192, pp. 45–73, 2019.

[66] S. Kanev, F. Savenije, and W. Engels, “Active wake control: An approach to optimize the lifetime operation of wind farms,” *Wind Energy*, vol. 21, no. 7, pp. 488–501, 2018.

[67] M. T. van Dijk, J.-W. van Wingerden, T. Ashuri, and Y. Li, “Wind farm multi-objective wake redirection for optimizing power production and loads,” *Energy*, vol. 121, pp. 561–569, 2017.

[68] S. Raach, S. Boersma, J.-W. van Wingerden, D. Schlipf, and P. W. Cheng, “Robust lidar-based closed-loop wake redirection for wind farm control,” *IFAC-PapersOnLine*, vol. 50, no. 1, pp. 4498–4503, 2017.

[69] P. Fleming, P. M. Gebraad, S. Lee, J.-W. van Wingerden, K. Johnson, M. Churchfield, J. Michalakes, P. Spalart, and P. Moriarty, “Simulation comparison of wake mitigation control strategies for a two-turbine case,” *Wind Energy*, vol. 18, no. 12, pp. 2135–2143, 2015.

[70] P. A. Fleming, P. M. Gebraad, S. Lee, J.-W. van Wingerden, K. Johnson, M. Churchfield, J. Michalakes, P. Spalart, and P. Moriarty, “Evaluating techniques for redirecting turbine wakes using sowfa,” *Renewable Energy*, vol. 70, pp. 211–218, 2014.

[71] J. van Wingerden, “Reconfigurable floating wind turbines,” *VENI project*, vol. 11930, 2011.

[72] A. J. Sørensen, "A survey of dynamic positioning control systems," *Annual reviews in control*, vol. 35, no. 1, pp. 123–136, 2011.

[73] S. Rodrigues, R. T. Pinto, M. Soleimanzadeh, P. A. Bosman, and P. Bauer, "Wake losses optimization of offshore wind farms with moveable floating wind turbines," *Energy Conversion and Management*, vol. 89, pp. 933–941, 2015.

[74] Y. Li and Z. Wu, "Stabilization of floating offshore wind turbines by artificial muscle based active mooring line force control," in *2016 American Control Conference (ACC)*. IEEE, 2016, pp. 2277–2282.

[75] C. Han, J. R. Homer, and R. Nagamune, "Movable range and position control of an offshore wind turbine with a semi-submersible floating platform," in *2017 American Control Conference (ACC)*. IEEE, 2017, pp. 1389–1394.

[76] P. A. Fleming, A. Scholbrock, A. Jehu, S. Davoust, E. Osler, A. D. Wright, and A. Clifton, "Field-test results using a nacelle-mounted lidar for improving wind turbine power capture by reducing yaw misalignment," in *Journal of Physics: Conference Series*, vol. 524, no. 1. IOP Publishing, 2014, p. 012002.

[77] D. Medici and J. Dahlberg, "Potential improvement of wind turbine array efficiency by active wake control (awc)," 2003.

[78] D. Medici and P. Alfredsson, "Measurements on a wind turbine wake: 3d effects and bluff body vortex shedding," *Wind Energy: An International Journal for Progress and Applications in Wind Power Conversion Technology*, vol. 9, no. 3, pp. 219–236, 2006.

[79] J. Schottler, F. Mühle, J. Bartl, J. Peinke, M. S. Adaramola, L. Sætran, and M. Hölling, "Comparative study on the wake deflection behind yawed wind turbine models," in *J. Phys. Conf. Ser*, vol. 854, 2017, p. 012032.

[80] P. Fleming, J. Annoni, A. Scholbrock, E. Quon, S. Dana, S. Schreck, S. Raach, F. Haizmann, and D. Schlipf, "Full-scale field test of wake steering," in *J. Phys. Conf. Ser*, vol. 854, no. 1, 2017, p. 012.

[81] P. M. Gebraad, M. J. Churchfield, and P. A. Fleming, "Incorporating atmospheric stability effects into the floris engineering model of wakes in wind farms," in *Journal of Physics: Conference Series*, vol. 753, no. 5. IOP Publishing, 2016, p. 052004.

[82] U. Ciri, M. A. Rotea, and S. Leonardi, "Effect of the turbine scale on yaw control," *Wind Energy*, vol. 21, no. 12, pp. 1395–1405, 2018.

[83] G.-W. Qian and T. Ishihara, "A new analytical wake model for yawed wind turbines," *Energies*, vol. 11, no. 3, p. 665, 2018.

[84] J. M. S. Bartl, F. V. Mühle, J. Schottler, L. R. Sætran, J. Peinke, M. S. Adaramola, and M. Holling, "Wind tunnel experiments on wind turbine wakes in yaw: effects of inflow turbulence and shear," *Wind Energy Science*, vol. 3, no. 1, pp. 329–343, 2018.

[85] P. M. Gebraad, F. Teeuwisse, J.-W. van Wingerden, P. A. Fleming, S. D. Ruben, J. R. Marden, and L. Y. Pao, "A data-driven model for wind plant power optimization by yaw control," in *2014 American*

Control Conference. IEEE, 2014, pp. 3128–3134.

[86] D. Dilip and F. Porté-Agel, "Wind turbine wake mitigation through blade pitch offset," *Energies*, vol. 10, no. 6, p. 757, 2017.

[87] J. Jonkman, S. Butterfield, W. Musial, and G. Scott, "Definition of a 5-mw reference wind turbine for offshore system development," National Renewable Energy Lab.(NREL), Golden, CO (United States), Tech. Rep., 2009.

[88] E. Bossanyi, "Optimising yaw control at wind farm level," in *Journal of Physics: Conference Series*, vol. 1222, no. 1. IOP Publishing, 2019, p. 012023.

[89] H. E. Jørgensen, M. Nielsen, R. J. Barthelmie, and N. G. Mortensen, "Modelling offshore wind resources and wind conditions," *Roskilde, Denmark: Risø National Laboratory*, 2005.

[90] E. Jones, T. Oliphant, P. Peterson *et al.*, "Scipy: Open source scientific tools for python," 2001.

[91] D. Kraft, "A software package for sequential quadratic programming." DLR German Aerospace Center – Institute for Flight Mechanics, Koln, Germany, techreport DFVLR-FB 88-28, 1988.

[92] C. L. Lawson and R. Hanson, "Solving least squares problems prentice-hall," *Englewood Cliffs, NJ*, 1974.

[93] P. A. Fleming, A. Ning, P. M. Gebraad, and K. Dykes, "Wind plant system engineering through optimization of layout and yaw control," *Wind Energy*, vol. 19, no. 2, pp. 329–344, 2016.

Annex A

Relevant FLORIS constants

The present annex provides information on the model-specific tuneable parameters and relevant atmospheric constants that had to be specified in FLORIS. These values are the defaults of FLORIS version 2.2.0.

Table A.1 Default model-specific parameters in FLORIS version 2.2.0

Jensen wake velocity deficit model parameters		
we	0.05	The linear wake decay constant that defines the cone boundary for the wake as well as the velocity deficit.
Gauss / GCH wake velocity deficit model parameters		
ka	0.38	Parameter used to determine the linear relationship between the turbulence intensity and the width of the Gaussian wake shape.
kb	0.004	Parameter used to determine the linear relationship between the turbulence intensity and the width of the Gaussian wake shape.
alpha	0.58	Parameter that determines the dependence of the downstream boundary between the near wake and far wake region on the turbulence intensity.
beta	0.077	Parameter that determines the dependence of the downstream boundary between the near wake and far wake region on the turbine's induction factor.
calculate_VW_velocities	True	Flag to enable calculation of spanwise and vertical velocity components needed to account for secondary steering effects (only GCH)
use_yaw_added_recovery	True	Flag to use yaw added recovery on the wake velocity (only GCH)
eps_gain	0.2	Tuning value for calculating the V- and W-component velocities (only GCH)
Jiménez wake deflection model parameters		
kd	0.05	Parameter used to determine the skew angle of the wake.
ad	0	Additional tuning parameter to modify the wake deflection with a lateral offset.
bd	0	Additional tuning parameter to modify the wake deflection with a lateral offset.
Bastankhah wake deflection model parameters		
ka, kb, alpha, beta, eps_gain	-	The same as for Gauss / GCH wake velocity deficit model parameters.
ad	0	Additional tuning parameter to modify the wake deflection with a lateral offset.
bd	0	Additional tuning parameter to modify the wake deflection with a lateral offset.
dm	1	Additional tuning parameter to scale the amount of wake deflection.
Crespo – Hernandez wake turbulence model		
initial	T_I	The initial ambient turbulence intensity expressed as a decimal fraction.
constant	0.5	The constant used to scale the wake-added turbulence intensity.
ai	0.8	The axial induction factor exponent used in the calculation of wake-added turbulence.
downstream	-0.32	The exponent applied to the distance downstream of an upstream turbine normalized by the rotor diameter used in the calculation of wake-added turbulence.

Table A.2 Relevant atmospheric constants set in FLORIS

Atmospheric constants		
Air density [kg/m^3]	1.225	
Wind shear coefficient	0.12	The power law wind shear exponent.
Wind veer coefficient	0	The vertical change in wind direction across the rotor.

Annex B

Optimization convergence

The following annex consists of the figures presenting optimization convergence tracking for each simulation scenario analysed in Chapter 5.

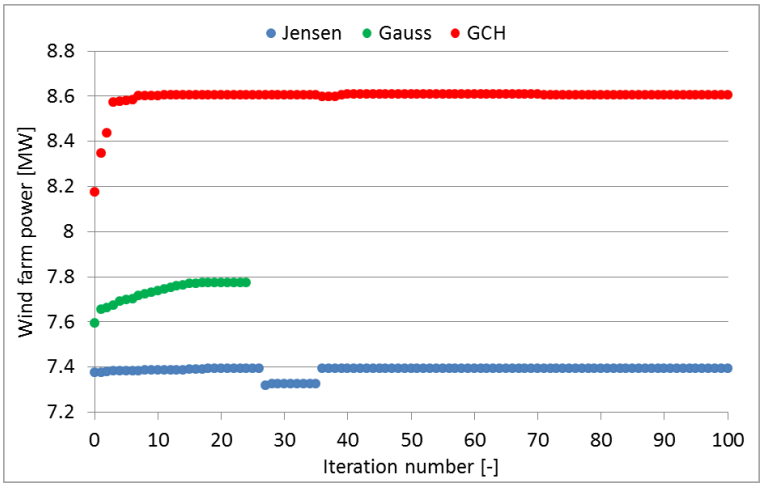

Figure B.1 Reference Case optimization convergence

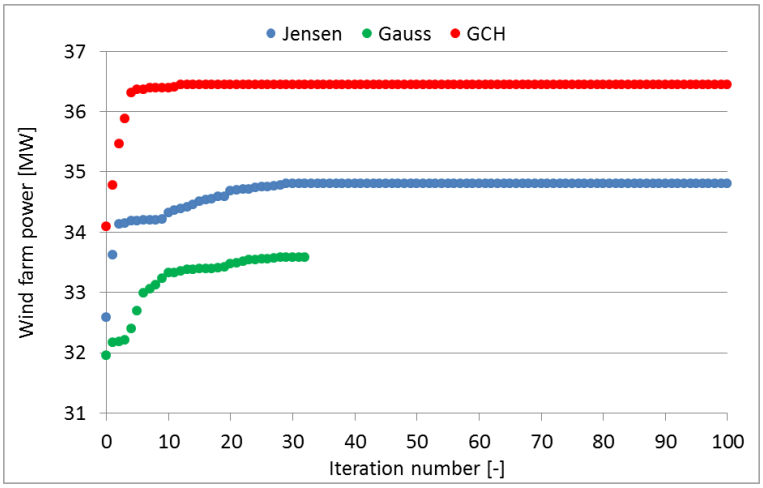

Figure B.2 High Wind Speed optimization convergence

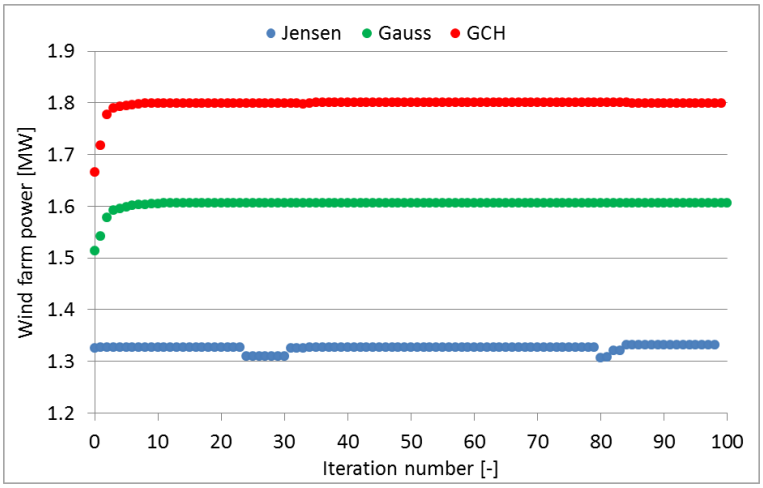

Figure B.3 Low Wind Speed optimization convergence

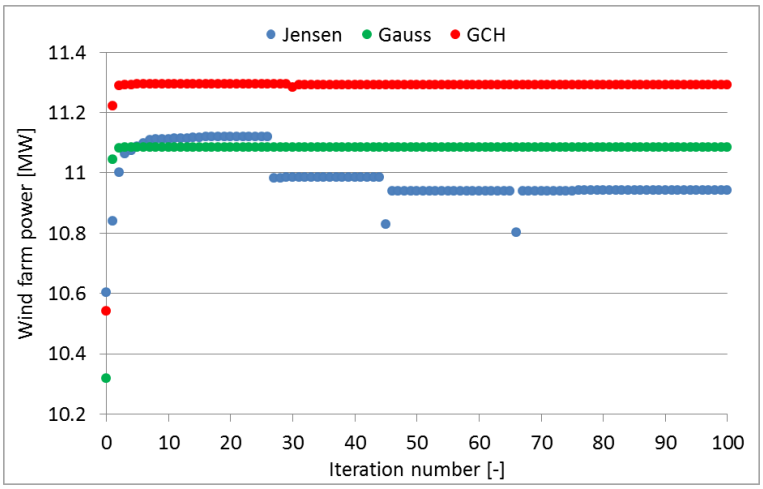

Figure B.4 Wind Direction 275° optimization convergence

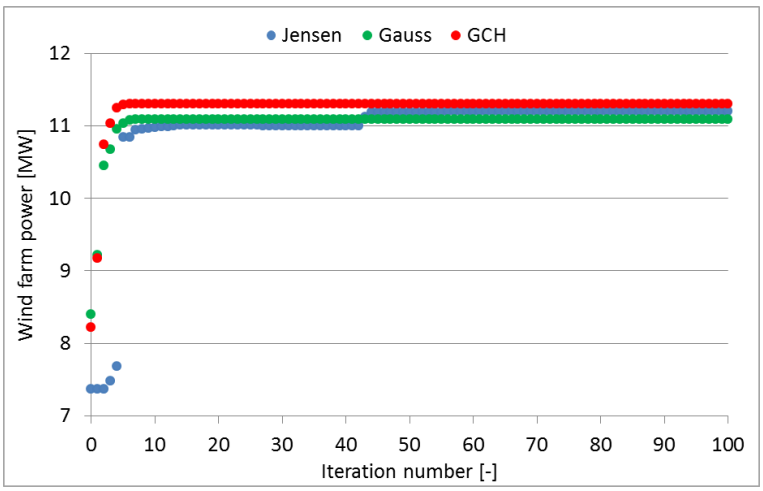

Figure B.5 Wind Direction 265° optimization convergence

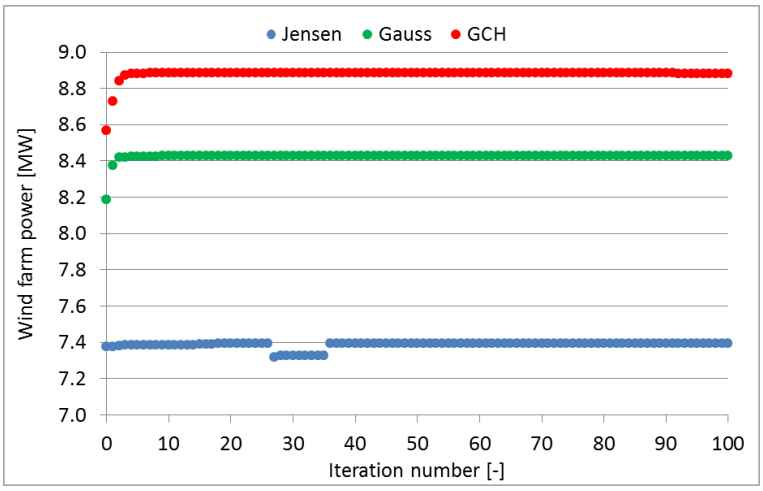

Figure B.6 High Turbulence Intensity optimization convergence

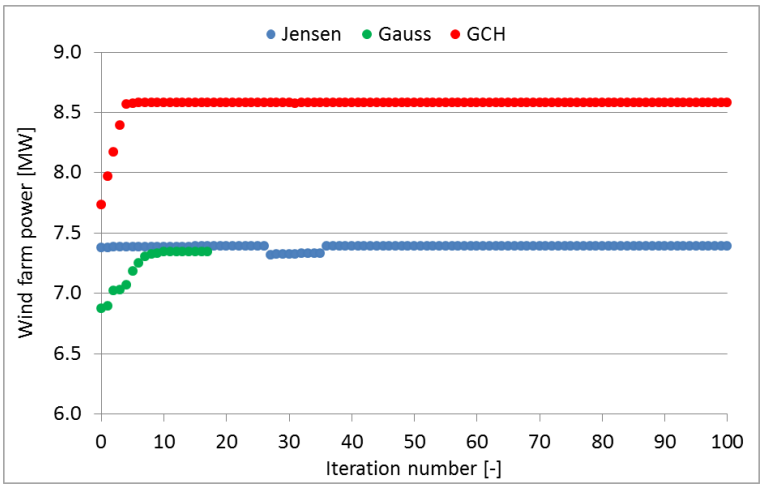

Figure B.7 Low Turbulence Intensity optimization convergence

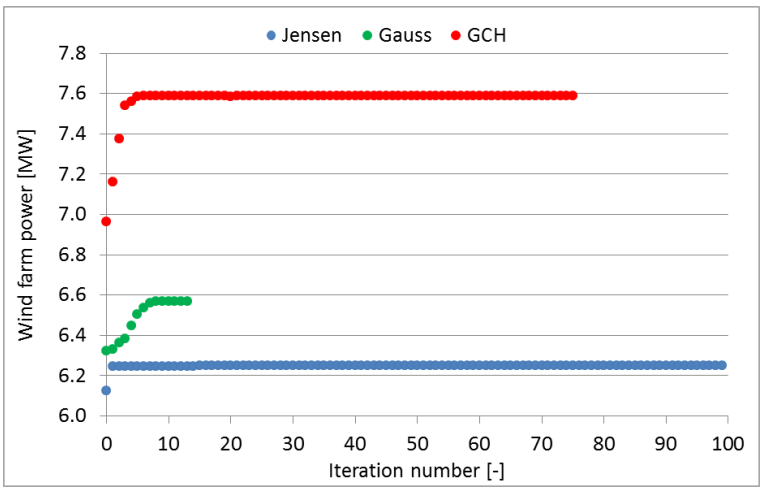

Figure B.8 Small Spacing optimization convergence

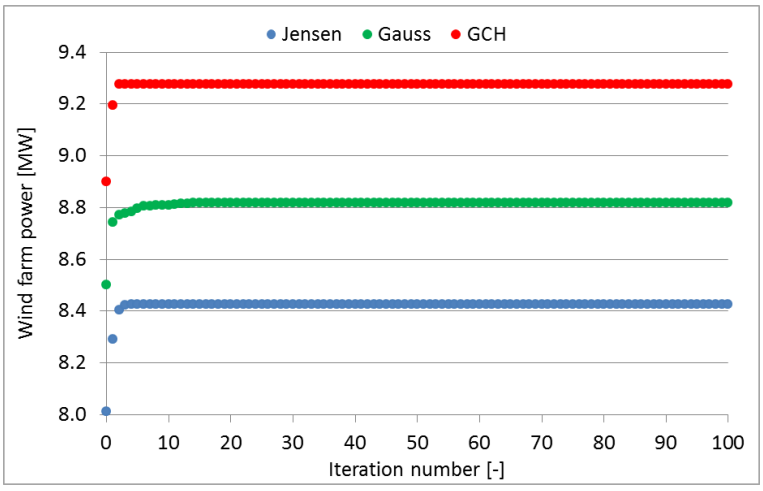

Figure B.9 Large Spacing optimization convergence

Annex C

Remaining figures

The present annex contains flow field visualization and rotor swept area wind velocity evolution throughout the park for LWS, WD_265°, LTI and LS simulation cases.

C.1 Low wind speed

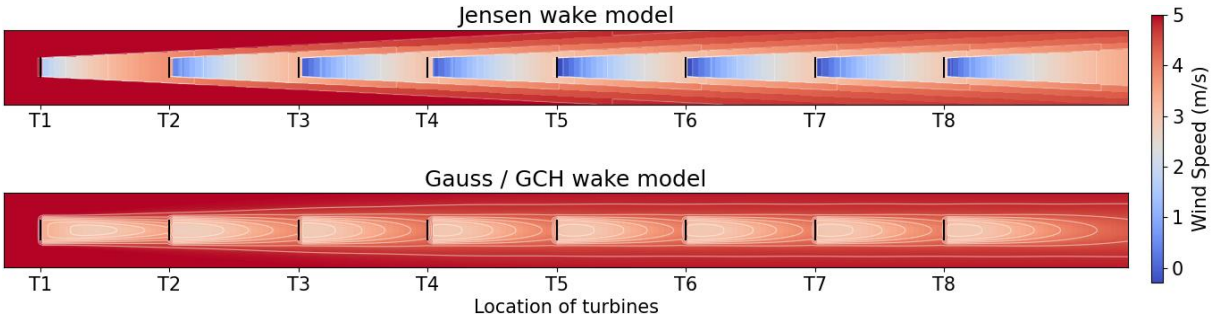

Figure C.1.1 Hub height flow field with baseline yaw settings – LWS

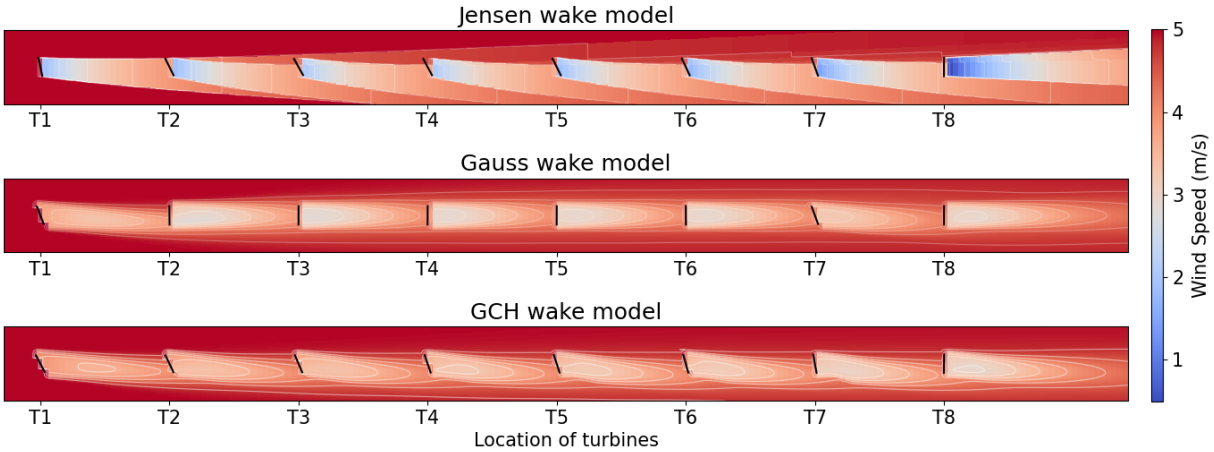

Figure C.1.2 Hub height flow field with optimized yaw settings – LWS

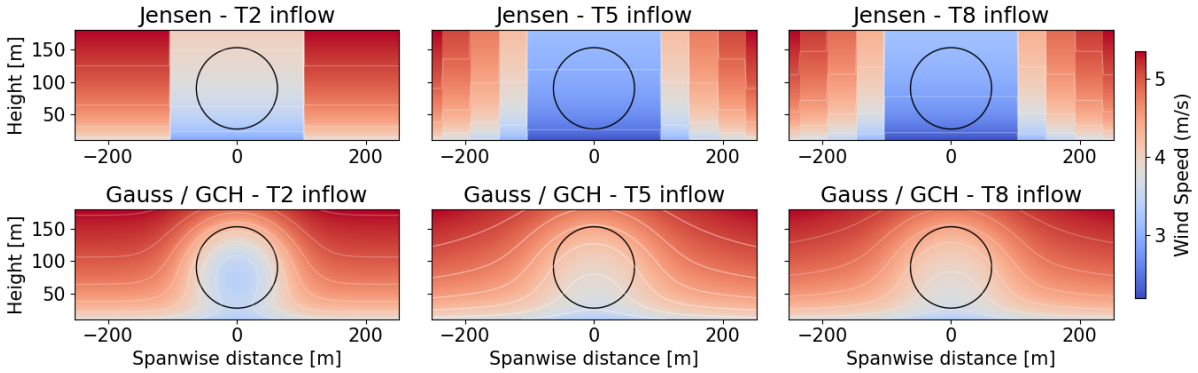

Figure C.1.3 Velocity field 0.5D ahead of T2, T5 and T8 with baseline yaw settings – LWS

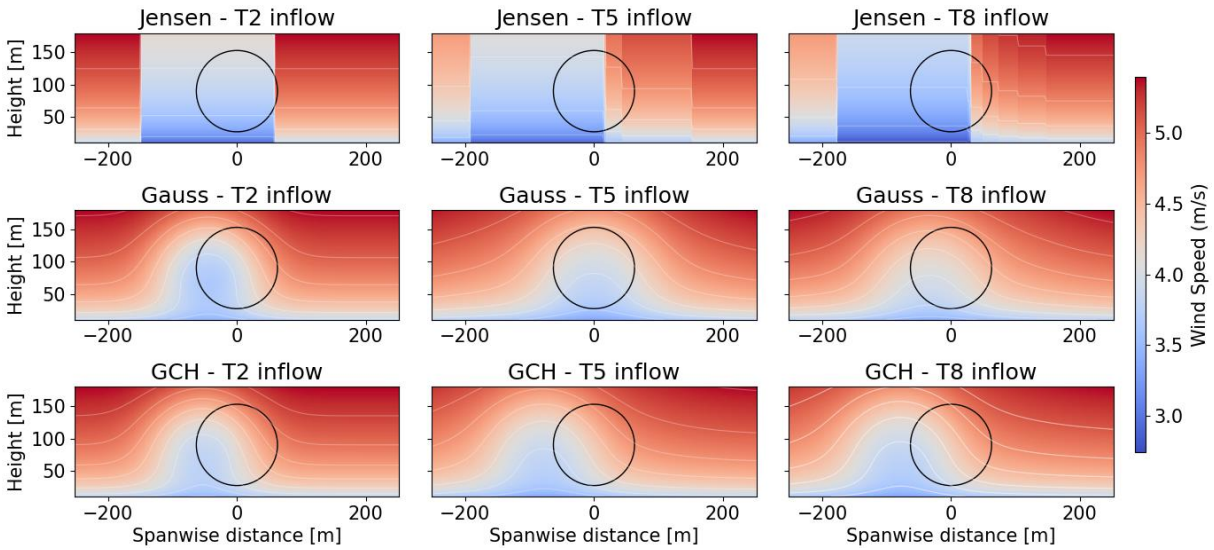

Figure C.1.4 Velocity field 0.5D ahead of T2, T5 and T8 with optimized yaw settings – LWS

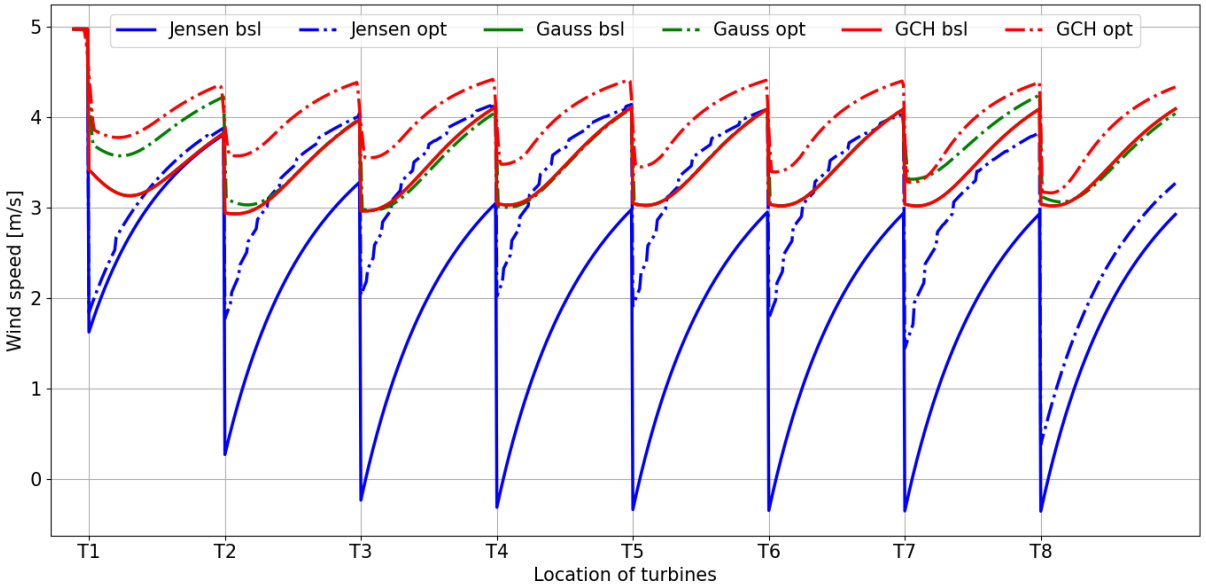

Figure C.1.5 Evolution of rotor swept area-averaged wind velocity along the wind farm – LWS

C.2 Wind direction 265°

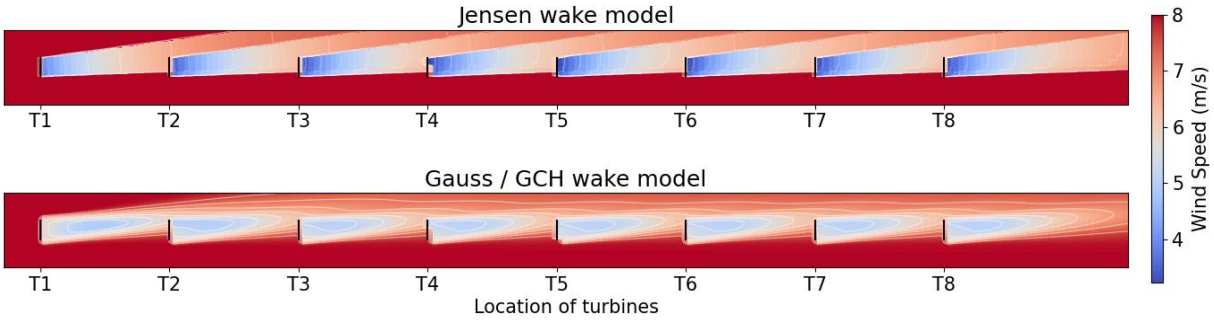

Figure C.2.1 Hub height flow field with baseline yaw settings – WD_265°

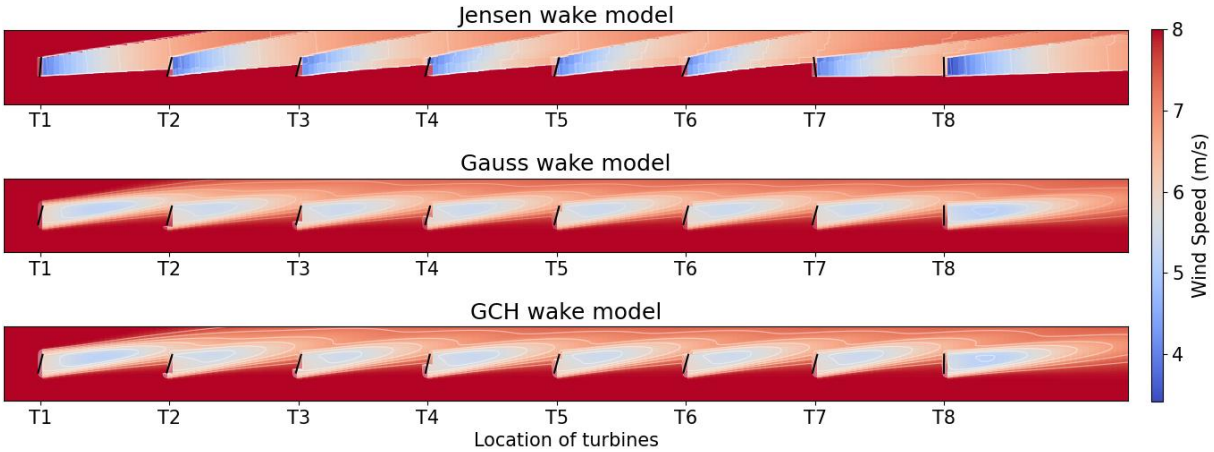

Figure C.2.2 Hub height flow field with optimized yaw settings – WD_265°

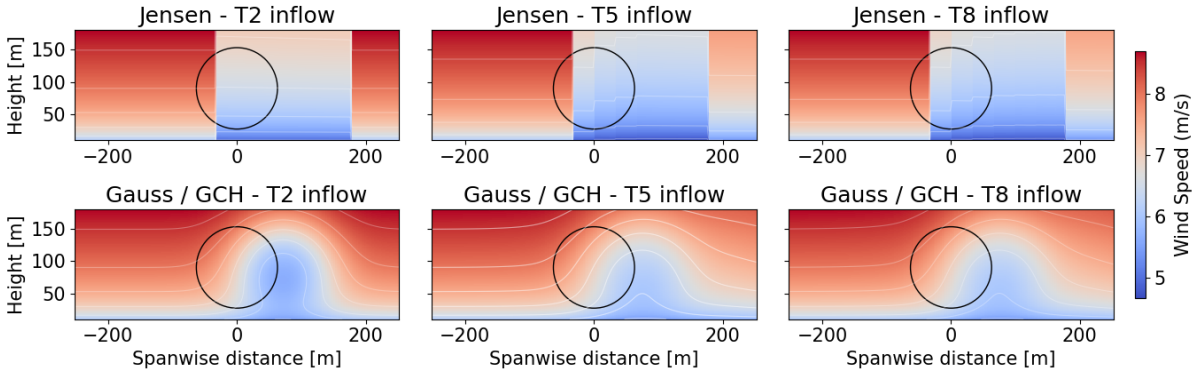

Figure C.2.3 Velocity field 0.5D ahead of T2, T5 and T8 with baseline yaw settings – WD_265°

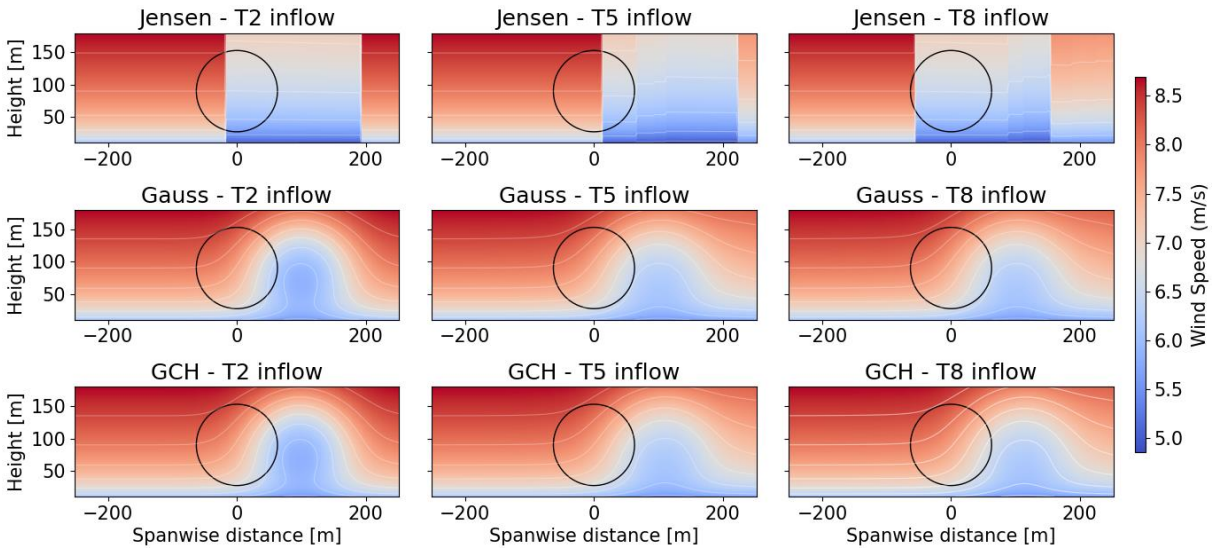

Figure C.2.4 Velocity field 0.5D ahead of T2, T5 and T8 with optimized yaw settings – WD_265°

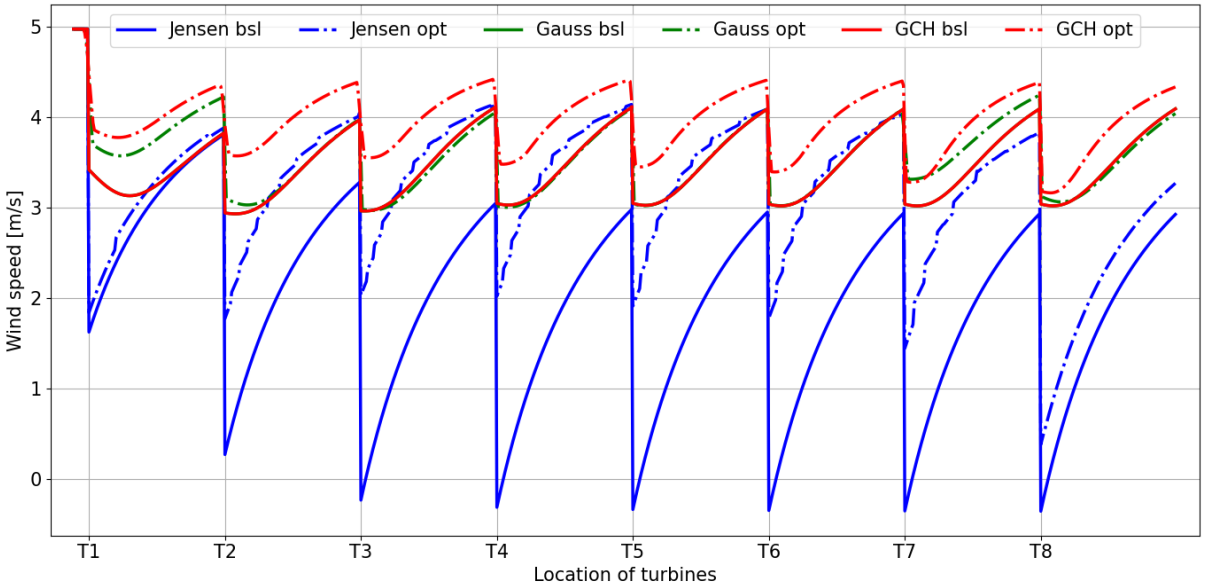

Figure C.2.5 Evolution of rotor swept area-averaged wind velocity along the wind farm – WD_265°

C.3 Low turbulence intensity

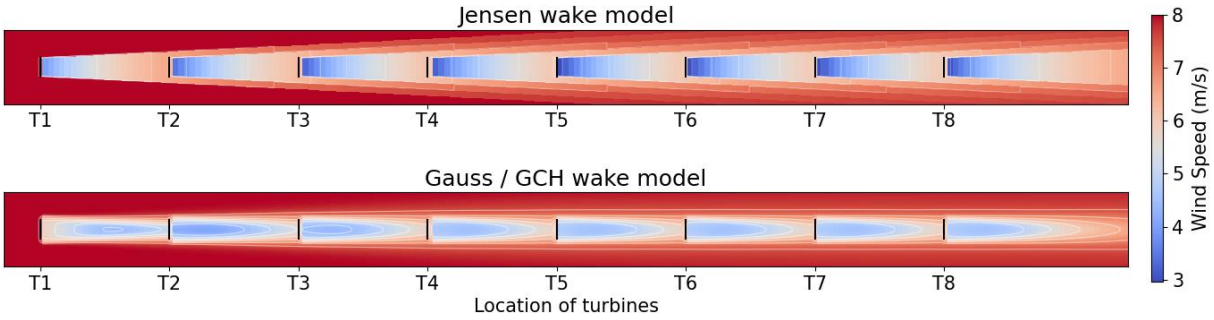

Figure C.3.1 Hub height flow field with baseline yaw settings – LTI

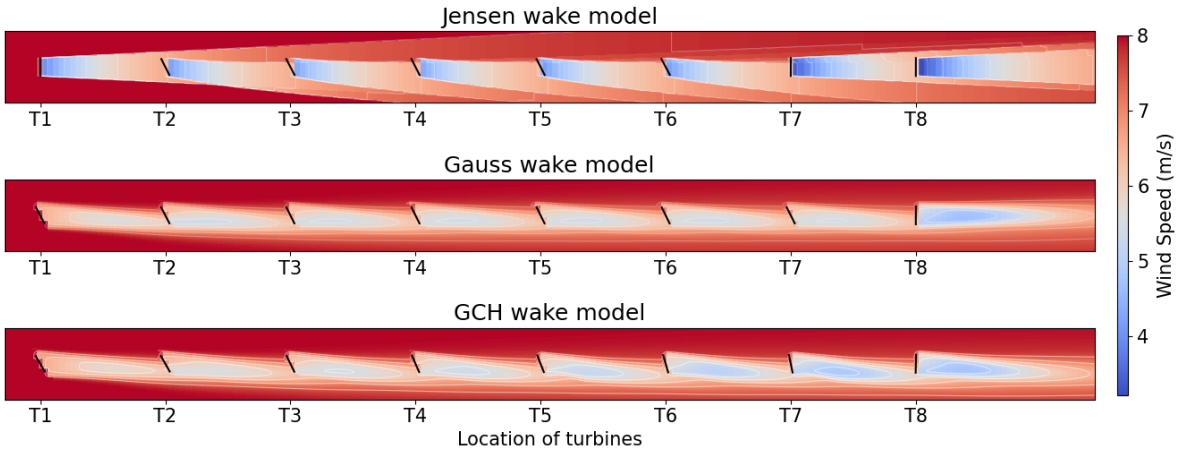

Figure C.3.2 Hub height flow field with optimized yaw settings – LTI

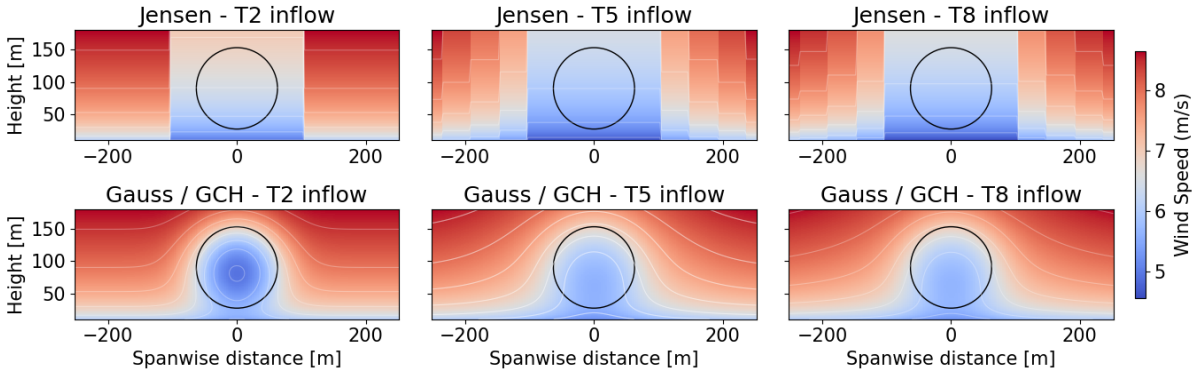

Figure C.3.3 Velocity field 0.5D ahead of T2, T5 and T8 with baseline yaw settings – LTI

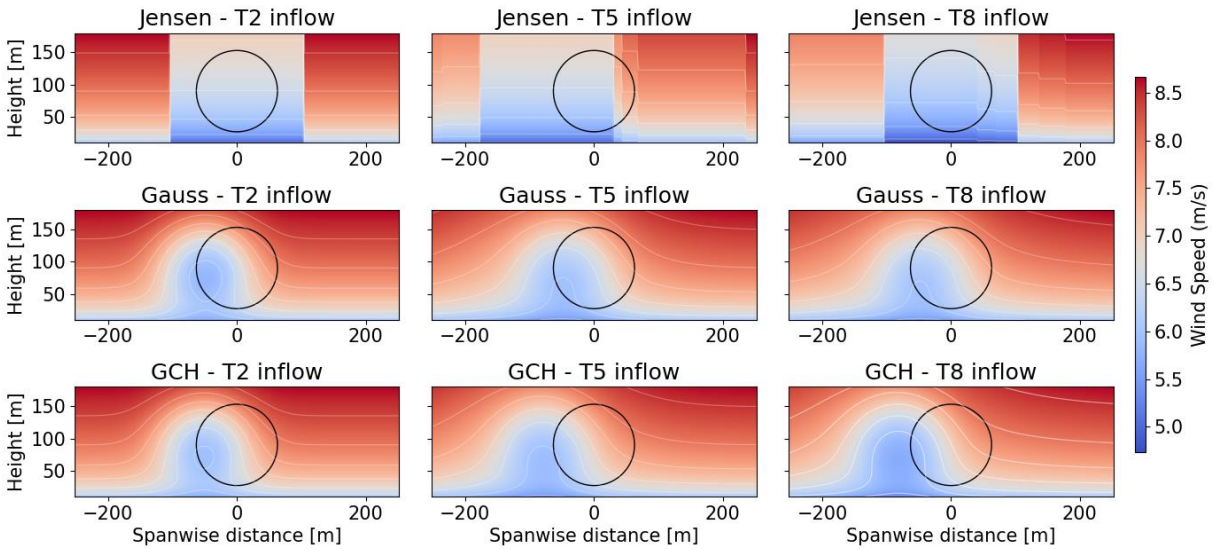

Figure C.3.4 Velocity field 0.5D ahead of T2, T5 and T8 with optimized yaw settings – LTI

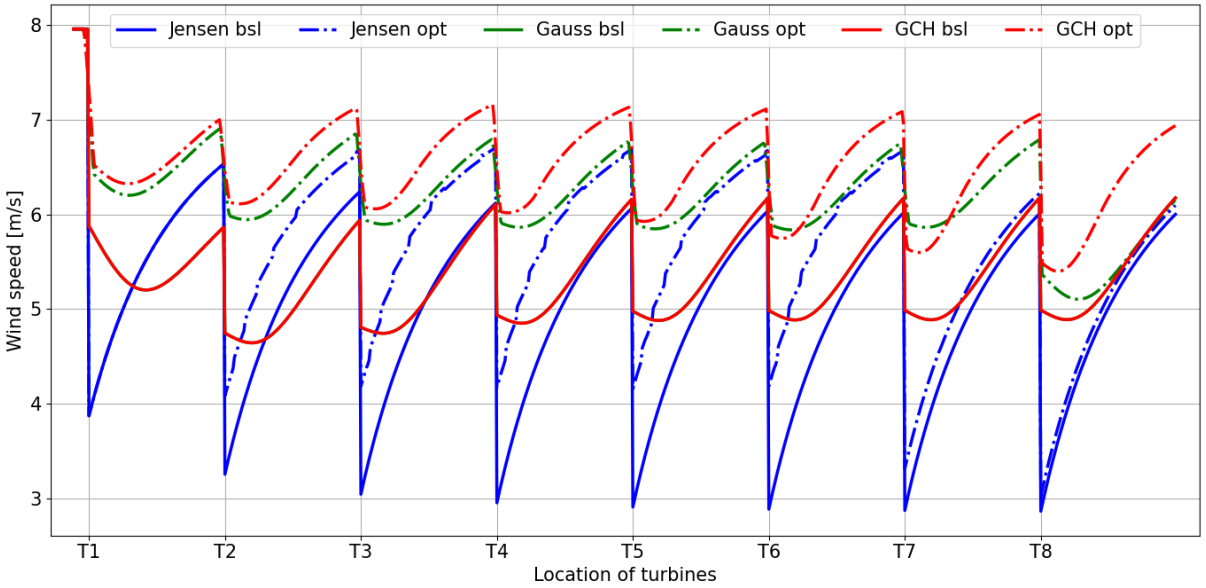

Figure C.3.5 Evolution of rotor swept area-averaged wind velocity along the wind farm – LTI

C.4 Large spacing

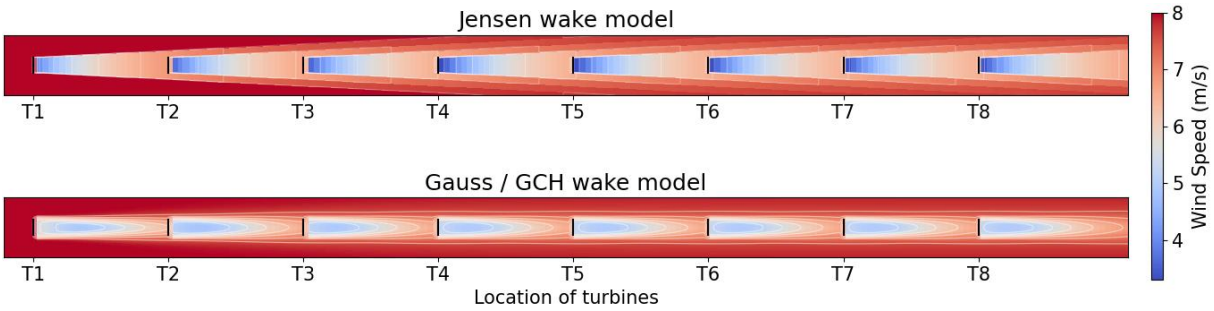

Figure C.4.1 Hub height flow field with baseline yaw settings – LS

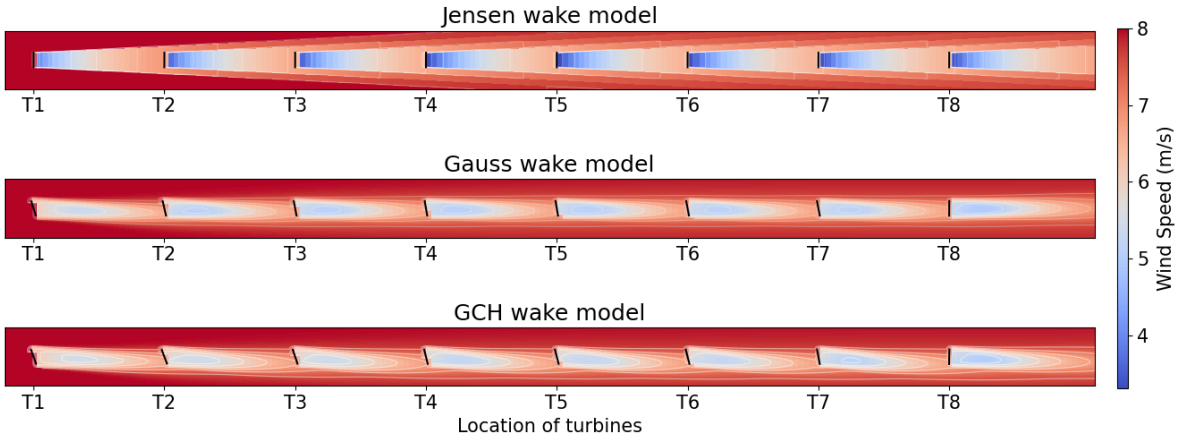

Figure C.4.2 Hub height flow field with optimized yaw settings – LS

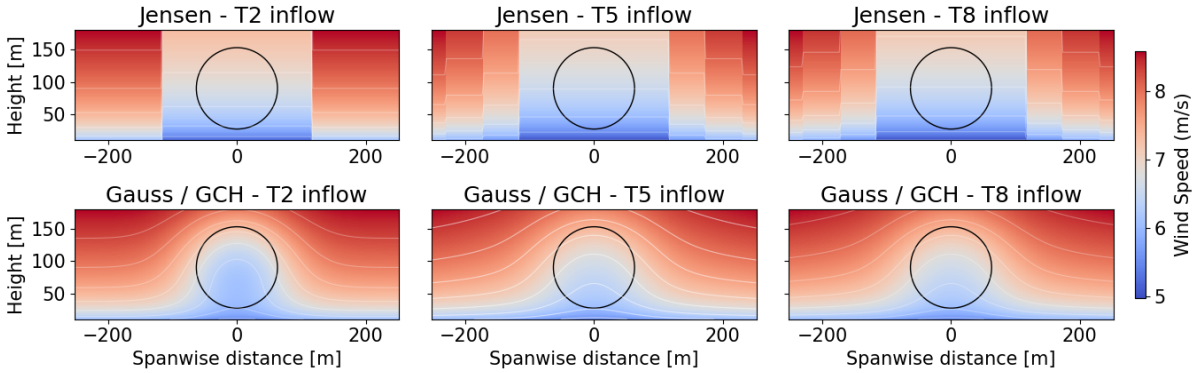

Figure C.4.3 Velocity field 0.5D ahead of T2, T5 and T8 with baseline yaw settings – LS

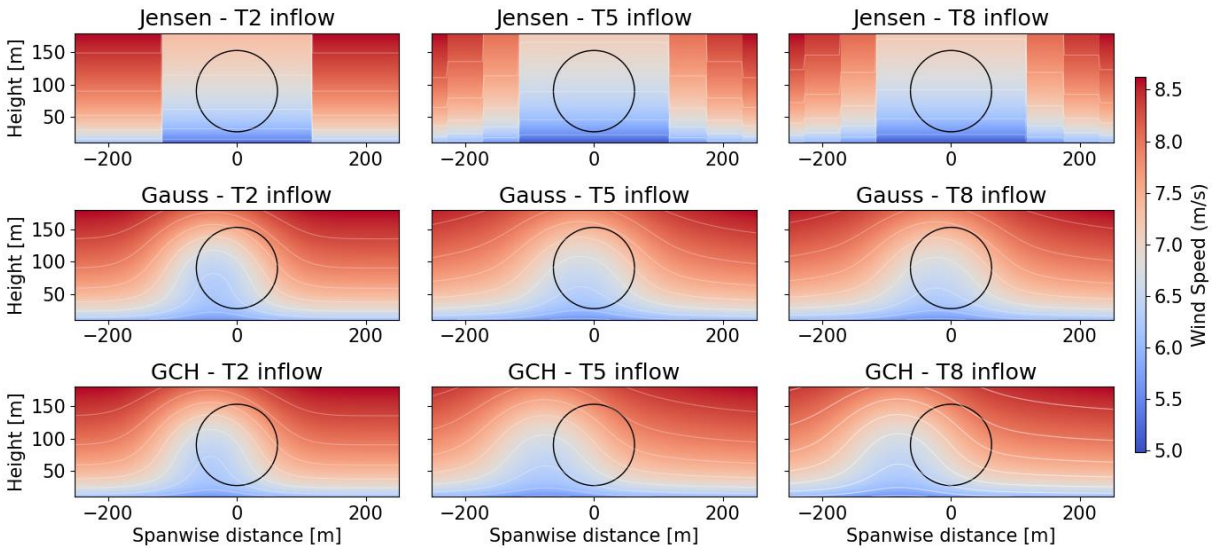

Figure C.4.4 Velocity field 0.5D ahead of T2, T5 and T8 with optimized yaw settings – LS

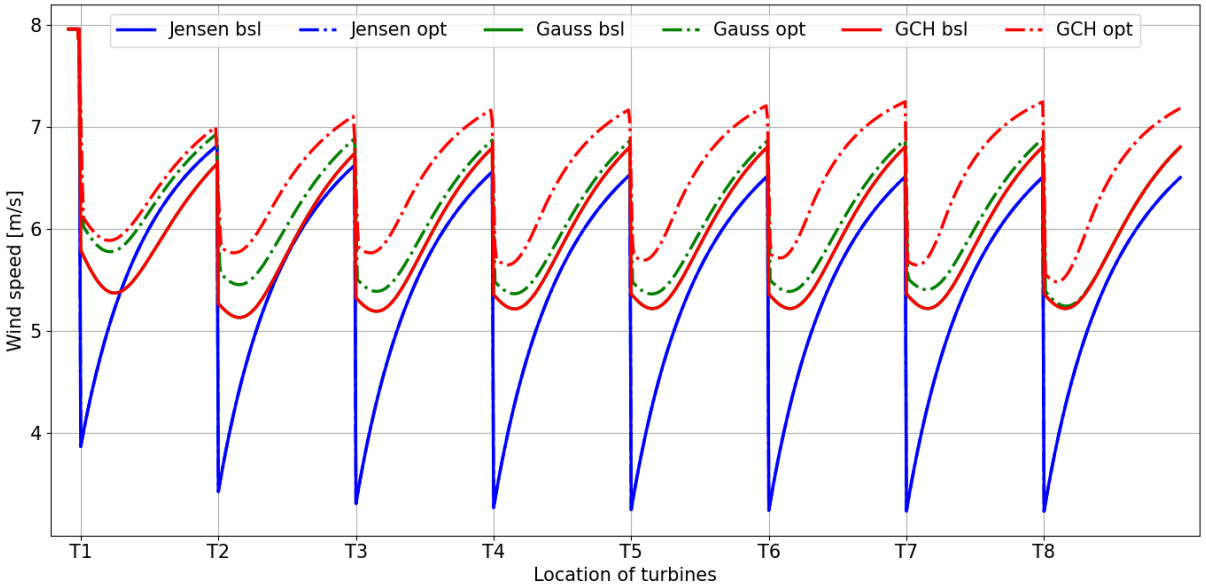

Figure C.4.5 Evolution of rotor swept area-averaged wind velocity along the wind farm – LS